Parvalbumin and Perineuronal net expression in the medial and lateral regions of the Dorsal Striatum in an Idiopathic model of ASD, through development.

A Thesis submitted in partial fulfilment of the requirements for the degree of MSc (by Research) at the University of Central Lancashire (UCLan)

Gabriel. E. Gibson

24th September 2024

RESEARCH STUDENT DECLARATION FORM

Type of Award _____MSc(by Research)_____

School _____Psychology and Humanities_____

*Sections marked * delete as appropriate*

1. **Concurrent registration for two or more academic awards**

Either *I declare that while registered as a candidate for the research degree, I have not been a registered candidate or enrolled student for another award of the University or other academic or professional institution

or

_____

_____

2. **Material submitted for another award**

Either *I declare that no material contained in the thesis has been used in any other submission for an

academic award and is solely my own work

or

_____

_____

3. Collaboration

Where a candidate's research programme is part of a collaborative project, the thesis must indicate in addition clearly the candidate's individual contribution and the extent of the collaboration. Please state below:

_____N/A_____

4. Use of a Proof-reader

Either

or   *No proof-reading service was used in the compilation of this thesis.

Signature of Candidate   _____ ⟨signature⟩ _____

Print name: _____Gabriel Edward Gibson_____

1 Abstract

2 Parvalbumin-expressing fast-spiking interneurons (PV+FSIs) within the dorsal striatum, associated with

3 the generation of habitual behaviour and motor stereotypy, are a commonly reported node of alteration

4 in various forms of autism spectrum disorder (ASD). Previous investigations of altered striatal PV+FSIs

5 and their associated perineuronal nets (PNNs) in ASD lack consideration of the potential differences

6 between dorsal striatum subregions (dorsomedial and dorsolateral striatum), sex, and developmental

7 stage. This study utilised immunohistochemical and qPCR methods on tissue from an idiopathic murine

8 model of ASD (BTBR T$^+$ Itpr3^{tf}/J mice; n = 20) and C57 L/J control mice (n = 20). The density of PV+FSIs,

9 PNNs, their colocalisation, and the relative intensity of fluorescent staining within the dorsal striatum was

10 compared between mouse strain, subregion, sex, and developmental stage. The relative expression of

11 pvalb, hapln1, tnr, and acan mRNA was compared between mouse strain, sex, and developmental stage.

12 A significantly lower density of PV+FSIs and colocalised PNN+PV+FSIs was observed within the

13 dorsomedial striatum of BTBR T$^+$ Itpr3^{tf}/J relative to C57 L/J mice ($F_{(1,58)}$ = 21.6, p = 0.0134; $F_{(1,58)}$ =

14 8.56, p = 0.007). Whilst a significant reduction in the density of PV+FSIs was identified through

15 development in C57 L/J mice, this was not significantly different between 3-4 and 6-8wk BTBR T$^+$

16 Itpr3^{tf}/J mice ($F_{(1,58)}$=18.9, p = 0.000138; p = 0.400). Further, a greater basal density of PV+FSIs

17 within the dorsomedial striatum was observed in male relative to female mice whereas a greater basal

18 density in the dorsolateral striatum was observed in female mice ($F_{(1,58)}$ = 25.91, p = 0.0002; p =

19 0.0427). A greater basal density of colocalised PNN+PV+FSIs within the dorsolateral striatum was also

20 observed in female mice ($F_{(1,58)}$ = 9.99, p > 0.0001). Altered expression of PV+FSIs and colocalised

21 PNN+PV+FSIs in the dorsal striatum may be a common biological phenotype for idiopathic and other

22 models of ASD, largely explained by downregulation within the dorsomedial striatum. These subregion

23 specific alterations may contribute to different elements of the ASD behavioural phenotype. Further, the

24 identification of basal sex differences in the expression of colocalised PNN+PV+FSIs within dorsal

25 striatum subregions highlights the importance of considering sex within investigations of ASD aetiology.

26

27 **Key words**: Parvalbumin, Perineuronal Nets, Excitation/Inhibition, Dorsal Striatum, Autism Spectrum
28 Disorder, BTBR, Dorsomedial Striatum, Dorsolateral Striatum

29

30

31

32   Abbreviations

ASD	Autism Spectrum Disorder	GOI	Gene of interest
AIS	Axonal initial segment	GWAS	Genome-wide association studies
BG	Basal Ganglia	LV	Lateral Ventricle
BTBR	BTBR T$^+$ Itpr3^{tf}/J	MSNs	Medium spiny projection neurons
C57	C57L/J	MSNs	Medium spiny projection neurons
DS	Dorsal Striatum	PV	Parvalbumin
DLS	Dorsolateral Striatum	PNN	Perineuronal net
DMS	Dorsomedial Striatum	PND	Postnatal day
E:I	Excitation:Inhibition	ROI	Region of interest
FSI	Fast-spiking interneurons	RRBIs	Restrictive, repetitive behaviours, interests, and activities
fEIB	Functional excitation-inhibition balance	TD	Typical development

33
34
35
36
37
38
39
40
41
42
43
44

45   (1.0)   Introduction

46

47   (1.1)   Autism Spectrum Disorder (ASD)

48

49   Autism spectrum disorder (ASD), as defined by the American Psychiatric Association

50   (2013), is a predominantly idiopathic neurodevelopmental condition with a potentially rising

51   (Casanova, et al., 2020; McConkey, 2020; Salari, et al., 2022), prevalence of 1 in 100 people

52   suggested to meet the diagnostic criteria worldwide (American Psychiatric Association, 2013;

53   World Health Organisation, 2022). As described in the Diagnostic and Statistical Manual of

54   Mental Disorders 5th edition, ASD is characterised by two core domains of deficit, namely: (1)

55   social/communication deficits and (2) restricted, repetitive behaviours, interests, and activities

56   (RRBIs; American Psychiatric Association, 2013). Deficits in the social/communication domain

57   include deficits to non-verbal communication behaviours, socio-emotional reciprocity, and

58   difficulties in developing, maintaining and understanding relationships, which often present as

59   poorly integrated verbal and non-verbal communication, abnormal social approach, and an

60   absence of interest in peers (American Psychiatric Association, 2013; World Health Organisation,

61   2022). In contrast deficits in the domain of RRBIs are thought to encompass stereotyped

62   movements and behaviour, restricted and fixated interests, and an insistence on sameness,

63   commonly presented as simple motor stereotypies, ritualised patterns of behaviour, and adverse

64   responses to sounds and textures (American Psychiatric Association, 2013). RRBIs have

65   previously been described as the symptom domain of greatest distress to autistic individuals and

66   their families, additionally disrupting further development of typical functioning (Boyd, et al.,

67   2011; Melo, et al., 2020). A great diversity (or "spectrum") in behavioural phenotype is reported

68   in the autistic population both between individuals and within individuals across development

69   (Richler, et al., 2010). Recent research suggests sex differences in RRBI expression in ASD,

70   potentially due to sexual dimorphic aetiology (van't Westeinde, et al., 2020; Amodeo, et al.,

71   2019; though see Ghandi, et al., 2023). Due to potential differences in ASD aetiology and

72   presentation between sexes, in addition to the previously reported sex bias in ASD diagnoses,

73   considering sex differences whilst investigating ASD aetiology has been emphasised as a key

74   research priority area (Pellicano, et al., 2014).

A diverse variety of environmental and genetic insults have been suggested to underlie the aetiology of ASD, but no single factor has yet been identified to underlie all cases (Casanova, et al., 2020; Ellegood, et al., 2015). This may suggest a shared biological phenotype, in addition to the above-described behavioural phenotype from which diagnosis is made, encapsulating a spectrum of observed biological differences in autistic individuals relative to the typically developing (TD) population. This biological phenotype of ASD may underlie observed morphological/volumetric differences between brain regions (Shan, et al., 2022; Lefebvre, et al., 2023), functional connectivity (Abbott, et al., 2018; Delmonte, et al., 2013), and alterations in Excitatory:Inhibitory (E:I) balance (Sohal & Rubenstein, 2019; Ferguson & Gao, 2018; Wöhr, et al., 2015) in ASD. Further investigation of these features within the context of a shared biological phenotype in ASD may facilitate the elucidation of convergent mechanisms underlying ASD aetiology, with biological phenotype severity potentially associated with behavioural phenotype severity.

(1.2)   E:I Balance

Alterations in E:I balance contributing to divergent brain development and function has gained traction as a prominent hypothesis of a convergent mechanism underlying ASD aetiology (Ferguson & Gao, 2018; Rubenstein & Merzenich, 2003; Sohal & Rubenstein, 2019). E:I balance within the brain traditionally refers to stable global levels of excitatory (E) and inhibitory (I) activity within specific circuits, typically explored through ratios of glutamate and γ-aminobutyric acid (GABA) -ergic signalling (the primary E and I neurotransmitters in the developmentally mature central nervous system; Rubenstein & Merzenich, 2003; Sohal & Rubenstein, 2019). E:I balance is often considered from both a global level of larger scale circuits (via the ratio of E and I neurons within and between different nodes of circuits, or general activity within circuits) and a neuronal level (considering ratios of E and I synapses, and the functioning and expression of components involved in E and I signalling within neuronal populations; Sohal & Rubenstein, 2019; Ferguson & Gao, 2018; Sohal & Rubenstein, 2019). Alterations of E:I ratio in ASD were initially suggested due to the observed high comorbidity of epilepsy in the autistic population, leading to the suggestion of increased excitation or reduced inhibition to modulate behaviour in ASD (Rubenstein & Merzenich, 2003; Ferguson & Gao, 2018; Sohal & Rubenstein, 2019).

Recently alterations in the overall ratio of E and I signalling in ASD have been identified through reports of altered functional E:I balance (fEIB) in "whole-brain" resting-state EEG with greater variability in fEIB reported in autistic children relative to age-matched TD children, suggesting bidirectional shifts from typical E:I signalling ratio may occur in ASD (Bruining, et al., 2020). Further reports of altered fEIB in ASD emphasise that these alterations may not simply reflect an increased or decreased E:I ratio, with differential fEIB developmental trajectories identified and the severity of deviance from typical ratios correlating with ASD symptom development and severity (Plueckebaum, et al., 2023; Bruining, et al., 2020). fEIB is suggested to relate to structural E:I balance measurements, such as the ratio of E-to-E and E-to-I synapses, inferring that the ratio of E and I signalling may be attenuated in ASD (Bruining, et al., 2020). However, this was not explored in females despite other functional imaging studies reporting differences in E:I ratio within the prefrontal cortex to be exclusive to autistic males, highlighting the need for further exploration of sex differences in ASD aetiology (Trakoshis, et al., 2020). The underlying signal alterations contributing to differences in E:I balance may be further understood by utilisation of animal models of ASD such as the Black and Tan Brachyury (BTBR) T[+]Itpr[3tf]/J mouse strain, known to exhibit reduced inhibitory post-synaptic current (IPSC) frequency relative to wild type (C57) mice (Sohal & Rubenstein, 2019; Hans, et al., 2014). Administration of low-dose benzodiazepine (a positive GABAa receptor allosteric modulator) increased the frequency of IPSCs to levels comparable to C57 mice in addition to reports of improved of behavioural deficits in both social/communication and RRBI domains, suggesting GABAergic system dysfunction to underlie an observed E:I signalling imbalance contributing to the behavioural phenotype of ASD (Han, et al., 2014).

Reduced concentrations of GABA have been previously reported in cortical regions in ASD with the severity of this reduction correlating with symptom severity, such as increased tactile hypersensitivity and poorer communication skills (Sapey-Triomphe, et al., 2019; Carvalho, et al., 2018). However, reduced GABA concentrations and altered GABA:Glutamate ratios were not observed universally, with reductions appearing to be localised to specific brain regions, suggesting GABA system dysfunction in ASD may occur in a region-specific manner (Edmonson, et al., 2018; Horder, et al., 2018; Kolondy, et al., 2020; Gonçalves, et al., 2017; Di, et al., 2020; See Zhao, et al., 2022 for review).

136	Several factors may contribute to GABAergic system dysfunction, and therefore E:I imbalance in
137	ASD, such as alterations in receptor and interneuron expression (Plueckebaum, et al, 2023;
138	Gonçalves, et al., 2017). Differences in GABA:Glutamate receptor ratios were observed in BTBR
139	mice relative to wild-type (C57) mice at post-natal day (PND) 28, though this difference was not
140	observed in BTBR mice at PND 84, suggesting alterations in E:I balance may be developmentally
141	dynamic in ASD (Nardi et al., 2023). Altered GABA receptor expression at earlier developmental
142	stages in ASD may have a greater impact on divergence from typical development than
143	alterations at later stages due to the protracted development of the GABAergic system, and the
144	involvement of GABA signalling in neurodevelopmental processes such as neuron maturation
145	and synaptogenesis (Di, et al., 2020; Sohal & Robenstein, 2019; Topchiy, et al., 2024). Beyond
146	the classical I role, GABA signalling possesses neurotrophic features through GABA receptor
147	triggered brain-derived neurotrophic factor release, promoting the development of GABAergic
148	synapses and dendritic spine formation (Fiorentino, et al., 2009; Owens & Kriegstein, 2002).
149	Prior studies further emphasise the neurodevelopmental contributions of GABA through GABA
150	blockades resulting in attenuated PV+FSI morphology and GABAa receptor inhibition resulting in
151	impaired survival and differentiation of striatal PV+FSIs in rodents (Cellot & Cherubini, 2013;
152	Ikeda, et al., 1997; Topchiy, et al., 2024; Wu, et al., 2012). As the development of the GABA
153	system is suggested to guide the development of other signalling pathways (e.g. glutamate), any
154	alterations of GABA signalling at earlier developmental stages may have widespread
155	consequences on brain wide development (Topchiy, et al., 2024).
156	Expression levels of various GABAa receptor subunits have previously been identified in
157	postmortem analysis in ASD (Adak, et al., 2023; Fatemi, et al., 2010; 2014; Hong, et al., 2020),
158	including reduced expression of the GABAa receptor α2 subunit around the axonal initial
159	segment (AIS) of cortical pyramidal neurons in ASD (Hong, et al., 2020). A reduction in GABA
160	receptors may be indicative of impaired GABA signalling received from presynaptic neurons,
161	such as parvalbumin (PV)+ interneurons that most often synaptically target the AIS in both
162	cortical and subcortical regions (Gonçalves, et al., 2017; Hong, et al., 2020). However, E:I
163	balance alterations in ASD may be region specific, the majority of studies investigate cortical
164	regions exclusively without considering the functional relevance of subcortical regions, such as
165	the striatum, to the ASD behavioural phenotype.
166	

167   (1.3)   Striatum/Striatal alterations in ASD

168

169   Both morphological and functional alterations of the striatum have been reported in

170   ASD, with dysfunction within this region postulated to underlie RRBIs (Evans, et al., 2023;

171   Fuccillo, 2016; Lauber, et al., 2016). The striatum is the main input nuclei of the basal ganglia

172   (BG)– a collection of heavily interconnected subcortical nuclei –subdivided into the caudate

173   (dorsomedial striatum (DMS)), putamen (dorsolateral striatum (DLS)), and ventral striatum (Filice,

174   et al., 2020; Langen, et al., 2009; Fuccillo, et al., 2016; van Rooij, et al., 2018). Approximately

175   95% of neurons within the striatum are GABAergic medium spiny neurons (MSNs), with

176   regulatory interneurons of various subtypes –with a key role in regulating the dynamics and flow

177   of information through the striatum– constituting the remaining 5% (Bolam, et al., 1983;

178   Briones, et al., 2022; Tepper, et al., 2010; 2018). The striatum facilitates motor behaviour in

179   addition to action selection mechanisms such as reward motivated behaviours, procedural

180   learning modulation, and behavioural flexibility (Hazlett, et al., 2024; Ma, et al., 2022; Nardi et

181   al., 2023; Evans, et al., 2023; Lauber, et al., 2016). Striatal involvement in these behaviours may

182   be pertinent to investigations of ASD aetiology as deficits within these functions may underlie

183   RRBI expression (D'Cruz, et al., 2013; Mostert-Kerckhoffs, et al., 2015). Morphological alteration

184   of the striatum has been reported in various murine models of ASD, with volumetric differences

185   noted in BTBR (increase) and CNTNAP2-/- mice (decrease; Ellegood, et al., 2013; Thabault, et al.,

186   2022) mirroring the bidirectional differences in striatal volume reported in the autistic

187   population (Turner, et al., 2016; Sussman, et al., 2015). However, the striatum is known to be a

188   heterogenous structure both in function and morphology with two distinct functional territories

189   within the dorsal striatum (DS) being the caudate and putamen (with anatomical analogues of

190   the DMS and DLS respectively in rodents; Hazlett, et al., 2024; Ma, et al., 2022; Nardi et al.,

191   2023). The DMS is reportedly associated with goal-directed behaviours whereas the DLS has

192   reported contribution to habit formation; underlying subregional differences in morphology may

193   be expected to underlie these functional differences and their alteration in ASD (Evans, et al.,

194   2023; Miyata & Kitigawa, et al., 2017; Fino, et al., 2018; O'Connor, et al., 2019). Post-mortem

195   investigations of striatal morphology emphasise the importance of considering striatal

196   subdivisions, reporting a significantly greater (~22%) increase in relative volume of the caudate

197   and reduced neuron density within the putamen relative to typical development (Wegiel, et al.,

10

2014). Volumetric striatal alterations in ASD may be a consequence of altered growth in childhood, potentially due to differential extrastriatal signalling (Abbott, et al., 2018; Langen, et al., 2009). Though static studies cannot provide this insight, longitudinal MRI investigations report almost doubled striatal growth rate within the caudate in autistic relative to TD children across development in contrast to reductions in putamen volume (Langen, et al., 2014; Langen, et al., 2009; van Rooij, et al., 2018). This greater striatal growth rate in ASD reportedly correlates with more severe RRBIs, suggesting alterations in the development of the striatum may contribute to the behavioural profile and aetiology of ASD (Langen, et al., 2014; Langen, et al., 2009).

As with most investigations of the striatum in the context of ASD, samples are predominantly male and therefore do not explore sex differences despite previous reports of greater relevance for brain structure alterations to RRBIs in autistic females (Abbott, et al., 2018; van't Westeinde, et al., 2020; Langen, et al., 2009; 2014). The striatum is a convergent node in multiple circuits of action selection and reward processing, therefore neuronal dysfunction within this primarily inhibitory nucleus may be uniquely sensitive in ASD with potentially wide-arching implications for E:I balance and circuits associated with RRBIs and behavioural-flexibility. One convergent locus that may underlie the morphological and functional alterations observed within the striatum in ASD may be parvalbumin-expressing fast-spiking interneurons (PV+FSIs) which, although only accounting for ~1% of neurons within the striatum, account for ~10% of all striatal activity (Briones, et al., 2022; Filice, et al., 2020).

(1.4)   Parvalbumin-expressing fast-spiking interneurons (PV+FSIs)

Despite relatively low numbers, striatal interneurons powerfully control the output of direct and indirect pathways through the striatum, with the parvalbumin-expressing subpopulation notably involved in establishing E:I signalling ratios in this region (Sreenivasan, et al., 2022; Eto, et al., 2010). Parvalbumin-expressing fast-spiking interneuron (PV+FSI) alterations in ASD may therefore influence E:I signalling ratios within the striatum, contributing to the observed behavioural phenotype (Wöhr, et al., 2015; Gritton, et al., 2019; Wingert & Sorg, 2021). PV+FSIs are a subpopulation of GABAergic interneurons found within the striatum, characterised by expression of the calcium binding protein parvalbumin and a fast-spiking

229   electrophysiological profile (Ghandi, et al., 2023; Inan, et al., 2016). These GABAergic

230   interneurons modulate the outputs of principal neurons (MSNs within the striatum) by forming

231   dense synapses in peri-somatic regions (e.g. the AIS) to facilitate inhibitory network motifs such

232   as feed-forward, feedback, and lateral inhibition, to influence striatal signalling output in larger

233   networks (Inan, et al., 2016; Wingert & Sorg, 2021; John, et al., 2022).

234   Reductions in cortical PV+FSI density have previously been identified in postmortem ASD cases,

235   with the severity of reductions correlating with the severity of reported motor stereotypies

236   (Dufour, et al., 2023; Hashemi, et al., 2017; Ariza, et al., 2018). However, it is unclear if

237   observed differences are exclusive to the cortex as alterations in PV+FSI density have been

238   reported in various cortical and subcortical regions, occurring in a region-specific manner across

239   development (Brandenberg & Blatt, 2022; Ueno, et al., 2017; 2018). Differences in cortical

240   PV+FSI density are reportedly attributed to reduction in the chandelier PV+FSI subtype (not

241   present within the striatum) rather than alterations in the basket PV+FSI subtype density (Ariza,

242   et al., 2018; Dufour, et al., 2023). Investigations of murine models of ASD reflect these cortical

243   findings whilst additionally reporting alterations in striatal PV+FSI expression (Ghandi, et al.,

244   2023; Lauber, et al., 2016; 2018; Filice, et al., 2020). Consideration of striatal subregional

245   differences reveals reductions in PV+FSI density to be representative of differences within the

246   DMS, with little or no differences observed within the DLS (Briones, et al., 2022). PV+FSIs are

247   suggested to be key in silencing non-motor outputs to facilitate task switching and action

248   selection, therefore a reduction in PV+FSI density may result in reduced inhibitory tone, altering

249   E:I signalling ratios in local striatal circuits in ASD with potential brain-wide impacts due to the

250   influence of PV+FSIs on striatal output (Lauber, et al.,, 2018; Gritton, et al., 2019). The

251   behavioural consequences of reduced PV+FSI expression may become apparent through

252   targeted ablation of FSIs within the striatum. With FSI ablation (~40% reductions) results in

253   increased motor stereotypy in male mice, this behavioural shift was not observed in female mice

254   (Rapanelli, et al., 2017; Xu, et al., 2016). Exploration of sex differences in striatal PV+FSI

255   expression has yet to be fully investigated in the context of ASD despite recent reports of

256   sexually dimorphic PV+FSI expression within the dorsal striatum of wild-type mice, with a greater

257   density within female mice (Van Zandt, et al., 2024; Lauber, et al., 2018). Subregional

258   differences in PV+FSI density within the DS between sexes has not yet been investigated, a gap

259   in the literature which this thesis aims to address. The presence of estrogen receptors on striatal

PV+FSIs may further emphasise the relevance of exploration into sex-differences in ASD as 17-β

estradiol exposure reported to increase PV expression and modify both RRBI and

social/communication deficits in PV deficient mice (Filice, et al., 2018).

Differences in PV expression are suggested to underlie reported alterations in PV+FSI density in

ASD, with low expression of PV causing PV+FSIs to fall under detection thresholds for PV+ cell

counts (Lauber, et al., 2018). Alterations in PV expression in ASD may be supported through

investigations of relative intensity of fluorescent staining for PV (a proxy for intensity of PV

expression within PV+FSIs), with decreased intensity reported within VPA mice (Xia, et al.,

2021). Genome-wide association studies (GWASs) support this with pvalb (the gene encoding for

PV) reported to be one of the most downregulated genes in ASD (Parikshak, et al., 2016;

Schwede, et al., 2018). Further, decreased pvalb mRNA was reported in the striatum in both

genetic and environmental models of ASD (Filice, et al., 2016; Lauber, et al., 2016; 2018),

reflecting reports of decreased in PV protein levels in multiple animal models of ASD (Filice, et

al., 2016; Lauber, et al., 2016). Recent research addresses concerns of miscounting PV+FSIs due

to reduced PV expression though the utilisation of secondary markers for PV+FSIs, typically

staining PV+FSI associated perineuronal nets (PNNs) often noting no significant changes in

numbers of PNN+ cells (Lauber, et al., 2018; Filice, et al., 2016; 2020; Lauber, et al., 2016;

2018). PV functions as a slow-onset intracellular calcium signalling modulator, regulating

calcium dependent processes such as neuronal signalling by modulating the availability of

calcium (Filice, et al., 2020; Fuccillo, 2016; Lauber, et al., 2016; Ghandi, et al., 2023; Lauber, et

al., 2018). A reduction in PV expression within the striatum in ASD, rather than reduced density

of PV+FSIs, may therefore lead to a differential impact on E:I signalling alterations as reduced

expression of PV may, in contrast, increase inhibitory tone by enhancing PV+FSI signalling

output (Lauber, et al., 2018; Ghandi, et al., 2023). Reported alterations in PV expression in

PV+FSIs have been suggested to occur due to an altered a PV-Perineuronal net (PNN)

expression relationship in ASD, which may hinder the use of PNN staining as a secondary marker

to overcome perceived loss of neurons due to altered protein expression (Xia, et al., 2021;

Slaker, et al., 2016; Xia, et al., 2021). Within the striatum a great proportion of PV+FSIs have

colocalised PNNs, known to enhance interneuron excitability, across a lateromedial gradient

within the dorsal striatum (Lee, et al., 2012; Slaker, et al., 2016; Lupori, et al., 2023). Previous

reports have identified alterations in this colocalisation in a variety of murine models of ASD

291 (BTBR, CNTNAP2-/-, SHANK3B-/-, and VPA mice) which may in turn influence PV+FSI function

292 (Balmer, 2016; Slaker, et al., 2018).

293

294 (1.5)   Perineuronal nets (PNNs)

295

296   PNNs are complex, specialised extracellular matrix (ECM) structures that preferentially

297 enwrap the soma and proximal dendrites of a small number of neurons –predominantly PV+FSIs

298 (Langen, et al., 2009; Briones, et al., 2022). The expression of PNN components is noted to

299 begin prenatally, as PNNs progressively aggregate across development in a regionally

300 dependent manner and are not considered fully developed –as compact structures with all

301 components in place– until adulthood (Eskici, et al., 2018; Langen, et al., 2009). The

302 development of well-defined PNNs is suggested to accompany the establishment of mature

303 neuronal circuits and the closure for critical periods of plasticity (Eskici, et al., 2018; John, et al.,

304 2022; Langen, et al., 2009; Mueller-Buehl, et al., 2023). With such dynamic expression across

305 development, PNNs are suggested to facilitate synaptic development and stabilisation (with

306 PNNS often described as the 4th component of the tetrapartite synapse), and the fast-spiking

307 properties of PV+FSIs (via various mechanisms such as the provision of ionic gradients and

308 protection from oxidative stress; Miyata & Kitigawa, et al., 2017; John, et al., 2022; Langen, et

309 al., 2009; Eskici, et al., 2018; Mueller-Buehl, et al., 2022; Hanssen, et al., 2023). Due to the

310 facilitation of the electrophysiological properties characteristic to PV+FSIs by PNNs, they may be

311 in a prime position for alterations in molecular profile to induce alterations in E:I balance

312 (Ghandi, et al., 2023; Burket, et al., 2021; Xia, et al., 2021).

313 Reduced PNN+ cell density was identified within the globus pallidus, though not the dentate

314 gyrus, suggesting a regional specificity of PNN alterations in postmortem cases of idiopathic

315 ASD (Brandenburg & Blatt, 2022). In contrast, an increased density of DMS PNN+ cells was

316 observed in the BTBR model of idiopathic ASD, suggesting the striatum (outlined in 1.3) as

317 another rationale BG nucleus of interest to investigate PNN expression alterations in ASD

318 (Briones, et al., 2022). Whilst unknown how alterations in PNN expression may contribute to

319 ASD aetiology, and the relevance of developmental stage when such alterations may manifest,

320 altered PNN expression has been observed to precede alterations in PV expression (Slaker, et al.,

321 2018; Brandenburg & Blatt, 2022; Briones, et al., 2022). This may be gleaned from both prior

14

reports of PNN expression alterations in CNTNAP2-/- mice, and reports of altered PV+PNN+ cell density, suggested to be due to alterations in specific subsets of PV+PNN+ cells with an altered expression relationship (Ghandi, et al., 2023; Xia, et al., 2021).

Altered PV-PNN colocalisation has been reported in animal models of ASD with an increased percentage of PV+ cells expressing PNNs within the striatum of SHANK3B-/-, CNTNAP2-/-, and VPA mice at PND 70-184 (Briones, et al., 2022). However, no significant difference in the percentage of PV+ interneurons expressing colocalised PNNs was observed in these mouse strains at PND 25, suggesting that observable differences in PV-PNN colocalisation in ASD may develop at a later developmental stage (Lauber, et al., 2016; 2018; Filice, et al., 2016). Though the direction of PV-PNN alterations in ASD has not been explored through multiple developmental stages in the striatum, something this study aims to explore. Attempts to correct perceived overexpression of PNNs in CNTNAP2-/- and BTBR mice via enzymatic digestion of PNNs resulted in electrophysiological and morphological shifts towards a TD electrophysiological profile with normalisation of RRBI and social/communication behaviours was observed (Ghandi, et al., 2023; Briones, et al., 2022). Alterations to PNNs within different regions may contribute to different elements of ASD-like behaviours, however the sexually dimorphic nature of PNN expression, which may lead to differentially altered E/I balance alterations, has not been considered within the striatum (Briones, et al., 2022; John, et al., 2022). This is therefore a gap within the current literature which we aim to address in the current study.

Conflicting findings in the direction of PNN expression alterations in ASD from post-mortem and animal models, though potentially attributable to interspecies differences, could be due to the immunohistochemical targeting of different PNN components (Brandenburg & Blatt, 2022; Briones, et al., 2022; van Rooij, et al., 2018). PNNs are not homogenous structures but possess great molecular diversity (Mueller-Buehl, et al., 2023; Schmidt, et al., 2020; Mueller-Buehl, et al., 2022). Multiple GWASs and molecular pathway analysis have identified a significant enrichment of mutant genes within an "extracellular matrix organisation" pathway in ASD datasets, including genes such as HAPLN1, Reelin, and semaphorins; all contributing to different elements of PNN expression (Drago, et al., 2018; Hussman, et al., 2011; Brandeburg & Blatt, 2022). PNNs are comprised of 3 key groups of components: glycosaminoglycans, tenascins, and link proteins; with alterations in various components noted to impact the structural properties and development of the PNN (Mueller-Buehl, et al., 2023; Schmidt, et al., 2020; Mueller-Buehl, et al.,

353	2022). Investigation of different elements contributing to this neural matrisome, rather than
354	alterations in PNNs as a whole may therefore be a rationale target for investigation potential
355	cause of the changes in expression of PV+PNN+ FSIs in ASD.
356	

| 357 | (1.6) PNN components |

| 358 | Despite reports of attenuated PV-PNN colocalisation, alterations in PNN density are not |
359	widely reported in animal models of ASD. Therefore, alterations in specific PNN components may
360	be a more rationale focus for investigation than PNN density alone when exploring PNN
361	alterations in ASD. PNNs are dynamic structures expressing a complex and diverse profile of
362	constituent components that both individually and collectively participate in stabilising E:I
363	balance (Jakovljević, et al., 2021; Mueller-Buehl, et al., 2023). The supramolecular organisation
364	of PNNs can be simplified by considering just the three core constituent component groups: link
365	proteins, glycosaminoglycans, and tenascins, as displayed in Figure 1.1 (Schmidt, et al., 2020;
366	Mueller-Buehl, et al., 2022; Mueller-Buehl, et al., 2023).
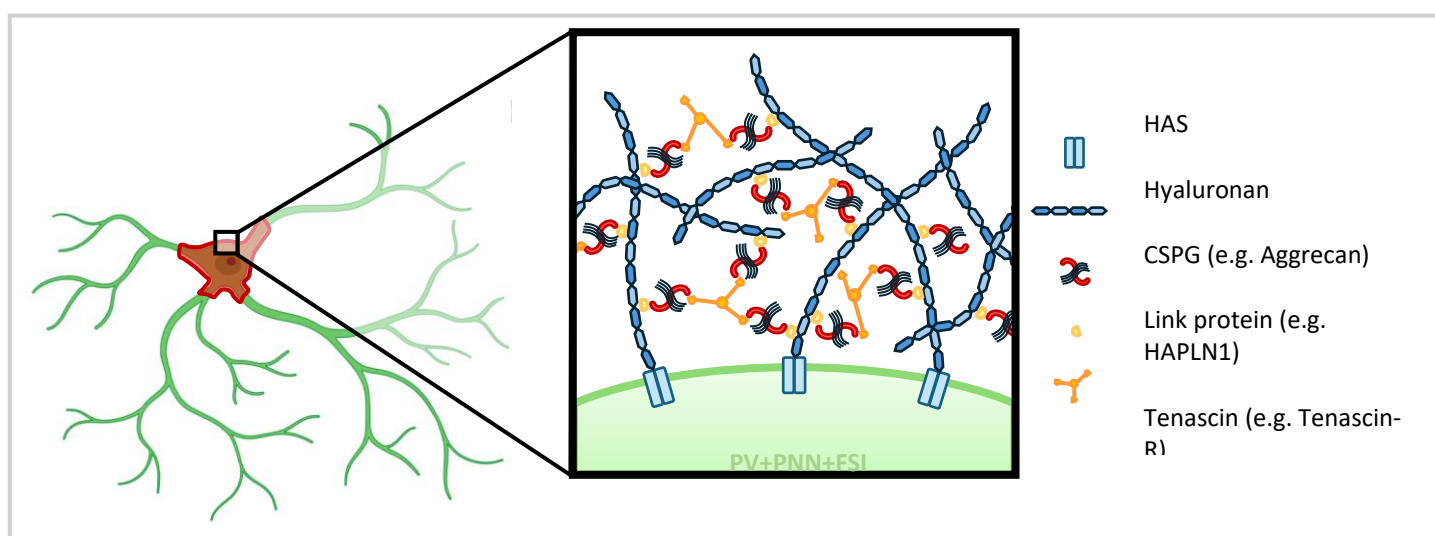
367 Fig. 1.1 Simplified Perineuronal Net Composition. A simplified diagram of a perineuronal net
368 encapsulating a PV+PNN+ FSI. The PNN is comprised of three core components (CSPGs, Link proteins,
369 and tenascins) in addition to hyaluronan chains synthesised by the PNN+ cell.

370	The hyaluronan and proteoglycan binding link protein (HAPLN) family (with HAPLN1 and
371	HAPLN4 expressed in the CNS) is considered critical to PNN formation (Balmer, et al., 2009;
372	Carceller, et al., 2023; Brandenburg & Blatt, 2022; Ghandi, et al., 2023). HAPLNs mediate the
373	binding of glycosaminoglycans to form condensed PNNs around neurons (Ghandi, et al., 2023;

374   John, et al., 2022). HAPLN1 is known to bind to all PNN glycosaminoglycan subtypes and is

375   reported to initiate PNN nucleation around prospective PNN+ neurons (Eskici, et al., 2018; John,

376   et al., 2022; Carceller, et al., 2023; Ghandi, et al., 2023). Due to this role in the formation of

377   typically arranged PNNs, alterations in HAPLN expression may result in altered PNN expression –

378   such as the diffuse formation and atypical presentation of PNNs reported in HAPLN1 deficient

379   mice (Mueller-Buehl, et al., 2023). Whilst alterations in PNN density are often not reported in

380   ASD, when staining for the HAPLN1 component to identify PNNs significant differences in PNN

381   expression are observed in ASD (Brandenburg & Blatt, 2022). Therefore, PNN expression

382   alterations in ASD may be a consequence of altered expression of specific PNN components. A

383   recent investigation of altered gene expression in foetal brains of VPA mice may support this,

384   identifying a 70% reduction in HAPLN1 gene expression (Dorsey, et al., 2023 [preprint]).

385   However, diffuse PNNs are not commonly reported in ASD animal models which may suggest

386   increased expression of other PNN components may act as a compensatory mechanism in

387   response to reductions HAPLN1 (Fawcett, et al., 2019; Carceller, et al., 2023). Due to the

388   inherent interconnectedness of link proteins to other PNN components, such as lecticans,

389   alterations in HAPLNs may not occur independent other alterations in other PNN components –

390   emphasised by the suggestion of distinct link protein-lectican pairs to describe the co-expression

391   and interaction of components such as HAPLN1 and aggrecan (Miyata & Kitigawa, et al., 2017;

392   John, et al., 2022).

393   A member of the lectican chondroitinsulfate (CSPG) family of glycosaminoglycans, aggrecan is

394   often described as the main functional constituent present within the majority of PNNs of the

395   CNS (Hanssen, et al., 2023; Giamanco & Matthews, 2012; Mueller-Buehl, et al., 2022; Miyata &

396   Kitigawa, et al., 2017). CSPGs facilitate the neuroprotective function of PNNs as their negative

397   charge enables the attraction and sequestration of cations to support rapid cation exchange with

398   PV+FSIs, in addition to restricting neuroplasticity (Mueller-Buehl, et al., 2023; Schmidt, et al.,

399   2020; Eskici, et al., 2018; Hanssen, et al., 2023). Like HAPLN1, CPSGs are expressed in an

400   activity dependent manner and synthesised within the neurons they will later enwrap (Oohashi,

401   et al., 2015; Giamanco & Matthews, 2012). Investigations of PNN density typically stain PNNs

402   with Vicia Villosa Agglutin (VVA) or Wisteria Floribunda Albumin (WFA), believed to bind to the

403   N-globular terminal domains of CSPGs (Ueno, et al., 2018). This may suggest previous reports of

altered PNN intensity and PV-PNN expression relationships may in fact reflect altered CSPG

expression and PV-CSPG expression relationships (Xia, et al., 2021; Ueno, et al., 2018). Further,

heterozygous and homozygous acan knockout mice present with reduced PV expression in

cortical PV+FSIs –suggesting a relationship between altered aggrecan and parvalbumin

expression (Rowlands, et al., 2018). Altered aggrecan expression was recently identified in the

FMR1-KO murine model of fragile X syndrome (the most common monogenetic cause of ASD),

with reduced expression noted at both PND 14 and to a lesser extent at PND 42 in cortical and

hippocampal regions (van't Spijker, et al., 2024). This may suggest a dynamic alteration of

aggrecan expression in PV+ cells in ASD. This has yet to be explored in the striatum, a region

with previously reported PV+FSI and PNN colocalisation alterations in ASD, this study aims to

address investigate this.

The third core component of PNNs are tenascins, a group of trimeric modular glycoproteins that

possess multiple lectican binding sites to facilitate the expansion of the net-like structure, and

strengthen the molecular meshwork of, PNNs (Mueller-Buehl, et al., 2023; Miyata & Kitigawa, et

al., 2017; Eskici, et al., 2018). Tenascin-R is known to stabilise PNN function by clustering

aggrecan to assemble PNNs, with a lack of this glycoprotein suggested to result in more

granular PNNs and have a knock-on effect on the electrophysiological profile of PNN+ neurons

(Wingert & Sorg, 2021; Ueno, et al., 2017; Mueller-Buehl, et al., 2023). Notably, tenascin

knockout mice present with attenuated mIPSCs and mEPSCs, with an increased amplitude, similar

to attenuations noted in mIPSCs from the DLS of BTBR mice (Wingert & Sorg, 2021; Briones, et

al., 2022). Little research has explored potential alterations in TNR in ASD despite the key role

of the tenascin protein family in PNN formation and support, this research aims to address this

through investigation of tenascin-r expression in BTBR mice at different developmental stages.

(1.7)   Research Aims and Hypotheses

Despite the previously identified functional differences between striatal subregions and

reports of subregional specificity in volumetric/morphological alterations in ASD, investigations

of PV and PNN expression in animal models of ASD often fail to consider how expression may be

differentially altered between striatal subregions (Filice, et al., 2016; Lauber, et al., 2016; 2018;

Fuccillo, 2016; Evans, et al., 2023). Further the inherent nature of ASD as a neurodevelopmental

434	condition, coupled with reports of a shift in behavioural phenotype through development,
435	suggest an underlying dynamic shift in molecular phenotype –particularly relevant to PV and
436	PNN expression due to their protracted development (Eskici, et al., 2018; Lauber, et al., 2018).
437	Sex differences in PV and PNN expression are frequently neglected in the context of ASD,
438	despite reported differences in the ASD behavioural phenotype between sexes and basal
439	differences in PV and PNN expression (van't Westeinde, et al., 2020; Amodeo, et al., 2019; Van
440	Zandt, et al., 2024; John, et al., 2022). Exploration of altered PV and PNN expression with
441	consideration of dorsostriatal subregions, sex, and developmental stage in ASD may allow for
442	greater understanding of ASD aetiology within the wider autistic population and provide insight
443	onto how sex differences in molecular phenotype may underpin sex differences in symptom
444	presentation/behavioural phenotype.
445	This thesis aims to explore this through investigation of PV and PNN expression within the DS in
446	an idiopathic murine model of ASD (BTBR mice) relative to typically developing control animals
447	(C57 mice) with consideration of sex, developmental stage and, striatal subregion via IHC and
448	qPCR techniques. An IHC approach was adopted to assess densities of PV+, PNN+ and,
449	colocalised PV+PNN+ cells, the percentage of PV+ cells with colocalised PNN staining, the
450	percentage of PNN+ cells with colocalised PV staining and, the relative intensity of fluorescence
451	of PV staining (as a proxy for the relative expression of PV protein in PV+FSIs). qPCR techniques
452	were undertaken to explore differences in gene expression of pvalb (encoding the PV protein),
453	hapln1, tnr and, acan (genes encoding for hapln1, tenascin-R and, aggrecan proteins
454	respectively; selected as representative proteins from the three main component classes
455	constituting PNNs) in ASD, relative to sex and developmental stage.
456	
457	Therefore, the main research objectives of this thesis are as follows:
458	▪ Investigate potential differences in PV+ cell density within the dorsal striatum relative to
459	animal strain (C57, BTBR), sex (male, female), developmental stage (3-4wk, 6-8wk), and
460	DS subregion (DMS, DLS).
461	▪ Investigate potential differences in PNN+ cell density within the dorsal striatum relative
462	to animal strain (C57, BTBR), sex (male, female), developmental stage (3-4wk, 6-8wk),
463	and DS subregion (DMS, DLS).

- Investigate potential differences in PV+PNN+ cell density within the dorsal striatum relative to animal strain (C57, BTBR), sex (male, female), developmental stage (3-4wk, 6-8wk), and DS subregion (DMS, DLS).
- Investigate potential differences in the percentage of PV+ cells with colocalised PNN staining within the dorsal striatum relative to animal strain (C57, BTBR), sex (male, female), developmental stage (3-4wk, 6-8wk), and DS subregion (DMS, DLS).
- Investigate potential differences in the percentage of PNN+ cells with colocalised PV staining within the dorsal striatum relative to animal strain (C57, BTBR), sex (male, female), developmental stage (3-4wk, 6-8wk), and DS subregion (DMS, DLS).
- Investigate potential differences in the relative intensity of fluorescence from PV staining in PV+FSIs within the dorsal striatum relative to animal strain (C57, BTBR), sex (male, female), developmental stage (3-4wk, 6-8wk), and DS subregion (DMS, DLS).
- Investigate potential differences in the relative expression of pvalb within the dorsal striatum relative to animal strain (C57, BTBR), sex (male, female), developmental stage (3-4wk, 6-8wk).
- Investigate potential differences in the relative expression of hapln1 within the dorsal striatum relative to animal strain (C57, BTBR), sex (male, female), developmental stage (3-4wk, 6-8wk).
- Investigate potential differences in the relative expression of tnr within the dorsal striatum relative to animal strain (C57, BTBR), sex (male, female), developmental stage (3-4wk, 6-8wk).
- Investigate potential differences in the relative expression of acan within the dorsal striatum relative to animal strain (C57, BTBR), sex (male, female), developmental stage (3-4wk, 6-8wk).

(2.0) Methods

(2.1) Experimental Design and Statistical Analysis

This study investigated the expression of parvalbumin (PV) and perineuronal nets (PNNs) in the dorsal striatum through both immunohistochemical (IHC) and qPCR analysis. In total 40 mouse brains were utilised, from 20 C57L/J and 20 BTBR T$^+$ltpr3^{+f}/J mice, each group contained 10 postnatal week (PNW) 3-4 and 10 PNW 6-8 mice, with 5 brains from mice of each sex (male, female) within each developmental stage group. The sample size of this study was based upon a conducted power analysis in G*Power (ver. 3.1.9.7; See Appendix A). Mice at these two developmental stages (PNW 3-4 and PNW 6-8) were selected for this study to investigate shifts in the molecular phenotype of ASD through development based on previous reports of shifts in the behavioural phenotype of ASD throughout these two developmental stages and estimated equivalencies to human development (Molenhuis, et al., 2014; Dutta, et al., 2016; Semple, et al., 2013).

For IHC analysis, this study utilised multiple mixed designs to explore PV and PNN expression via: PV+ cell density, PNN+ cell density, PV+PNN+ cell density, the percentage of PV+ cells with colocalised PNN staining, percentage of PNN+ cells with colocalised PV staining, and the relative fluorescent intensity of PV staining (as a proxy for relative expression of PV protein in interneurons). Between group variables of all mixed designs were animal strain (C57L/J and BTBR T$^+$ltpr3^{+f}/J), sex (male and female), and developmental stage (PNW 3-4 and PNW 6-8). The within group variable of interest in this study was dorsal striatal subregion (DMS and DLS). 3-5 brain slices were utilised in IHC data collection for each animal. For qPCR analysis, this study utilised between subjects designs to investigate the relative gene expression of pvalb, hapln1, tnr, and aggrecan. The between group IVs for these designs were animal strain (C57L/J and BTBR T$^+$ltpr3^{+f}/J), sex (male and female) and developmental stage (PNW 3-4 and PNW 6-8).

All data was analysed in R statistical software (ver. 4.3.3; R Core Team 2024). The Shapiro-Wilk test was utilised to assess normality. For IHC data analysis, if normality within distributed residuals could not be assumed, QQ plots were screened and appropriate transformations were performed on the data to achieve normality where possible (for detail on specific transformations, see relevant subsections of (3.0) Results). Transforming data to achieve normality was preferred due to interests in interaction effects between IVs. Where normality was assumed, data was analysed via Analysis of Variance (ANOVA) with

524 post-hoc analysis performed via Tukey's HSD test. For qPCR data analysis, if normality of residuals was

525 assumed, then Student's t-tests were performed on ΔCq values. If normality of residuals could not be

526 assumed, Wilcoxon rank-sum tests were performed. An alpha level of 0.05 was set, with $p < 0.05$

527 considered statistically significant.

528 (2.2) Animals

529 C57L/J (C57; Stock No. 000688) and BTBR T$^+$Itpr3^{+f}/J (BTBR; Stock No. 002282;) mouse brain

530 tissue obtained from The Jackson Laboratory (USA), was utilised in this study. All mice were housed in a

531 controlled animal facility (12:12hr light/dark cycle) at The Jackson Laboratory (USA) and fed ad libitum.

532 (2.3) Tissue preparation

533 Brain tissue was requested from The Jackson Laboratory (USA) as follows. Mice were culled via

534 cervical dislocation with confirmation of death via cessation of circulation. This procedure, approved by

535 the Home Office Code of Practice under Schedule 1 techniques, is in line with the Animals (Scientific

536 Procedures) Act 1986. Post-culling, brains were removed and post-fixed in 4% paraformaldehyde (PFA)

537 with 0.03% Sodium Azide. Isolated tissue was then dehydrated in 30% sucrose -0.01M Phosphate-

538 buffered Saline (PBS) at 3-5°C for 24 hours before returning to 4% PFA for storage at 3-5°C until further

539 processing. All procedures for the use of this secondary tissue were approved by the animal welfare and

540 ethics review board (AWERB) at the University of Central Lancashire (UCLan; approval no. 23_02).

541 (2.4) Vibratome

542 Left hemispheres, previously separated with a razor blade down the longitudinal fissure, were

543 then sectioned with a vibrating microtome (Campden Instruments model 5000mz). Initially, the olfactory

544 bulb was removed in addition to the cerebellum, providing a flat surface to mount the hemisphere to the

545 vibratome chuck. Before sectioning, a vibratome blade was visually assessed to be level and central, and

546 a metal bath surrounded by ice was filled with 200ml of 0.01M PBS. Hemispheres were then individually

547 mounted to the vibratome chuck via superglue, pipetting a few drops of 0.01M PBS on top. The

548 vibratome chuck was then placed inside the metal bath, allowing for individual sectioning to commence.

549 Dorsoventrally sliced 25μm coronal sections were cut at 100Hz frequency, 0.5mm amplitude, with a

550 0.23mm/s advance. Slices were manipulated with a fine paintbrush to prevent curling and collected into

551 6-well plates filled with 9ml of 0.01M PBS in each well. Once all sections for a hemisphere were

552   collected, slices were transferred into a second 6-well plate with 9ml cryoprotectant (30% ethylene

553   glycol, 30% glycerol, 30% dH$_2$O, 10% 0.01M PBS) in each well. All 6-well plates were fitted with a lid

554   and stored at -20°C until further processing.

555   (2.5)   Slice selection

556   To select sections containing the region of interest (ROI), namely the dorsal striatum (DS), the

557   Paxinos & Franklin (2007) Mouse Brain Atlas was used to identify and select coronal slices within

558   bregma -0.10 to 1.10mm (See Fig. 2.1A).

559   The DS was identified to be laterally adjacent to the lateral ventricle (LV), dorsal to the anterior

560   commissure (AC), and ventral to the corpus callosum (CC; A, B, C, and D in Fig. 2.1A respectively). Slices

561   were identified based on the appearance of the LV, AC, and CC. Spanning dorsoventrally, the LV appears

562   as an inverted triangle, progressively narrowing ventrally in each slice (see B in Fig. 2.1A). The LV

563   narrows further throughout this bregma range, then merging with the dorsal third ventricle indicating the

564   posterior end of this bregma range. Ventrolateral to the LV, the presence of the AC (first observed with a

565   rounded morphology) also indicates brain slices within this bregma range, wherein it progressively

566   elongates toward the posterior end of this range (see C, in Fig. 2.1A).

Anterior

A

Bregma: 1.10mm

B

Posterior
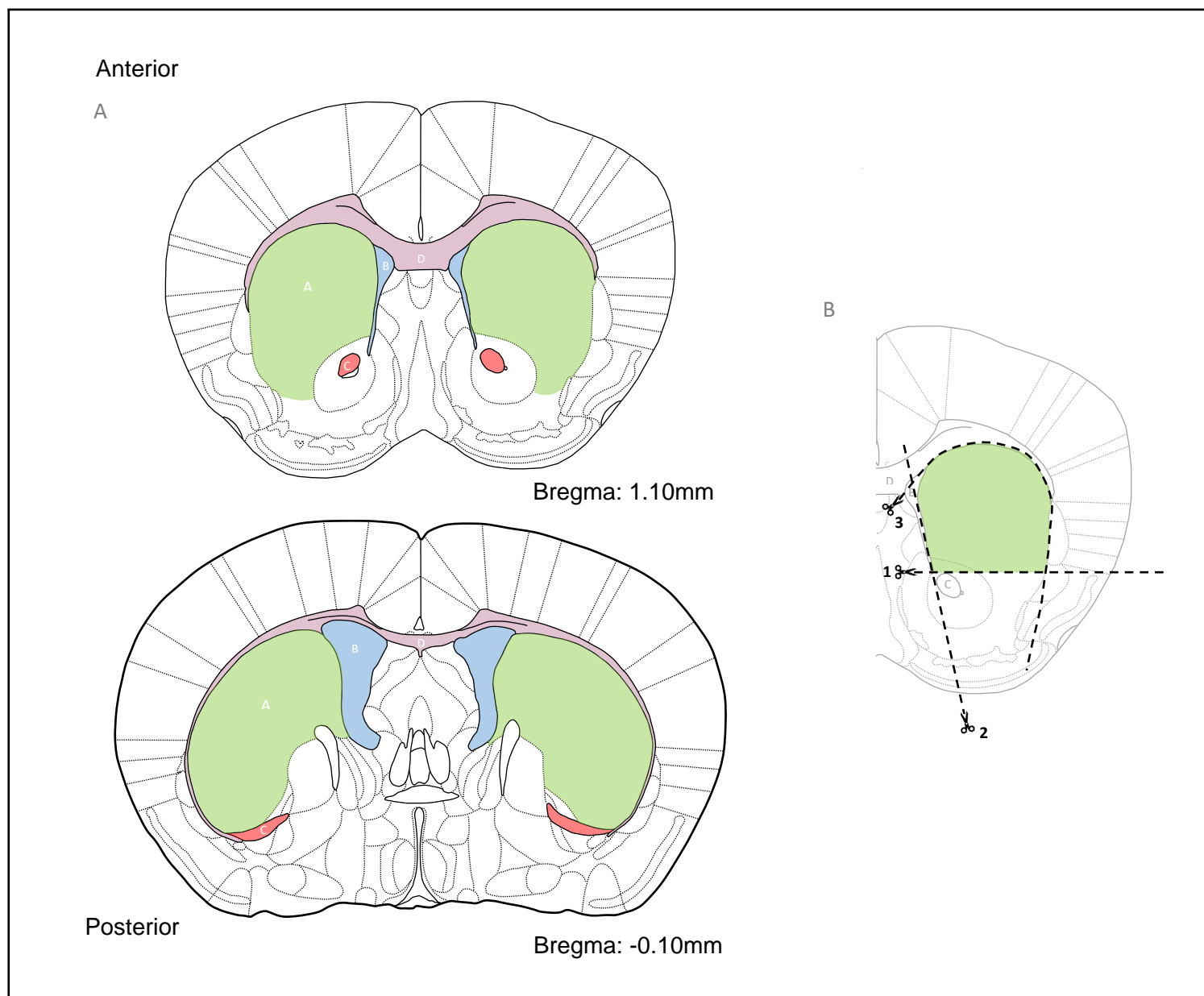
Bregma: -0.10mm

568   Fig. 2.1. Adapted from Mouse Brain atlas (Paxinos & Franklin, 2007).

569   A) Coronal sections of mouse brain at bregma 1.10mm and –0.10mm were selected for use in IHC and

570   qPCR analysis, the anterior and posterior ends of the defined bregma range are displayed here. The

571   striatum (A) is indicated in green. Regions used to identify slices within this Bregma range are indicated

572   as (B) LV in blue, (C) AC in red, and (D) CC in purple. B) Coronal section of the left hemisphere at bregma

573   1.10mm, indicative of the incisions made to extract striatal tissue from all slices in this bregma range for

574   use in IHC and qPCR.

575

576   (2.6)   Slice dissection

577   Striatal regions were dissected as follows from 6 slices within this predefined bregma range

578 (outlined above) from each animal for subsequent use in qPCR. Slices were floated in 0.01M PBS under a

579 stereoscopic microscope. Regions ventral to the striatum were first removed with a horizontal cut ventral

580 to the LV but dorsal to the AC (see 1 in Fig. 2.1B). Secondly, a probe was used to gently separate septal

581 regions from the striatum before cortical regions and the CC were additionally removed, with only striatal

582 tissue remaining (see 2 and 3 in Fig.2.1B). Separated striatal tissue was then stored in cryoprotectant at

583 -20°C until further use.

584   (2.7)   Immunohistochemistry (IHC)

585   Free floating sections in glass vials were initially washed for 10 minutes in 0.01M PBS, followed

586 by a 5-minute wash in 0.01M PBS plus 0.2% Triton-X (TX). After a further 10-minute wash in 0.01M PBS,

587 selected slices were incubated in Image IT FX Signal Enhancer (Invitrogen, Cat No. 136993) on a Stuart

588 SSL4 rocker at 30 oscillations/min for 30 minutes at room temperature (RT). Sections were then washed

589 for 10 minutes in 0.01M PBS before a 30-minute wash in 0.01M PBS plus 0.3% TX with 2.5% bovine

590 serum albumin (BSA), and a subsequent 30-minute wash in 0.01M PBS.

591 The free floating sections were then incubated in a cocktail of guineapig anti-PV antibody (1:2000;

592 Synaptic Systems, Cat No. 195004, RRID:AB_2156476), biotinylated Wisteria Floribunda Albumin (WFA)

593 for juvenile tissue (1:200; Vector Labs, Cat No. B1355, RRID:AB_2336874) or biotinylated Vicia Villosa

594 Agglutin (VVA) for adult tissue (1:200, Vector Labs, Cat No. B1235, RRID:AB_2336855), in 0.01M PBS

595 plus 0.3% TX with 2.5% BSA and 5% normal goat serum (NGS). Sections were then incubated overnight,

596 protected from light and incubated for 30 minutes at RT with 30 oscillations/minute agitation. No

597 significant difference in PNN+ cell densities was identified when PNNs were stained with WFA or VVA

598 (data not presented).

599 All sections were twice washed in 0.01M PBS for 10 minutes. Sections were then incubated for 2 hours

600 with Alexaflour 488 goat anti-guineapig (1:500; Abcam, Cat No. Ab150185, RRID: AB_2736872) and

601 Texas Red streptavidin (1:200; Vector Labs, Cat No. SA-5006) in 0.01M PBS plus 0.3% TX and 2.5%

602 NGS at RT and protected from light. Separate slices were used at negative controls, processed in the

603 same manner as other slices but with primary antibodies omitted. After which sections were washed in

604 0.01M PBS for 5 minutes twice, before mounting to glass slides. Slices were left to dry for 15 minutes at

605   RT and protected from light before cover slipping with Vectashield mounting medium containing a

606   fluorescent DAPI label (Alexa Flour 405; Vector Labs, Cat No. H2000). Slices were stored at 4°C until

607   visualisation.

608   (2.8)   Image acquisition and region of interest (ROI) selection

609   Brain slices were visualised with a ZEISS Axio Observer widefield microscope (Zeiss, Germany),

610   equipped with a motorised x-y stage, and Apotome 3. An ORCA-Fusion Digital CMOS camera (Hamatsu

611   Photonics, Japan; C14440-20UP) and Colibri 7 FR-R (G/Y) BV-UV Light Source (Zeiss, 423052-9770-

612   000) were used to visualise all adult and juvenile female mouse brain slices. An AxioCamMRm camera

613   (Zeiss, Germany, cat. no. 426509-9901-000) and Colibri.2 LED light source (Zeiss, Germany, 423052-

614   9501-000) were used to visualise juvenile male mouse brain slices. A computer managed by UCLan,

615   running Zeiss Zen Blue software (3.9.0) was connected to the microscope.

616   Left hemisphere slices were visualised with a 20x dry lens. The DS was considered dorsal to a borderline

617   determined to be adjacent to the ventral end of the LV and dorsal to the most medial extension of the

618   AC, with consideration to the Paxinos and Franklin mouse brain atlas (2007; as described by Voorn, et

619   al., 2004; as shown by A in Fig. 2.2). Images of the DMS and DLS were taken as z-stacks within the

620   centre of the tissue comprising two stitched tiles, containing twenty focal planes (1μm/plane) with three

621   apotome phases per plane, and deconvoluted using the apotome deconvolution software (Zen pro,

622   3.9.0; as shown by B in Fig. 2.2). Exposure times were kept the same for all imaging sessions.

623   ROI placement within the DMS was defined with the upper right vertex placed laterally adjacent to the LV

624   and vertically adjacent to the CC. Further, ROI placement within the DLS was performed with the upper

625   left vertex placed ventromedially adjacent to the external capsule of the CC. ROI dimensions were

626   determined within the ImageJ Software as 447.6 x 637.3μm rectangular area (as shown in Fig. 2.2 A).
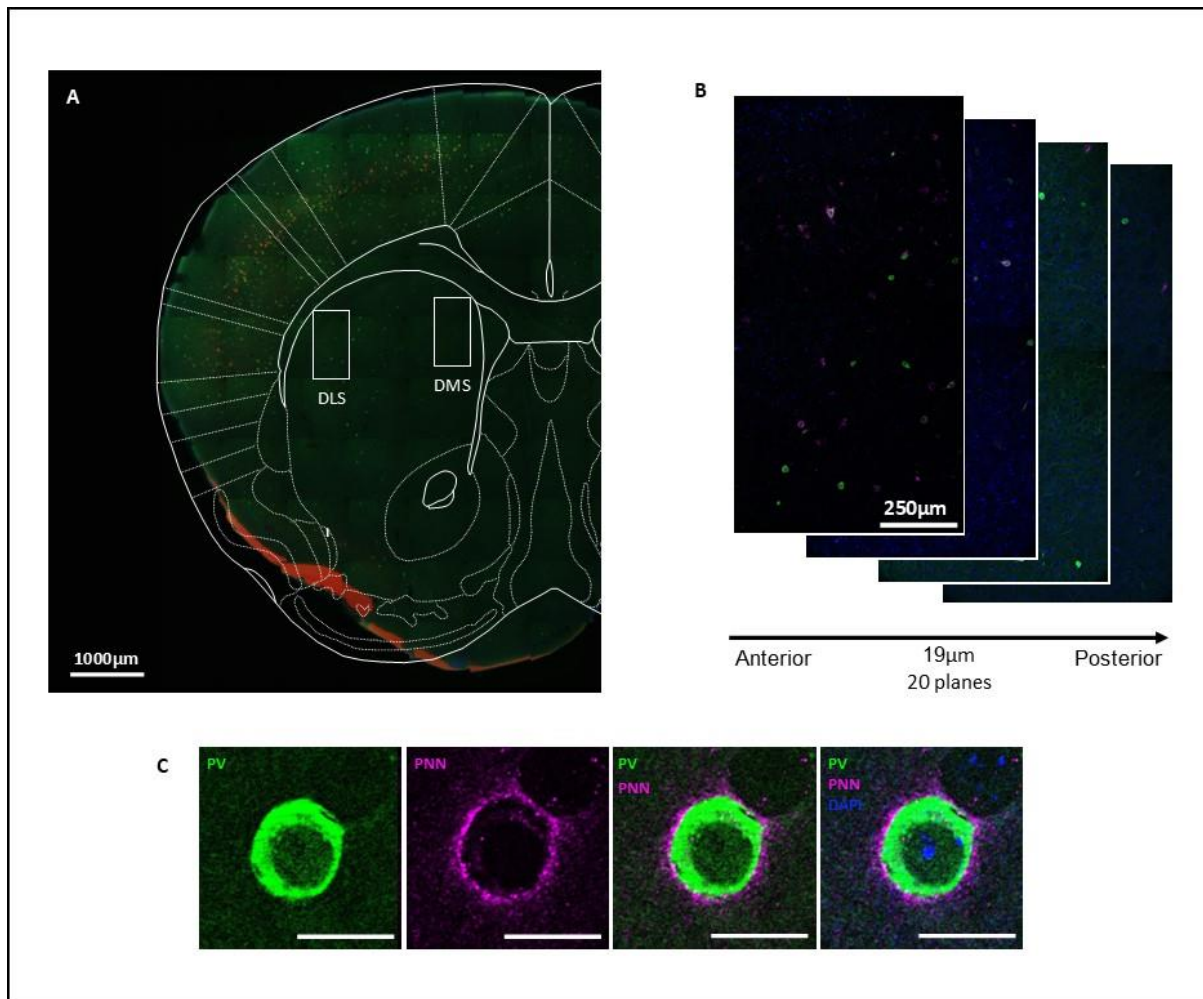
627

Fig. 2.2. Identifying ROI, collecting z-stacks, and identifying PV and PNN expressing cells.

A) Coronal sections of mouse brain at bregma 1.10mm, fluorescently stained for parvalbumin (green), perineuronal nets (red), and DAPI (blue) overlain with a diagram of a coronal section adapted from the Paxinos & Franklin mouse brain atlas (2007). ROIs within this study are identified (DMS and DLS). B) Z-stacks were obtained by taking 20 sequential images along the z-axis within each ROI, with each frame 1μm from the last. C) Cells were initially counted with only the filters for PV and PNN staining separately in addition to DAPI staining, before images were combined to obtain PV-PNN colocalisation data.

(2.9) Image processing and counting criteria

All images were acquired, processed and analysed manually by an experimenter once blinded to experimental conditions. Initially, collected z-stacks were summed using the sum slice feature of z-project in ImageJ (ver. 2.9.0). Background brightness was then subtracted from images using the rolling-ball radius function (as described in Slaker, et al., 2016). Identification of parvalbumin expressing (PV+) and

642 perineuronal net expressing (PNN+, defined by either WFA or VVA staining) cells was conducted in

643 ImageJ with each fluorophore imaged independently (as shown by C in Fig. 2). In each slice, number of

644 PV+ cells, PNN+ cells, PV+PNN+ cells, in addition to the relative intensity of PV fluorescent staining, was

645 quantified within each ROI imaged. Counting criteria for PV+ and PNN+ cells were as follows: cells must

646 be in sharp focus, wholly within the ROI and not overlapping with another cell, and the presence of a

647 clearly stained soma surrounding a visible DAPI stained nucleus. Further, the PNN must be noted to

648 surround more than 75% of the soma to be counted as a PNN+ cell. Each PV+ and PNN+ cell was

649 manually delineated as a ROI.

650 Raw counts of PV+, PNN+ and colocalised PV+PNN+ cells were then converted into cell densities per

651 region. These raw counts were divided by the ROI area (mm^3) to obtain cell densities (cells/mm^3). The

652 percentage of PV+ cells with PNN+ staining was obtained by division of PV+PNN+ cell counts by PV+

653 cell counts per region, followed by multiplication by 100. Percentage of PNN+ cells with PV+ staining

654 was obtained in a similar manner, with PV+PNN+ cell counts divided by PNN+ counts before multiplying

655 by 100. The relative intensity of fluorescence, a proxy of relative PV expression (525nm emission)

656 expression, was determined by firstly recording mean grey values for each cell. Background intensity

657 measurements were recorded via mean grey value measurements from two 100x100μm squares in

658 randomly determined locations within the ROI that did not contain stained cells. These background

659 intensity values were then averaged to create an average background intensity per section, then

660 subtracted from raw PV and PNN cell mean grey values from their respective fluorophores. PV intensities

661 from here on reflect this background subtracted values, reported in arbitrary units (a.u.). Cell densities,

662 relative intensities, and proportional colocalisation values were then averaged between all sections from

663 the same animal.

664   (2.10) Nucleic Acid Extraction and Purification

665   RNA was isolated and further purified from three dissected striatal tissue slices with the

666 Thermofisher RecoverAll Total Nucleic Acid Isolation Kit, as part of the RecoverAll Multisample RNA/DNA

667 Isolation Workflow (Thermofisher, Cat No. A26069) with minor deviation from manufacturer protocol.

668 Namely, supplied collection tubes and filter cartridges were substituted with PureLink viral collection

669 tubes and RNA minicolumns respectively, to increase RNA yields (Thermofisher, Cat No. 12282100,

670 A29837). An Eppendorf Centrifuge 5430 and ThermomixerC were utilised for all extraction steps

671 (Eppendorf, Germany). RNA yield and purity for each sample was assessed using a NanoDrop 2000

672   spectrophotometer (Thermofisher, UK; for complete spectrophotometry data see Appendix B). Extracted

673   RNA was immediately reverse transcribed as described below.

674   (2.11) Reverse Transcription

675   Total extracted RNA was used as a template for reverse transcription (RT) via random hexamers,

676   with 1μL RNA mix in a 20μl reaction volume. GDNase digestion and subsequent RT reactions and no-RT

677   controls were performed with SuperScript IV VILO Master Mix (Thermofisher, Cat no. 11766050) as per

678   manufacturer's protocol. A ThermomixerC (Eppendorf, Germany) was utilised for all incubation steps.

679   Synthesised cDNA and no-RT controls were stored at -70°C until further analysis.

680   (2.12) qPCR

681   qPCR was employed to quantify expression of multiple genes of interest (GOIs): pvalb, hapln1,

682   tnr, and acan, relative to expression of reference gene Rn18s, a commonly utilised reference gene

683   (Chapman & Waldenström, 2015; Trent, et al., 2014). Further information on these targets can be found

684   in Table 2.1.

685   **Table 2.1:** *qPCR target information for GOIs and reference gene.*

Gene Symbol	Gene Name	Sequence Accession No.	Chromosome Location
Rn18s	18S ribosomal RNA	NR_003278	NA
pvalb	parvalbumin	NM_013645	Chr.15: 78191117 - 78206351
hapln1	hyaluronan and proteoglycan link protein 1	NM_013500	Chr.13: 89540529 - 89611832
tnr	tenascin R	NM_022312	Chr.1: 159523741 - 159931729
acan	aggrecan	NM_007424	Chr.7: 79053202 - 79115099

686   Validated TaqMan Gene Expression Assays (Thermofisher, Cat. No. 4331182), containing specific

687   hydrolysis MGB probes with forward and reverse primers were utilised in the qPCRs (Table 2.2). FAM

688   fluorescent probes spanning exon junctions were used for all assays, whilst a VIC fluorescent probe was

689   included in the reference gene assay. ROX passive reference dye was included in all premade assays.

690   Further primer information can be found in Table 2.2.

691

692

Table 2.2: qPCR primer/oligonucleotide information

Target Gene Symbol	Assay ID	Probe Context Sequence	Amplicon Context Sequence	Amplicon Length
Rn18s	Mm03928990_g1	TACTTGGATAACTGTGGTAATTCTA	AATGGCTCATTAAATCAGTTATGGTTCCTTTGGTCGCTCGCTCCTCTCCTACTTGGATAACTGTGGTAAT TCTAGAGCTAATACATGCCGACGGGCGCTGACCCCCCTTCCCGGGGGGGGGATG	61
pvalb	Mm00443100_m1	GAGCCTTTGCTGCTGCAGACTCCTT	TCATCCAAGTTGCAGGATGTCGATGACAGACGTGCTCAGCGCTGAGGACATCAAGAAGGCGATAGGAGCC TTTGCTGCTGCAGACTCCTTCGACCACAAAAGTTCTTCCAGATGGTGGGCCTGAAGAAAAAGAACCCGG ATGAGGTGAAGAAGG	77
hapln1	Mm00488952_m1	CAACTTCAACGGCCGATTTTACTAC	CACCAAACCACGAGAGCCCTGCGGGGGCCAAAACACGGTGCCTGGAGTCAGGAACTACGGGTTTTGGGAC AAGGATAAAAGCAGATATGACGTTTTCTGTTTTACATCCAACTTCAACGGCCGATTTTACTACCTGATCC ACCCCACCAAACTCACCTACGATGAGGCGGTGCAAGCTTGTCTCAATGACGGTGCTCAGATCGCGAAAGT GGGCCAGATATTTGCTGCCTGGAAGCT	118
tnr	Mm00659075_m1	AGTCCAGGCACAGTCAGGGGATCAA	ACAGAGACAATGATGTTGCAGTCACCAACTGTGCCATGTCCTACAAGGGTGCTTGGTGGTATAAGAACTG CCACCGGACCAACCTCAACGGGAAGTACGGGGAGTCCAGGCACAGTCAGGGGATCAACTGGTACCATTGG AAAGGCCATGAATTCTCCATCCCCTTTGTAGAAATGAAGATGAGGCCCTACATCCATCGTCTCACAGCCG GGAGGAAACGGCGAGCCTT	114
acan	Mm00545794_m1	CTCAGAAGAAGTTCCAGACCATGAC	GACCACTTTACTCTTGGTCTTTGTGACTCTGAGGGTCATCGCTGCAGTGATCTCAGAAGAAGTTCCAGAC CATGACAACTCACTGAGCGTGAGCATCCCTCAACCATCCCCATTGAAGGTCCTCCTA	63

qPCR reactions were performed in duplex, with prior assessment of primer efficiency and duplex viability

(duplexed primer efficiency curves displayed in Appendix C) A 10μL qPCR reaction mix containing: 5μL

TaqMan Fast Advanced Master Mix (2x) (Thermofisher, Cat. No. 4444557), 3μL nuclease-free water

(Thermofisher, Cat. No. AM9915G), 1uL of sample cDNA, 0.5μL of one GOI TaqMan assay, and 0.5μL of

Rn18S TaqMan assay was placed in each well of a 0.1mL MicroAmp Fast Optical 96-well reaction plate

(Thermofisher, Cat. No. 4346907) before sealing with MicroAmp Optical Adhesive Film (Thermofisher,

Cat. No. 4313663). All reactions were run in triplicate with a no-RT control for each duplex assay per

biological replicate (wherein 1μL of cDNA is replaced with 1μL of the NoRT control), and one no template

control (NTC) per plate (with 1μL cDNA substituted for 1μL nuclease-free water). Once sealed, plated

were spun in a temperature-controlled centrifuge (Centrifuge 5430 R, Eppendorf, Cat. No. 5428000255)

for 30s at 1000 x g before thermocycling.

705　Fast qPCR thermocycling was then performed in a QuantStudio5 Real Time PCR system (Thermofisher,

706　UK) connected to a laptop running Design and Analysis 2 (DA2) software (v.2.7.0, Thermofisher, UK)

707　managed by UCLan. Thermocycling conditions were as follows: i) 50°C for 2 minutes, ii) 95°C for 20

708　seconds, iii) 95°C for 1 second, iv) 60°C for 20 seconds, v) iii-iv repeated 39 times.

709　　　　　　(2.13)　qPCR Data analysis

710　　　　　qPCR data was analysed with the $2^{-\Delta\Delta Cq}$ method (Schmittgen & Livak, 2008). Quantification

711　cycles (Cq) were collected from each well for both assays within the DA2 software by setting thresholds

712　at 0.06 ΔRn for the pvalb and Rn18s duplex, and 0.07 ΔRn for all other duplexes. Acquired Cq values

713　from technical replicates within 1 Cq of each other were included in further analysis, with Cq values

714　outside of this range excluded for analysis. Absence of amplification curves from NTC and NoRT controls

715　was recorded. Cq data was averaged across technical replicates, with gene expression data then

716　normalised to reference gene expression by subtraction of Rn18s average Cq values from average GOI

717　Cq values from the same well/duplex. These ΔCq values were used for later statistical analysis. Fold

718　changes in the expression of GOIs in BTBR relative to C57 mice were calculated using the $2^{-\Delta\Delta Cq}$ method,

719　with Cq values of GOIs normalised to Rn18s (ΔCq) then to age- and sex-matched C57 mice (ΔΔCq) as

720　previously described (Schmittgen & Livak, 2008).

721

722

723

724

725

726

727

728

729

730

731

732

733

734

735

736 (3.0) Results

737   (3.1) IHC Results

738   Through immunohistochemical analysis, this study investigated: densities of parvalbumin-

739 expressing (PV+) (3.1.1), perineuronal net-expressing (PNN+) (3.1.2), and colocalised PV+PNN+ (3.1.3)

740 cells, in addition to percentages of PV+ cells with colocalised PNN expression (3.1.4) (vice versa (3.1.5)),

741 and relative intensities of fluorescence in PV (3.1.6) fluorescent staining, within the DS (both DMS and

742 DLS) at two developmental stages (PNW 3-4 and PNW 6-8) in both BTBR and C57 mice of both sexes

743 (Male and Female).

744   (3.1.1) PV+ cell density (cells per mm^3)

745   A 4-way mixed analysis of variance (ANOVA; Strain*Sex*Age*ROI) was performed on PV+ cell

746 density values (cells per mm^3), with normality assumed within this data as supported by nonsignificant

747 results from a Shapiro-Wilk Test. Descriptive statistics of PV+ cell density can be found in **Table 3.1.**

748 *Table 3.1: Mean and standard deviation of the density of Parvalbumin-expressing cells per mm^3 within*

749 *the Dorsal Striatum between C57 and BTBR mice. Note SD = standard deviation.*

PV+ Cell Density (cells/mm³)					
			ROI		
Strain	Age	Sex	DMS (SD)	DLS (SD)	Row Mean (SD)
C57L/J	3-4wk	M	2177 (336)	2495 (364)	2336 (350)
		F	1559 (335)	2721 (315)	2140 (325)
	6-8wk	M	1629 (334)	1720 (165)	1675 (250)
		F	996 (450)	2189 (321)	1593 (386)
BTBR T+tf/j	3-4wk	M	1469 (361)	2765 (350)	2117 (356)
		F	470 (239)	2710 (175)	1590 (207)
	6-8wk	M	1395 (227)	2310 (494)	1853 (361)
		F	1399 (553)	3213 (1053)	2306 (803)
	Column Mean (SD)		1387 (354)	2515 (405)	

750 **Table 3.1** shows the mean cell density and standard deviation (SD) of PV+ cells per mm^3 within the

751 dorsomedial- and dorsolateral striatum (DMS and DLS) of C57 and BTBR mice with reference to sex and

752 age. **Fig. 3.1** displays main effects and two-way interaction effects of the density of parvalbumin

753 expressing cells presented in **Table 3.1,** with reference to strain, sex, age, and ROI.
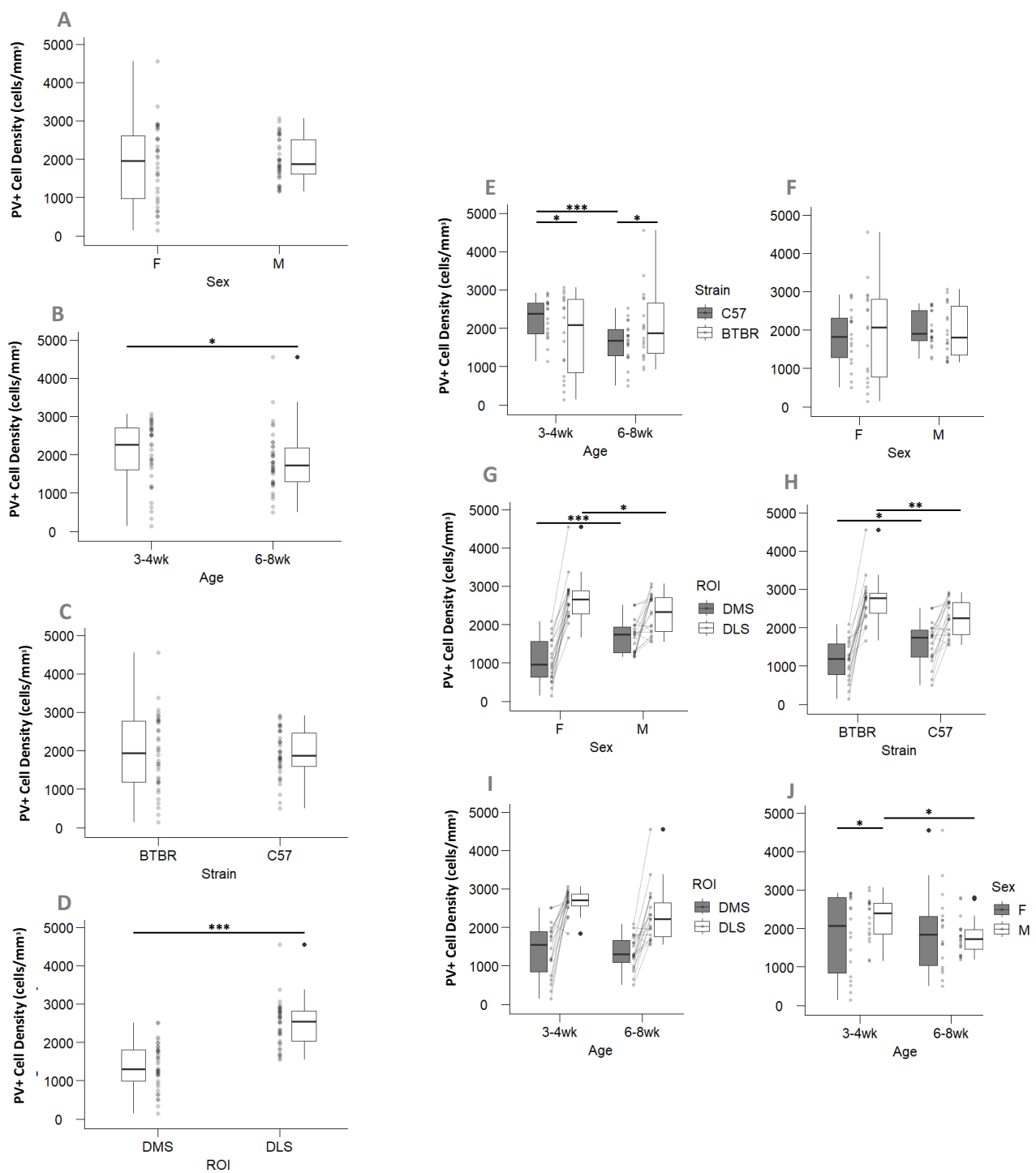
755   Fig. 3.1. Mean Density of PV+ Cells per mm3 in the Dorsal Striatum.

756   Box plots displaying mean density of PV+ cells per mm3 in the DS (±SD) with regards to (A) Sex (male &

757   female), (B) Age (3-4wk & 6-8wk), (C) Strain (C57 & BTBR), and (D) Subregion (DMS & DLS).

758   Box plots displaying mean density of PV+ cells per mm3 in the DS (±SD) with regards to interactions of

759   (E) strain: age, (F) sex:age, (G) sex:ROI, (H) strain: ROI, (I) age: ROI, (J) age:sex. Asterixis represent * p ≤

760   0.05, ** p ≤ 0.01, and *** p ≤ 0.001. Small dots represent individual data points.

761   (K) Indicative images of PV+ cells within the DS within each group investigated, PV staining is

762   represented as green, with blue indicating DAPI staining. Scale bar = 250μm.
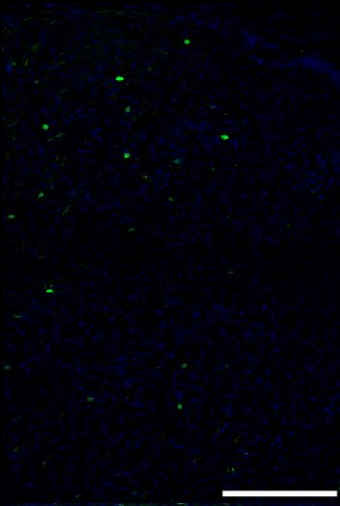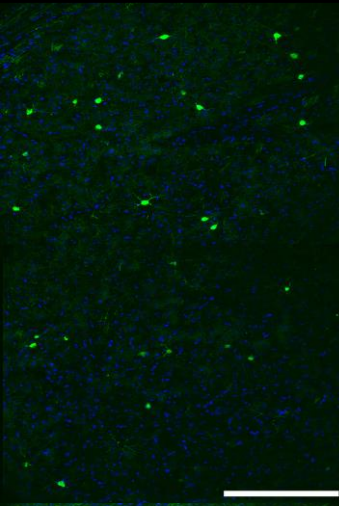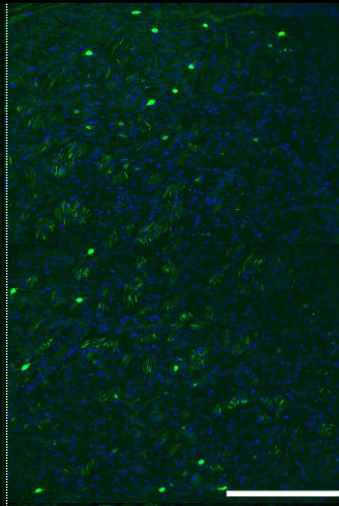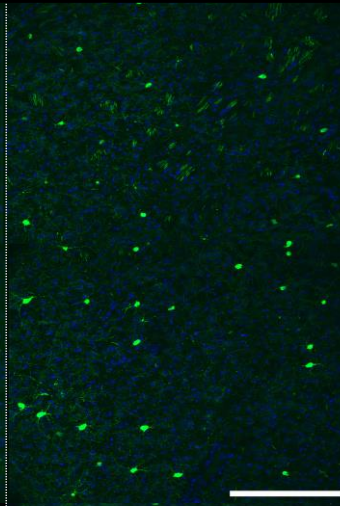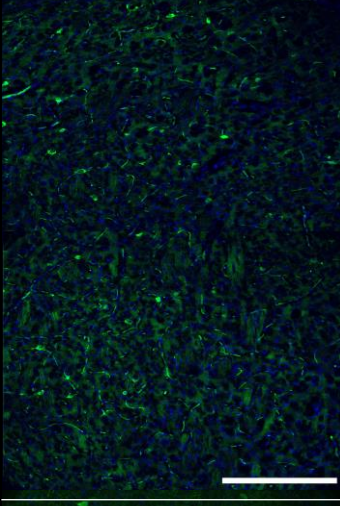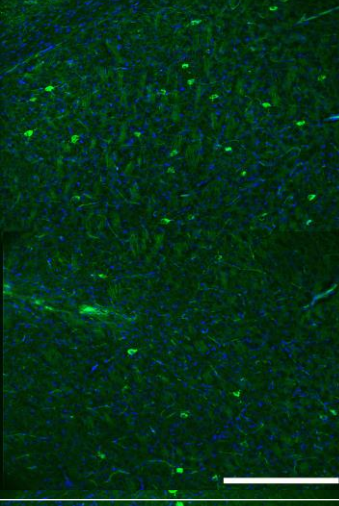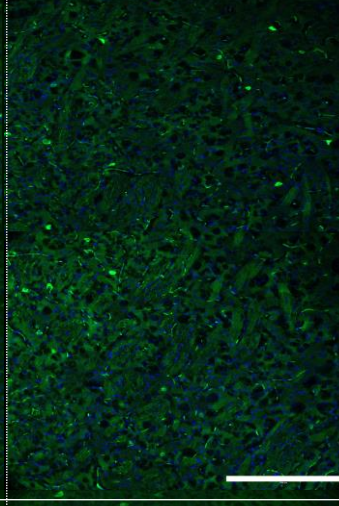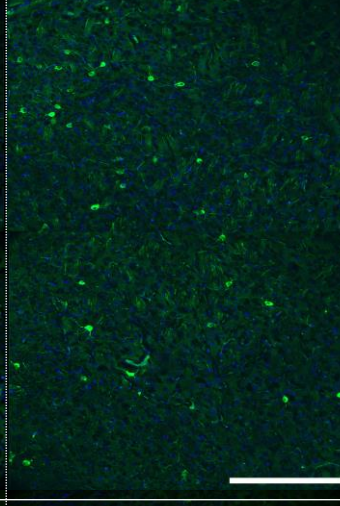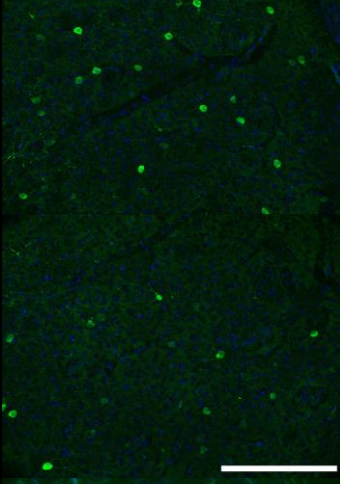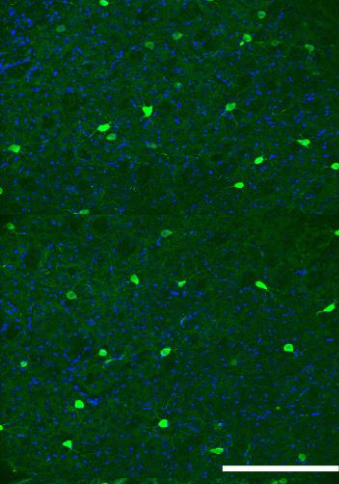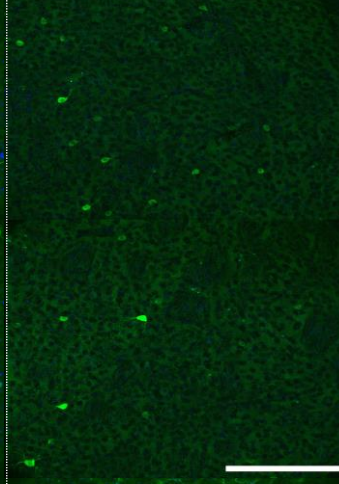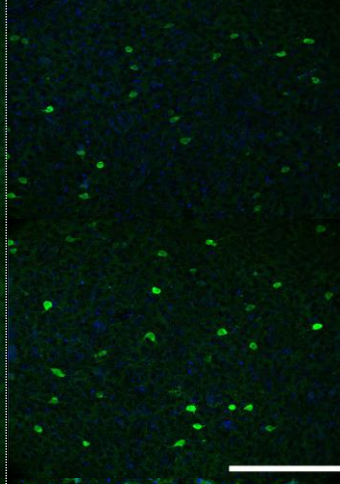
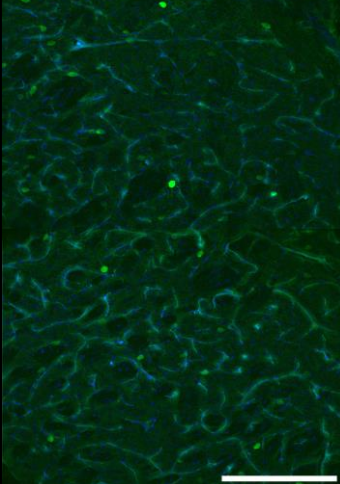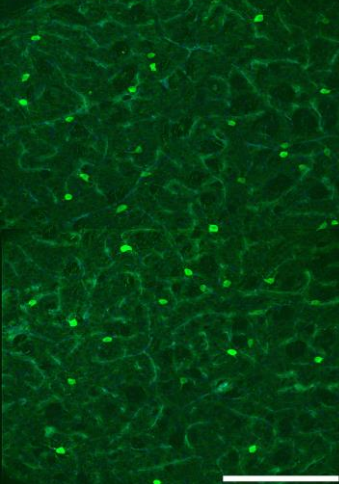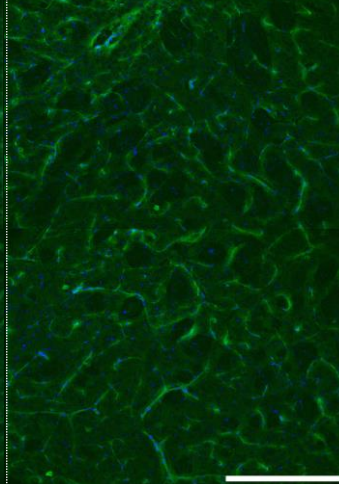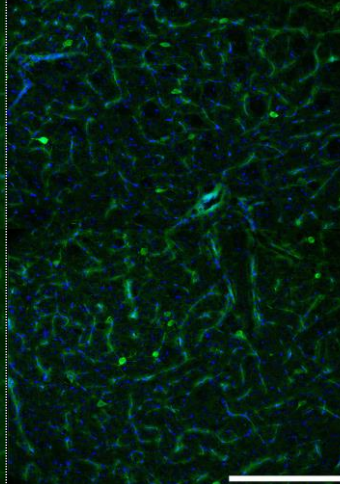|	C57		BTBR	
	DMS	DLS	DMS	DLS

6-8wk Male

6-8wk Female

3-4wk Male

3-4wk Female

764 Fig. 3.1.1. Indicative images of PV+ cells within the DS within each group investigated.

765 PV staining is represented as green, with blue indicating DAPI staining. Scale bar = 250μm

766

767 Between group main effects analysis found no significant main effect of strain (F(1,58)=0.0360, p =

768 0.850; See Fig. 3.1 C) or sex (F(1,58)=1.58, p=0.214; See Fig. 3.1 A) on the density of PV+ cell within

769 the DS wholly. However, a significant between group effect of age on the density of PV+ cells within the

770 DS (F(1,58)=4.80, p = 0.0326; See Fig. 3.1 B) irrespective of strain and sex. Namely, 6-8wk (1856

771 ±450 cells/mm^3) mice show a significantly lower (~10.02%) density of PV+ cells within the DS wholly

772 than in 3-4wk (2046 ±309 cells/mm^3) mice. Further, a significant within group main effect of DS

773 subregion was identified (F(1,58)=132.88, P<2e-16; See Fig. 3.1 D) with a greater density of PV+ cells

774 within the DLS (2515 ±405 cells/mm^3) than the DMS (1387 ±354 cells/mm^3) irrespective of strain, age,

775 and sex.

776 Multiple significant interaction effects were noted as follows. A significant interaction effect of strain*ROI

777 was observed (F(1,58)=21.6, p=2.01e-05; See Fig. 3.1. H). Within the DMS, C57 mice (1590 ±364

778 cells/mm^3) show a greater density of PV+ cells than BTBR mice (1183 ±345 cells/mm^3; p=0.0134).

779 However, within the DLS, BTBR mice (2750 ±518 cells/mm^3) present with a greater density of PV+ cells

780 than C57 mice (2281 ± 291; p=0.00621). A significant sex*ROI interaction effect was also observed

781 (F(1,58)=25.91, p=4.06e-06; See Fig. 3.1 G). As within the DLS, female mice (2708 ±466 cells/mm^3)

782 show a greater PV+ cell density than male mice (2323 ± 343 cells/mm^3; p=0.0427), whereas in the

783 DMS a significantly greater PV+ cell density is apparent in male (1668 ±315 cells/mm^3) relative to

784 female mice (1106 ± 394 cells/mm^3; p=0.0002).

785 Further, a significant interaction effect of strain*age (F(1,58)=18.9, p=5.63e-05; See Fig. 3.1 E) with

786 greater PV+ cell density in 3-4wk C57 mice (2238 ±338 cells/mm^3) than 3-4wk BTBR mice (1854 ±281

787 cells/mm^3; p = 0.0195), a relationship further observed between 6-8wk C57 (1634 ±318 cells/mm^3)

788 and BTBR (2079 ±582 cells/mm^3) mice (p=0.0145). Additionally, a significantly greater density of PV+

789 cells was recorded in 3-4wk C57 mice than 6-8wk C57 mice (p=0.000138). Notably a similar significant

790 difference between age groups was not observed between BTBR mice of 3-4wk and 6-8wk (p=0.400). A

791 significant sex*age interaction effect on PV+ cell density was identified (F(1,58)=7.43, p=0.00848; See

792 Fig. 3.1 F) with greater PV+ cell density recorded in 3-4wk male mice (2227 ±353 cells/mm^3) than 3-

793   4wk female mice (1865 ±266 cells/mm^3; p=0.0291), a relationship not observed between sexes at 6-

794   8wk (p=0.776). Additionally, significantly greater PV+ cell density was observed in 3-4wk male mice and

795   6-8wk male mice (1764 ±305 cells/mm^3; p=0.00543), a significant interaction not similarly observed

796   between 3-4wk and 6-8wk female mice (1949 ±594 cells/mm^3; p=0.973).

797   Finally, a significant three-way interaction effect of strain*sex*age was noted age ($F_{(1,58)}$=5.19,

798   p=0.0264). As 6-8wk female BTBR mice (2306 ±803 cells/mm^3) show a significantly greater PV+ cell

799   density than 3-4wk female BTBR mice (1590 ±207 cells/mm^3; p=0.0124). No further significant

800   interaction effects were noted to influence PV+ cell density.

801   (3.1.2) PNN+ cell density (cells per mm^3)

802   A 4-way mixed ANOVA (Strain*Sex*Age*ROI) was performed on square root transformed PNN+

803   cell density data (as previously described in: St-Pierre, et al., 2018; Lee, 2020; McDonald, 2009), with

804   normality assumed within this data, supported by nonsignificant results from a Shapiro-Wilk test.

805   Descriptive statistics of PNN+ cell density can be found in **Table 3.2.**

806   *Table 3.2: Mean and standard deviation of the density of Perineuronal net-expressing cells per mm^3*

807   *within the Dorsal Striatum between C57 and BTBR mice. Note SD = standard deviation.*

PNN+ Cell Density (cells/mm^3)					
			ROI		
Strain	Age	Sex	DMS (SD)	DLS (SD)	Row Mean (SD)
C57L/J	3-4wk	M	1347 (704)	1584 (634)	1466 (669)
		F	2391 (616)	2391 (378)	2391 (497)
	6-8wk	M	1082 (341)	1129 (233)	1106 (287)
		F	1063 (297)	1656 (213)	1360 (255)
BTBR T+tf/j	3-4wk	M	961 (967)	1513 (1116)	1237 (1042)
		F	1310 (550)	2500 (236)	1905 (393)
	6-8wk	M	999 (260)	1211 (423)	1105 (342)
		F	906 (337)	1927 (366)	1417 (352)
	Column Mean		1257 (509)	1739 (450)	

808   **Table 3.2** shows the mean cell density and standard deviation of PNN+ cells per mm^3 within the

809   dorsomedial- and dorsolateral striatum (DMS and DLS) of C57 and BTBR mice with reference to sex and

810   age. **Fig. 3.2** displays main effects and two-way interaction effects of density of PNN+ cells presented in

811   **Table 3.2.** with reference to strain, sex, age, and ROI.
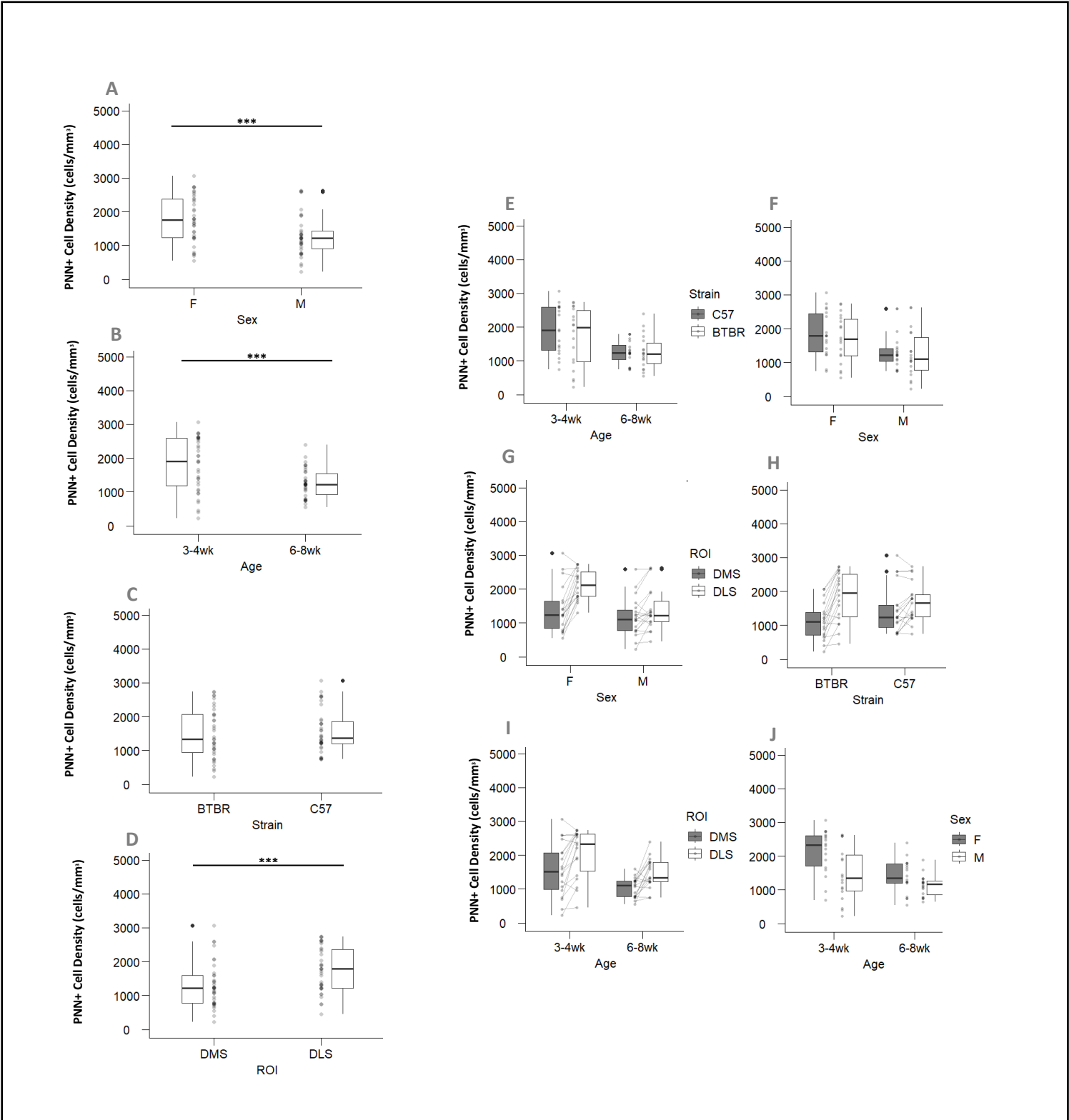
Fig. 3.2. Mean Density of PNN+ Cells per mm^3 in the Dorsal Striatum.

Box plots displaying mean density of PNN+ cells per mm^3 in the DS (±SD) with regards to (A) Sex (male & female), (B) Age (3-4wk & 6-8wk), (C) Strain (C57 & BTBR), and (D) Subregion (DMS & DLS). Box plots

816   displaying mean density of PNN+ cells per mm^3 in the DS (±SD) with regards to interactions of (E) strain:

817   age, (F) sex:age, (G) sex:ROI, (H) strain: ROI, (I) age: ROI, (J) age:sex. Asterixis represent * $p \le 0.05$, ** $p \le$

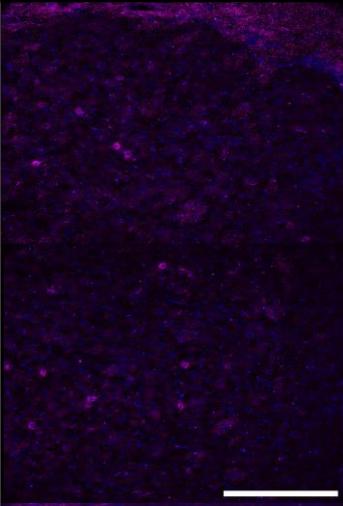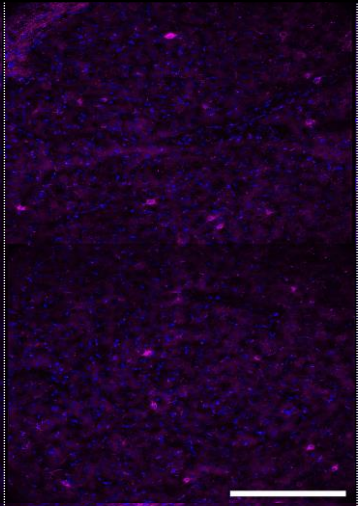818   0.01, and *** $p \le$ 0.001. Small circles represent individual data points.
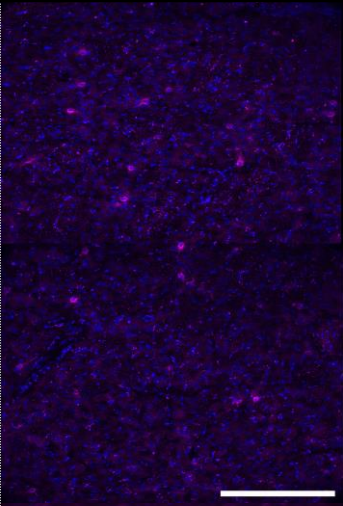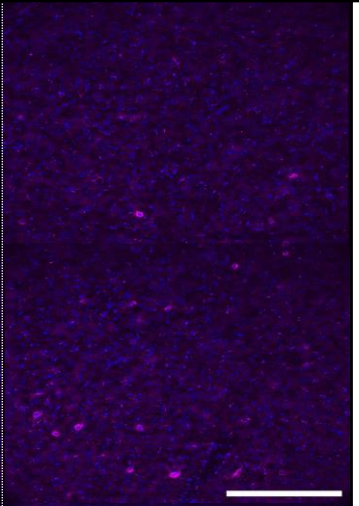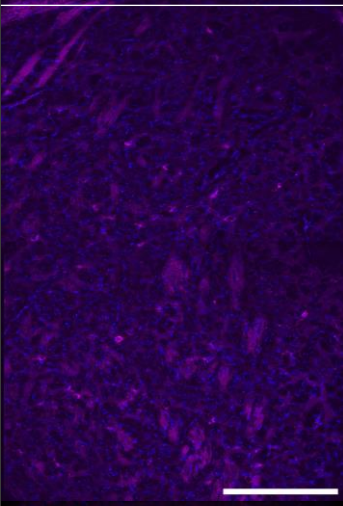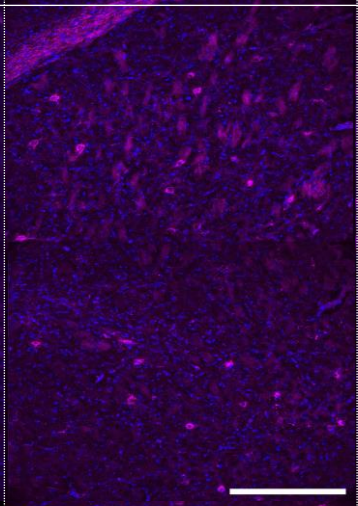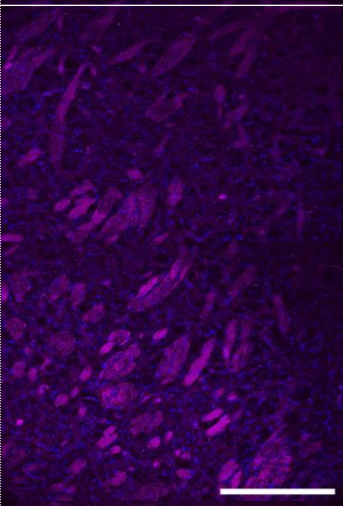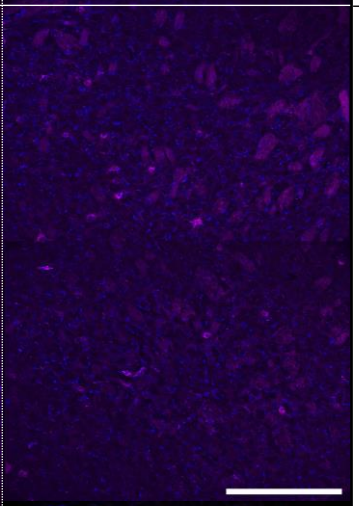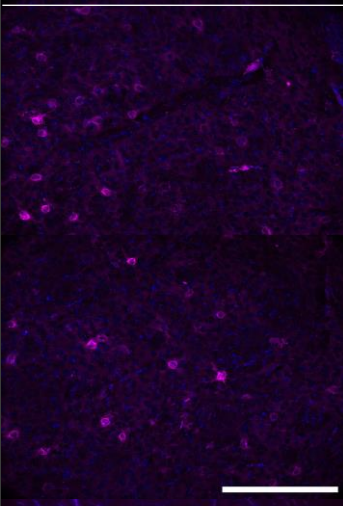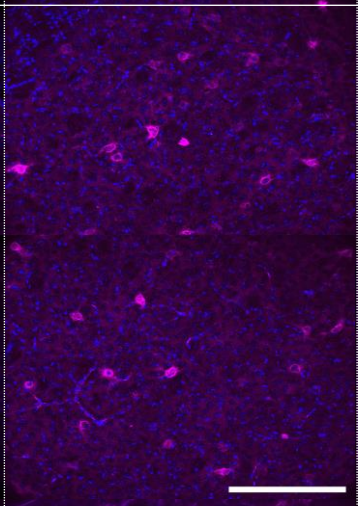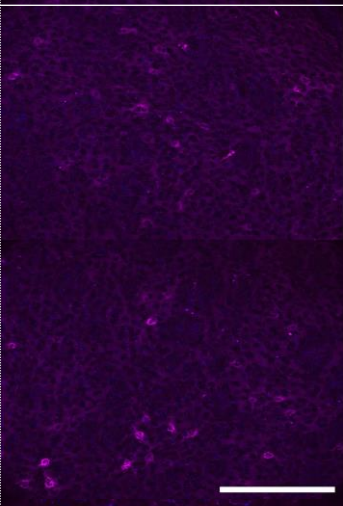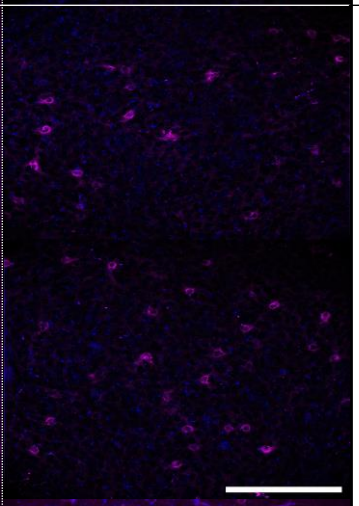
	C57		BTBR	
	DMS	DLS	DMS	DLS

6-8wk Male

6-8wk Female

3-4wk Male

3-4wk Female

820   Fig. 3.2.1 Indicative images of PNN+ cells within the DS within each group investigated.

821   PNN staining is represented as magenta, with blue indicating DAPI staining. Scale bar = 250µm.

822

823   Between group main effects analysis found no significant main effect of strain ($F_{(1,58)}$=0.875, p =

824   0.353; See Fig. 3.2. C) on the density of PNN+ cells within the DS wholly, irrespective of sex or age.

825   However, a significant main effect of sex on PNN+ cell density within the DS was identified

826   ($F_{(1,58)}$=14.37, p = 0.00036; See Fig. 3.2 A), with an increased PNN+ cell density in female (1768

827   ±374 cells/mm^3) compared to male (1228 ± 585 cells/mm^3) mice. A significant main effect of age was

828   identified ($F_{(1,58)}$=13.57, p = 0.00051; See Fig. 3.2 B), with a greater density of PNN+ cells in the DMS

829   of 3-4wk (1750 ± 650 cells/mm^3) than 6-8wk (1247 ± 309 cells/mm^3). Further, a significant within

830   group main effect of DS subregion was observed ($F_{(1,58)}$=18.80, p = 0.00046; See Fig. 3.2 D), with a

831   greater density of PNN+ cells within the DLS (1739 ± 450 cells/mm^3) than the DMS (1257 ± 509

832   cells/mm^3). No statistically significant interaction effects were observed (See Fig. 3.2 E-J).

833   (3.1.3) PV+PNN+ cell density (cells per mm^3)

834   A 4-way mixed ANOVA (Strain*Sex*Age*ROI) was performed on square root transformed

835   PV+PNN+ cell density data (as previously described in: St-Pierre, et al., 2018; Lee, 2020; McDonald,

836   2009), with normality assumed within this data as supported by nonsignificant results from a Shapiro-
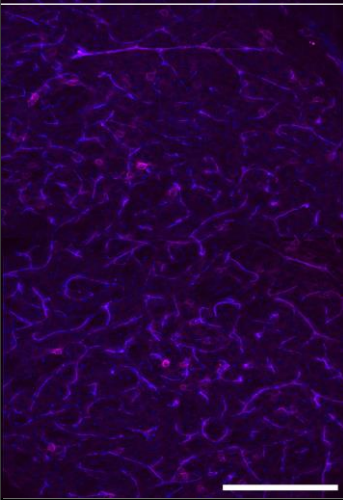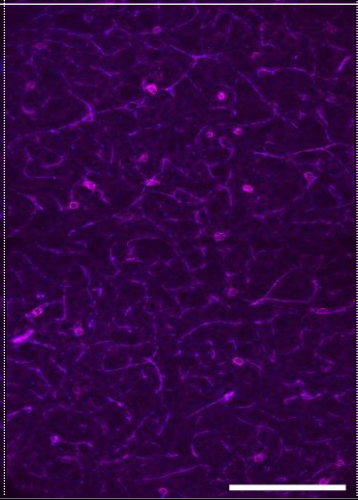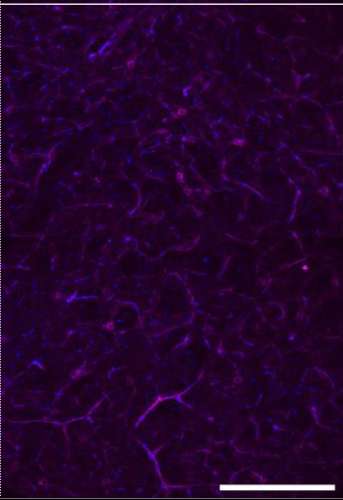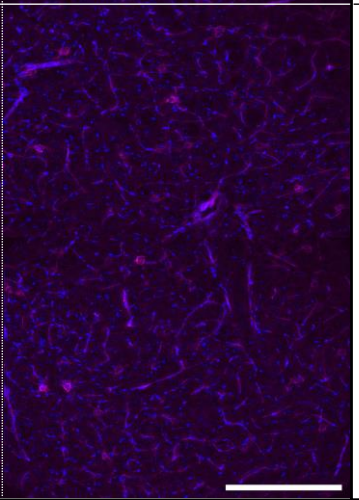
837   Wilk test. Descriptive statistics of PV+PNN+ cell density can be found in **Table 3.3.**

838   *Table 3.3: Mean and standard deviation of the density of Perineuronal net and Parvalbumin-expressing*

839   *cells per mm^3 within the Dorsal Striatum between C57 and BTBR mice. Note SD = standard deviation.*

PV+PNN+ Cell Density (cells/mm^3)					
			ROI		
Strain	Age	Sex	DMS (SD)	DLS (SD)	Row Mean (SD)
C57L/J	3-4wk	M	745(240)	1391 (547)	1068 (394)
		F	1096 (275)	2107 (414)	1602 (345)
	6-8wk	M	595 (251)	1063 (193)	829 (222)
		F	640 (249)	1490 (303)	1065 (276)
BTBR T+tf/j	3-4wk	M	408 (236)	1347 (984)	878 (610)
		F	1096 (248)	2181 (240)	1639 (244)
	6-8wk	M	615 (188)	1129 (419)	872 (304)
		F	458 (209)	1714 (225)	1086 (217)
	Column Mean		707 (237)	1553 (416)	

840   **Table 3.3** displays the mean density and standard deviation (SD) of PV+PNN+ cells per mm^3 within the

841   dorsomedial- and dorsolateral striatum (DMS and DLS) of C57 and BTBR mice with reference to sex and

age. **Fig. 3.3** displays main effects and two-way interaction effects on densities of PV+PNN+ cells, as

presented in **Table 3.3**, with reference to strain, sex, age, and ROI.

844
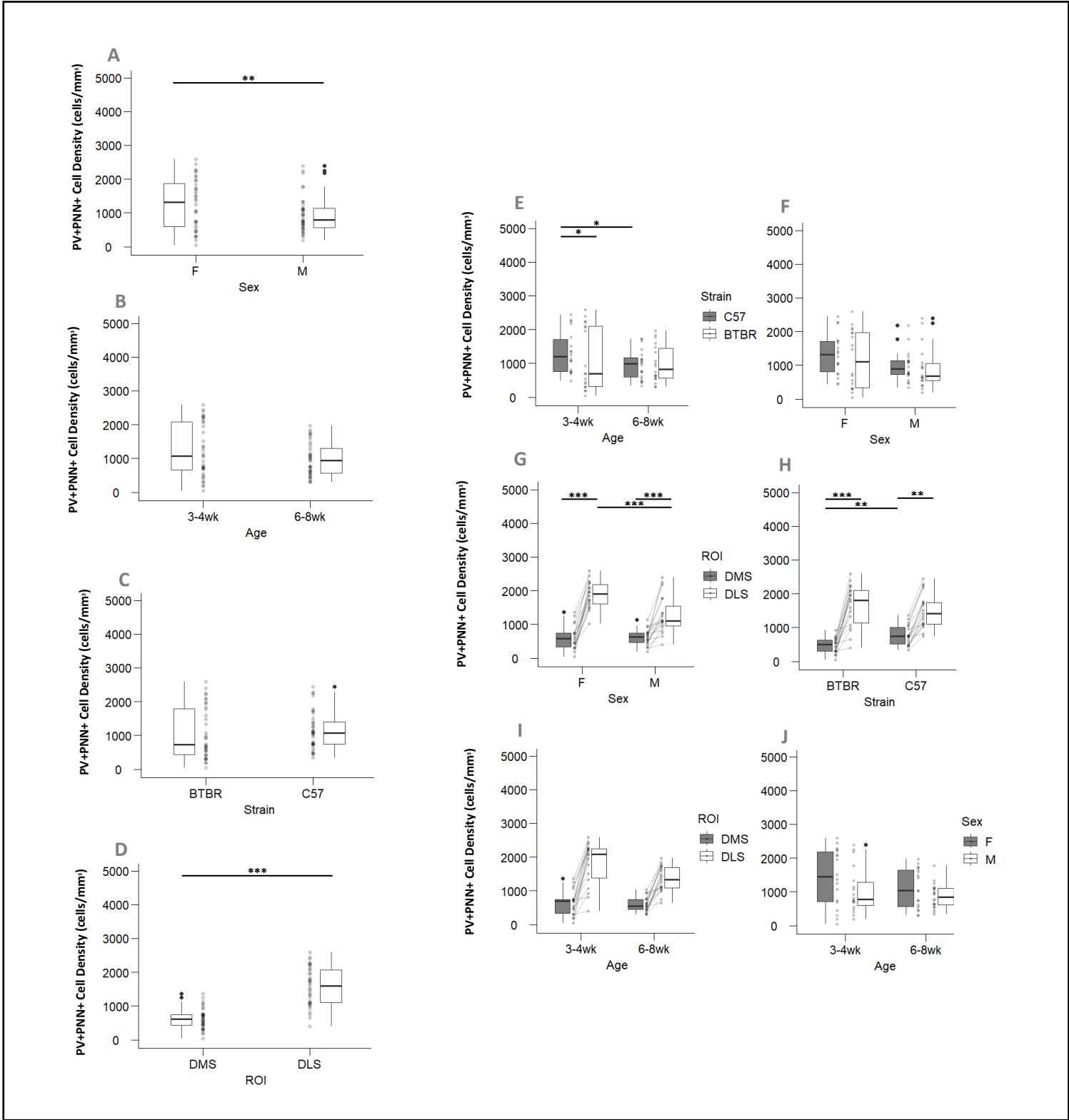
Fig. 3.3. Mean Density of PV+PNN+ Cells per mm^3 in the Dorsal Striatum.

846 Box plots displaying mean density of PV+PNN+ cells per mm^3 in the DS (±SD) with regards to (A) Sex

847 (male & female), (B) Age (3-4wk & 6-8wk), (C) Strain (C57 & BTBR), and (D) Subregion (DMS & DLS).

848 Box plots displaying mean density of PV+PNN+ cells per mm3 in the DS (±SD) with regards to

849 interactions of (E) strain: age, (F) sex:age, (G) sex:ROI, (H) strain: ROI, (I) age: ROI, (J) age:sex. Asterixis

850 represent * $p \leq 0.05$, ** $p \leq 0.01$, and *** $p \leq 0.001$. Small circles represent individual data points.

	C57		BTBR		
	DMS	DLS	DMS	DLS	
					6-8wk Male
					6-8wk Female
					3-4wk Male
					3-4wk Female

Fig. 3.3.1 Indicative images of PV+PNN+ cells within the DS within each group investigated PV staining is representing in green, PNN staining is represented as magenta, with blue indicating DAPI staining. Scale bar = 250μm.

Between group main effects analysis found no significant main effect of strain ($F_{(1,58)}$ = 3.32, p = 0.0734; See Fig. 3.3 C) on the density of PV+PNN+ cells within the DS wholly, irrespective of sex or age. A significant main effect of sex on PV+PNN+ cell density within the DS was identified ($F_{(1,58)}$=8.34, p = 0.0055; See Fig, 3.3 A), with a greater density of PV+PNN+ cell density in female mice (1348 ± 270 cells/mm^3) relative to male mice (912 ± 382 cells/mm^3). However, no significant between group effect of age PV+PNN+ cell density within the DS was observed ($F_{(1,58)}$ = 3.93, p = 0.052; See Fig. 3.3. B). A significant within group main effect of DS subregion on PV+PNN+ cell density was observed ($F_{(1,58)}$=121.91, p = 6.96e-16; See Fig. 3.3. D), with a greater density of PV+PNN+ cells within the DLS (1553 ± 416 cells/mm^3) than the DMS (707 ± 237 cells/mm^3), irrespective of strain, age, and sex.

A number of significant interaction effects were observed, such as a significant interaction effect of strain*ROI on the density of PV+PNN+ cells within the DS ($F_{(1,58)}$ = 8.56, p = 0.0049; See Fig. 3.3 H). 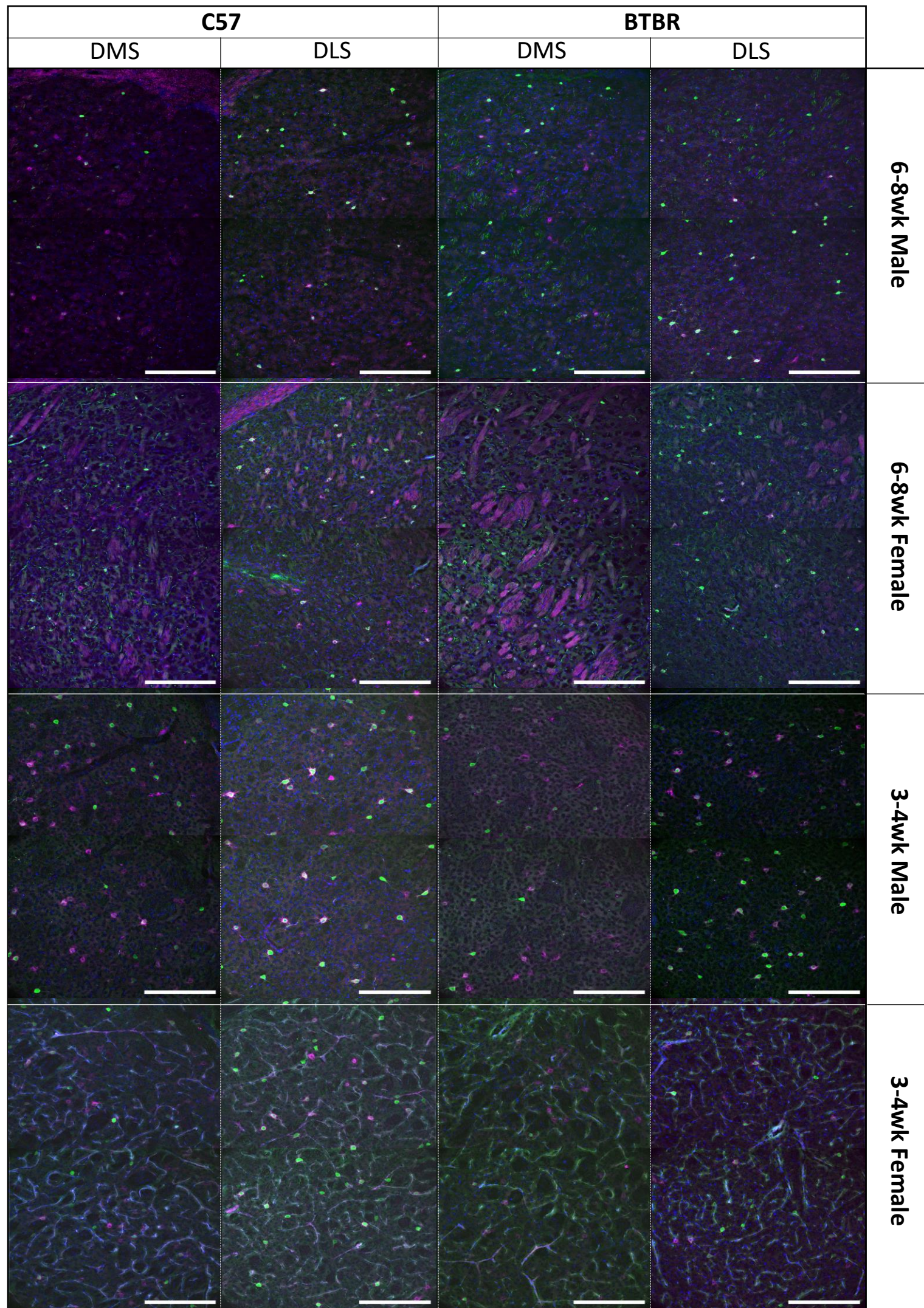A greater density of PV+PNN+ cells was observed within the DLS than the DMS in both C57 (DMS = 769 ±254 cells/mm^3, DLS = 1512 ±364 cells/mm^3, p = 0.000) and BTBR (DMS = 644 ±220 cells/mm^3, DLS = 1593 ±467 cells/mm^3, p = 0.000) mice. Further, the density of PV+PNN+ cells within the DMS was found to be significantly greater in C57 mice than BTBR mice (p = 0.007). This difference was not significant within the DLS (p = 0.863).

A significant interaction effect of sex*ROI was noted ($F_{(1,58)}$ = 9.99, p = 0.0025; See Fig. 3.3 G), with a greater density of PV+PNN+ cells within the DLS than the DMS seen in both males (DMS = 591 ±229 cells/mm^3, DLS = 1233 ±536 cells/mm^3, p = 0.000) and females (DMS = 823 ±245 cells/mm^3, DLS = 1873 ±230 cells/mm^3, p = 0.000). Additionally, a greater density of PV+PNN+ cells within the DLS was reported in females than males (p = 0.000) however no similar relationship was observed within the DMS (p = 0.999).

Further, a significant interaction effect of strain*age was observed ($F_{(1,58)}$ = 4.52, p = 0.0378; See Fig. 3.3. E) with a greater density of PV+PNN+ cells in 3-4wk C57 (1335 ±369 cells/mm^3) than 3-4wk BTBR mice (1258 ±427 cells/mm^3; p=0.318). Additionally, significantly lower PV+PNN+ cell density was noted in 6-8wk C57 mice (947 ±249 cells/mm^3) in comparison to 3-4wk C57 mice was observed (p=0.026).

882 Of note, no equivalent significant difference was found between 3-4wk BTBR and 6-8wk BTBR (979

883 ±260 cells/mm^3) mice (p=0.999). No further significant interactions were noted to influence the density

884 of PV+PNN+ cells within the DS.

885   (3.1.4) Percentage of PV+ cells with PNN staining

886   A 4-way (Strain*Sex*age*ROI) mixed ANOVA was performed on ART-transformed percentage of

887 PV+ cells with colocalised PNN staining data (as previously described by Elkin, et al., 2021; Wobbrock, et

888 al., 2011). Normality was assumed within this transformed data, supported by non-significant results

889 from a Shapiro-Wilk test. Descriptive statistics can be found in **Table 3.4.**

890 *Table 3.4:* *Mean and standard deviation of the Percentage PV+ Cells with PNN Staining (%) within the*

891 *Dorsal Striatum between C57 and BTBR mice. Note SD = standard deviation.*

			Percentage PV+ Cells with PNN Staining (%)		
			ROI		
Strain	Age	Sex	DMS (SD)	DLS (SD)	Row Mean (SD)
C57L/J	3-4wk	M	35.16 (14.55)	56.80 (16.27)	45.98 (15.41)
		F	70.01 (5.33)	78.09 (8.33)	74.05 (6.83)
	6-8wk	M	37.17 (10.55)	65.02 (9.72)	51.10 (10.14)
		F	71.76 (17.65)	69.71 (13.76)	70.74 (15.71)
BTBR T+tf/j	3-4wk	M	32.78 (21.05)	53.09 (33.01)	42.94 (27.03)
		F	65.74 (29.65)	81.89 (8.05)	73.82 (18.85)
	6-8wk	M	43.09 (8.59)	50.42 (10.32)	46.76 (9.46)
		F	39.50 (27.59)	58.93 (24.02)	49.22 (25.81)
	Column Mean		49.40 (16.87)	64.24 (15.44)	

892 Table 3.4 shows the mean and standard deviation (SD) of the percentage of PV+ cells with colocalised

893 PNN staining within the dorsomedial- and dorsolateral striatum (DMS and DLS) of C57 and BTBR mice

894 with reference to sex and age. **Fig. 3.4** displays main effects and two-way interaction effects of the

895 percentages of PV+ cells with colocalised PNN staining, as presented in **Table 3.4,** with respect to strain,

896 sex, age, and ROI.

Fig. 3.4. Mean % of PV+ cells with PNN staining in the Dorsal Striatum

Box plots displaying mean % of PV+ cells with PNN staining in the DS (±SD) with regards to (A) Sex (male & female), (B) Age (3-4wk & 6-8wk), (C) Strain (C57 & BTBR), and (D) Subregion (DMS & DLS). Box plots displaying mean % of PV+ cells with PNN staining in the DS (±SD) with regards to interactions of (E) strain: age, (F) sex:age, (G) sex:ROI, (H) strain: ROI, (I) age: ROI, (J) age:sex. Asterixis represent * $p \leq$ 0.05, ** $p \leq$ 0.01, and *** $p \leq$ 0.001. Small circles represent individual data points.

Between group main effect analysis revealed no significant main effect of strain on the percentage of PV+ cells with colocalised PNN expression within the DS wholly, irrespective of sex and developmental stage ($F_{(1,29)}$=8.4893e-01, p = 0.364; See Fig. 3.4. B). However, a significant main effect of sex was

906   demonstrated (F(1,29) = 1.6971e+01, p = 0.000289; See Fig. 3.4. D), with a greater percentage of

907   PV+ cells with colocalised PNN expression in female (66.95 ± 16.80 %) than male (46.69 ± 15.51 %)

908   mice. No significant main effect of age on the percentage of PV+ cells with PNN colocalised expression

909   within the DS wholly was identified (F(1,29) = 6.7275e-01, p = 0.419; See Fig. 3.4. C). A significant

910   within group main effect of DS subregion was noted (F(1,29) = 3.3839e+01, p = 2.634e-06, See Fig.

911   3.4. A), with a greater percentage of PV+ cells with colocalised PNN expression within the DLS (64.24

912   ±15.44 %) relative to the DMS (49.40 ±16.87 %).

913   No significant two-way interaction effects were observed, however a significant three-way strain*sex*ROI

914   interaction effect was noted (F(1,29)= 6.6108e-00, p = 0.0155), suggesting a greater percentage of

915   PV+ cells were colocalised with PNNs within the DMS of C57 female mice (70.89 ±11.49 %) than BTBR

916   female mice (52.62 ±28.62 %).

917   (3.1.5) Percentage of PNN+ cells with PV staining

918   A 4-way (Strain*Sex*age*ROI) mixed ANOVA was performed on ART-transformed percentage of

919   PNN+ cells with colocalised PV staining data (as previously described by Elkin, et al., 2021; Wobbrock, et

920   al., 2011). Normality was assumed within this transformed data, supported by non-significant results

921   from a Shapiro-Wilk test. Descriptive statistics can be found in **Table 3.5.**

922   *Table 3.5: Mean and standard deviation of the Percentage PNN+ Cells with PV Staining (%) within the*

923   *Dorsal Striatum between C57 and BTBR mice. Note SD = standard deviation.*

			Percentage PNN+ Cells with PV Staining (%)		
			ROI		
Strain	Age	Sex	DMS (SD)	DLS (SD)	Row Mean (SD)
C57L/J	3-4wk	M	58.59 (7.59)	87.57 (6.35)	73.08 (6.97)
		F	43.13 (3.16)	88.38 (6.73)	65.76 (4.95)
	6-8wk	M	53.83 (13.52)	93.10 (5.69)	73.47 (9.61)
		F	63.62 (22.05)	90.02 (10.71)	76.82 (16.38)
BTBR T+tf/j	3-4wk	M	57.04 (30.56)	88.85 (3.09)	72.95 (16.83)
		F	23.94 (12.60)	87.85 (7.52)	55.90 (10.06)
	6-8wk	M	61.41 (20.07)	94.79 (3.59)	78.10 (11.83)
		F	53.51 (15.31)	88.86 (8.98)	71.19 (12.15)
	Column Mean		51.88 (15.61)	89.93 (6.58)	

924   **Table 3.5** shows the mean and standard deviation (SD) of the percentage of PNN+ cells with PV staining

925   within the dorsomedial- and dorsolateral striatum (DMS and DLS) of C57 and BTBR mice with reference

926   to sex and age. **Fig. 3.5** displays main effects and two-way interaction effects of the percentages of

927   PNN+ cells with PV staining, as presented in **Table 3.5.** with respect to strain, sex, age, and ROI.
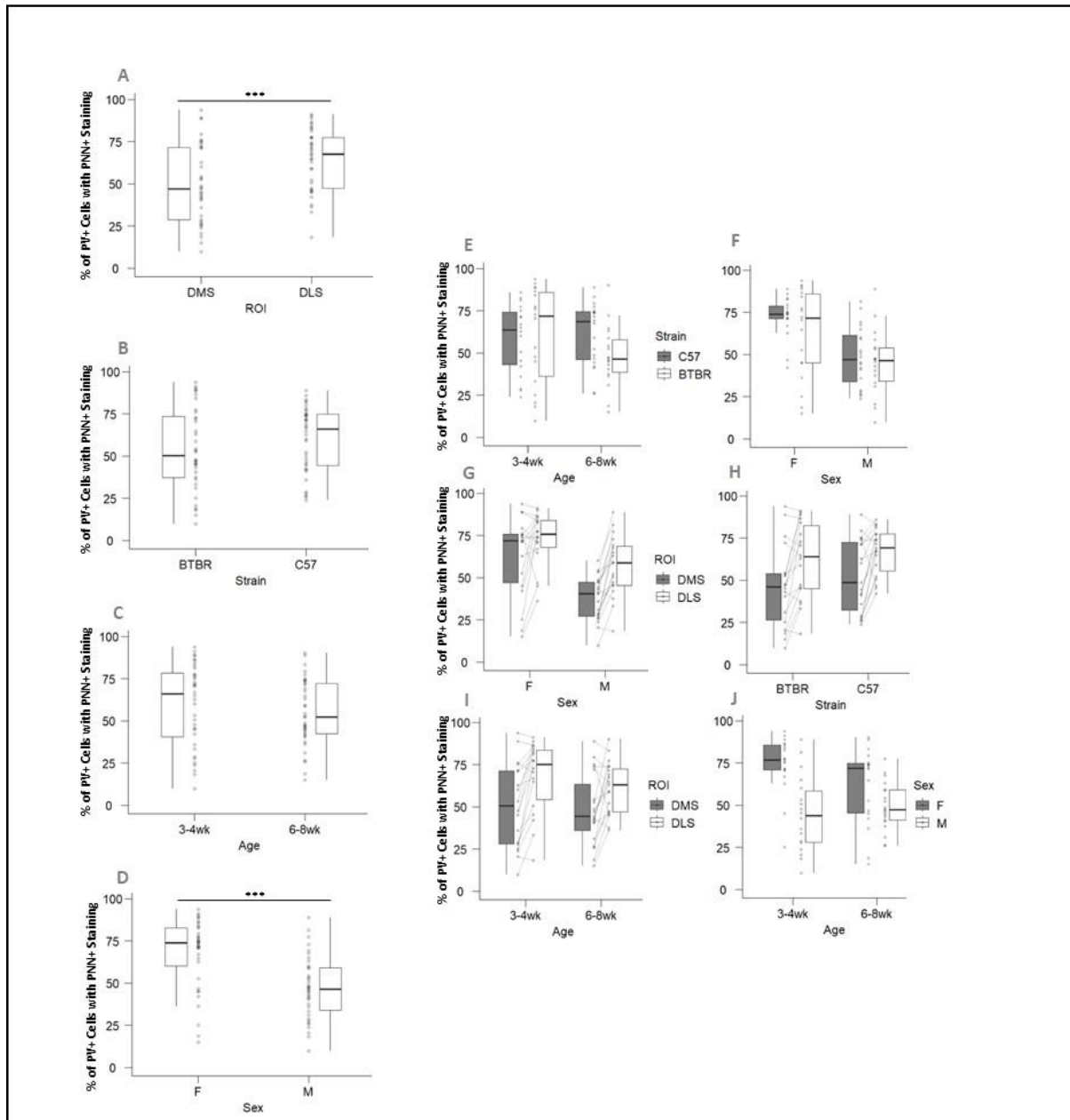
928

929 Fig. 3.5. Mean % of PNN+ cells with PV staining in the Dorsal Striatum

930 Box plots displaying mean % of PNN+ cells with PV staining in the DS (±SD) with regards to (A) Sex

931 (male & female), (B) Age (3-4wk & 6-8wk), (C) Strain (C57 & BTBR), and (D) Subregion (DMS & DLS).

932 Box plots displaying mean % of PNN+ cells with PV staining iin the DS (±SD) with regards to

933 interactions of (E) strain: age, (F) sex:age, (G) sex:ROI, (H) strain: ROI, (I) age: ROI, (J) age:sex. Asterixis

934 represent * p ≤ 0.05, ** p ≤ 0.01, and *** p ≤ 0.001. Small circles represent individual data points.

935 Between group main effect analysis revealed no significant main effect of strain on the percentage of

936 PNN+ cells with colocalised PV expression within the DS wholly, irrespective of sex and developmental

937 stage ($F_{(1, 29)}$ = 1.8165e-00, p = 0.188; See Fig 3.5 B). However, a significant main effect of sex was

938 demonstrated sex (F(1,29)=5.8363e+00, p = 0.022; See Fig 3.5 D)), with male mice (57.72 ±17.93 %)

939 presenting a higher percentage of PNN+ cells expressing colocalised PV than female mice (46.05

940 ±13.28 %). A significant main effect of age was also found (F(1,29)=4.144e+00, p = 0.0052; See Fig.

941 3.5 C), with 6-8wk mice (74.89 ±12.49 %) presenting a greater percentage of PNN+ cells expressing PV

942 in the DS wholly than 3-4wk mice (66.92 ±9.70 %), irrespective of sex or strain. Additionally, a

943 significant within groups main effect of DS subregion was noted (F(1,29)=1.5495e+02, p=3.7003e-13;

944 See Fig, 3.5 A) with a greater percentage of PNN+ cells with colocalised PV staining found in the DLS

945 (89.93 ±6.58 %) in comparison to the DMS (51.88 ±15.61 %) irrespective of age, strain, or sex.

946 A significant sex*age interaction effect was noted (F(1,29)=4.2993e+00, p = 0.0471164; See Fig. 3.5

947 J), with a significantly greater percentage of PNN+ cells with PV staining in 3-4wk male (73.01

948 ±11.90 %) mice than 3-4wk female (60.83 ±7.50 %) mice. A further significant three-way sex*age*ROI

949 interaction effect was noted (F(1,29)=8.3671e+00, p = 0.71761), suggesting a reduced percentage of

950 PNN+ cells with PNN colocalised staining within the DMS of 3-4wk female relative to juvenile male mice.

951   (3.1.6) Relative Intensity of fluorescence for PV staining (525nm)

952   PV fluorescence intensity (the relative intensity of fluorescence at 525nm, calculated as

953 described in subsection 2.9) was investigated as a proxy for the relative intensity of PV protein

954 expression within PV+FSIs in this study. Data from juvenile male animals was not included within this

955 analysis due to the difference in camera and light source utilised to capture images of DS ROIs impacting

956 PV fluorescence intensity values. Two 3-way mixed ANOVAs (Strain*Age*ROI on Female only data, and

957 Strain*Sex*ROI on 6-8wk only data) were performed on cube-root transformed PV fluorescence intensity

958 data (a.u.; Cox, 2011; Mangiafico, 2016), with normality assumed within this transformed data as

959 supported by non-significant results from Shapiro-wilk testing. Descriptive staistics can be found in Table

960 3.6.

961

962

963

964

965 *Table 3.6: Mean and standard deviation of the PV fluorescence intensity (a.u) within the Dorsal Striatum*

966 *between C57 and BTBR mice. Note SD = standard deviation.*

			PV Fluorescence Intensity (a.u.) ROI		
	Age	Sex	DMS (SD)	DLS (SD)	Row Mean (SD)
C57L/J	3-4wk	M	1948.96 (240.00)	2366.87 (546.96)	2157.92 (393.50)
		F	3845.24 (274.50)	7074.07 (413.67)	5459.66 (344.09)
	6-8wk	M	8479.52 (250.83)	17669.94 (193.12)	13074.73 (221.98)
		F	3158.37 (249.44)	5580.14 (302.86)	4369.26 (276.15)
BTBR T+tf/j	3-4wk	M	2251.81 (236.04)	5712.92 (983.50)	3982.37 (609.77)
		F	3613.93 (248.31)	7368.99 (240.04)	5491.46 (244.18)
	6-8wk	M	7921.18 (188.16)	15477.46 (418.71)	11699.32 (303.44)
		F	3414.62 (209.32)	7352.18 (224.57)	5383.40 (216.95)
	Column Mean		4329.20 (237.08)	8575.32 (415.43)	

967 **Table 3.6** shows the mean and standard deviation (SD) of the mean fluorescent intensity of PV staining

968 (a.u.) within the dorsomedial- and dorsolateral striatum (DMS and DLS) of C57 and BTBR mice with

969 reference to sex and age.

970 Between group main effect analysis (Strain*Sex*ROI) revealed no significant main effect of strain on PV

971 fluorescent intensity ($F_{(1,30)}$=0.161, p = 0.691). However, a significant main effect of sex on PV

972 fluorescent intensity was observed, with a greater PV fluorescent intensity in male than female mice

973 ($F_{(1,30)}$=111.982, p = 1.21e-11). A significant main effect of ROI, with greater PV fluorescent intensity

974 noted also within the DLS than the DMS ($F_{(1,30)}$=24.493, p = 2.69e-05). No significant interaction

975 effects were identified.

976 Between group main effects analysis (Strain*Age*ROI) revealed no significant main effect of strain

977 ($F_{(1,28)}$=0.613, p = 0.440), or age ($F_{(1,28)}$ = 1.286, p = 0.266) on PV fluorescent intensity. However a

978 significant main effect of DS subregion was identified ($F_{(1,28)}$ = 29.28, p = 9.04e-6), with greater PV

979 intensity again noted within the DLS than the DLS. No significant interaction effects were identified.

980 **(3.2) qPCR results**

981 Utilising qPCR techniques/gene expression analysis, this study has investigated the relative gene

982 expression of pvalb, hapln1, tnr, and acan within the dorsal striatum of both C57 and BTBR mice through

983 development (3-4wk and 6-8wk) and between sexes (Male and Female). ΔCq values were calculated (as

984 described in 2.13) and utilised for statistical analysis. Fold changes in relative gene expression in BTBR

985 mice, relative to sex and age matched C57 mice, were visualised using the 2- ΔΔCq method, as shown in

Fig 3.6 (Schmittgen & Livak, 2008). Full descriptions of statistical analysis performed on ΔCq values for

each GOI are described in their relevant subsections.
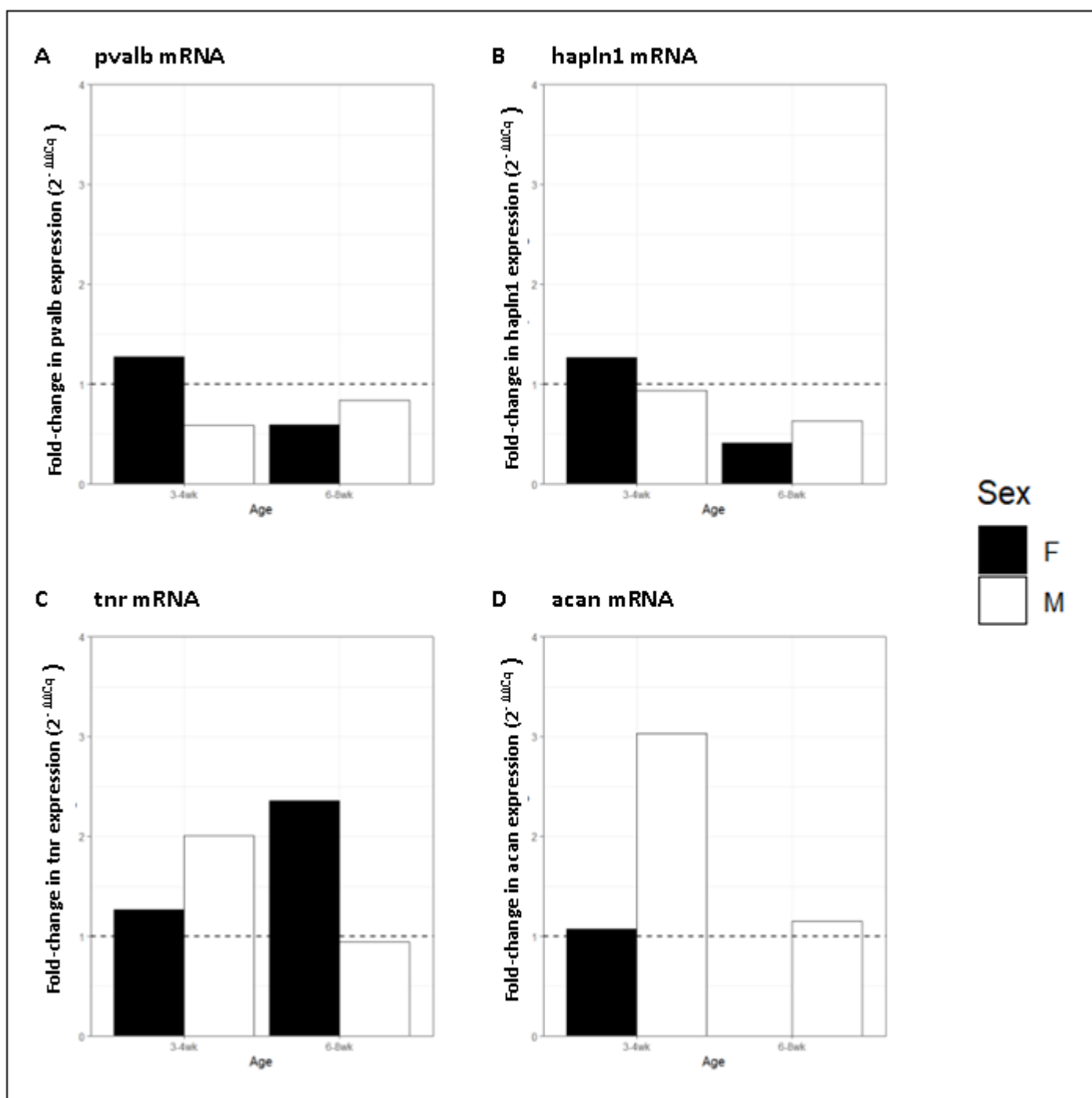
Fig. 3.6. Mean 2- ΔΔCq values (±SEM) from striatal samples representing mRNA levels for (A) pvalb, (B)

hapln1, (C) tnr, and (D) acan. mRNA levels were normalised to Rn18s mRNA levels and represented as

fold change relative to WT mice (shown as the dashed horizontal line at 1).

992   (3.2.1) pvalb mRNA expression

993   Multiple Student's t-tests were performed on pvalb ΔCq values, with normality assumed within

994   this data supported by a nonsignificant result from a Shapiro-Wilk test. Student's t-tests revealed a

995   significant difference in relative expression of pvalb in 3-4wk male BTBR mice (ΔCq = 16.12 ± 0.24) than

996   3-4wk female BTBR mice (ΔCq = 15.40 ± 0.22; $t(6.18)=4.11$, p = 0.00587). In turn suggesting a lower

997   relative expression of pvalb in 3-4wk male BTBR mice than 3-4wk female BTBR mice. A similar sex

998   difference in 3-4wk C57 mice was not observed ($t(7.87)=-0.796$, p = 0.4494). Further, a significant sex

999   difference was not observed in 6-8wk BTBR ($t(3.4555)=0.97107$, p = 0.3945) or C57

1000   ($t(2.7965)=0.71813$, p = 0.528) mice. No further significant differences in relative expression of pvalb

1001   were observed.

1002   (3.2.2) hapln1 mRNA expression

1003   Multiple Student's t-tests were performed on halpn1 ΔCq values, with normality assumed within

1004   this data supported by a nonsignificant result from a Shapiro-Wilk test. Student's t-tests revealed a

1005   significant difference in the relative expression of hapln1 in 3-4wk male BTBR mice (ΔCq = 17.78 ±

1006   0.44) and 3-4wk female BTBR mice (ΔCq = 16.77 ± 0.26; $t(4.63)=3.57$, p = 0.0183). Suggesting a

1007   significantly lower expression of hapln1 in 3-4wk male than 3-4wk female BTBR mice. A similar

1008   significant difference between C57 3-4wk mice was not observed ($t(6.05)=0.154$, p = 0.882). Further

1009   sex differences were observed between 6-8wk male BTBR mice (ΔCq = 17.71) and 6-8wk female BTBR

1010   mice (ΔCq = 19.23; $t(4.04)=3.44$, p = 0.02588). In turn suggesting a significant sex difference in hapln1

1011   relative gene expression in the opposite direction in adulthood, with lower relative expression of hapln1

1012   in female than male 6-8wk BTBR mice. Again, no significant sex differences were apparent in 6-8wk C57

1013   mice ($t(4.9938)=1.7841$, p = 0.1346). No futher significant differences in the relative expression of

1014   hapln1 were observed

1015   (3.2.3) tnr mRNA expression

1016   Multiple Student's t-tests were performed on tnr ΔCq values, with normality assumed within this

1017   data supported by a nonsignificant result from a Shapiro-Wilk test. Student's t-tests revealed a significant

1018   difference in the relative expression of tnr in 3-4wk male C57 mice (ΔCq = 15.17) in comparison to 3-

1019   4wk female mice (ΔCq = 14.13; $t(6.66)=2.80$, p = 0.0278). Suggesting a significantly lower relative

1020 expression of tnr in 3-4wk male than 3-4wk female C57 mice. This significant sex-based difference in tnr

1021 expression was not apparent in 3-4wk BTBR mice (t(3.29)=0.522, p = 0.6348). No significant sex

1022 differences were observed in 6-8wk C57 (t(1.29)=2.14, p = 0.231) and 6-8wk BTBR (t(5.95)=0.754, p

1023 = 0.496) mice. No further significant differences in the relative expression of tnr were observed.

1024   (3.2.4) acan mRNA expression

1025   Multiple Wilcoxon Rank-Sum tests were performed on acan ΔCq values, as normality was not

1026 assumed due to significant results from a Shapiro-Wilk test. Acan ΔCq values from adult female animals

1027 were not included in this analysis due to a high incidence of non-detects. Additionally, when exploring

1028 differences in the relative expression of acan in juvenile animals, a significant difference was noted

1029 between 3-4wk male (ΔCq = 15.15) and female mice (ΔCq = 18.23; p = 0.000250). Suggesting a

1030 reduced relative expression of acan in 3-4wk female mice than 3-4wk male mice. Further, a significant

1031 difference in the relative expression of acan was noted between 3-4wk male (ΔCq = 14.67) and female

1032 (ΔCq = 18.28) C57 mice (p = 0.01587). No such significant difference was observed within 3-4wk BTBR

1033 mice (p = 0.09524). No further statistically significant differences in the relative expression of acan were

1034 observed.

1035

1036

1037

1038

1039

1040

1041

1042

1043

1044

1045

1046

1047

1048

1049

1050

(4.0) Discussion

(4.1) No strain-wide alterations of PV and PNN expression in BTBR mice DS

Significant reductions in the density of PV+FSIs have been reported in the striatum of various genetic (CNTNAP2-/- and multiple SHANKopathies) and pharmacological (VPA) mouse models of ASD (Lauber, et al., 2016; 2018; Filice, et al., 2020; Briones, et al., 2022). However, most investigations into PV+FSI density in the striatum utilise exclusively male mice at once developmental stage. In contrast, within a mixed population of BTBR mice, irrespective of sex and developmental stage, we found no significant difference in the density of PV+FSIs in the DS wholly. Further, no significant difference in the relative intensity of fluorescent PV staining (a proxy for PV protein expression) was identified in the DS between strains. This agrees with previous research by Filice, et al., (2016), noting no significant difference in PV fluorescent intensity in the striatum of SHANK1-/- mice. A significant reduction of PV fluorescent intensity has been reported in cortical regions of various other models of ASD (both genetic and pharmacological) which may suggest PV intensity alterations in ASD to occur in a region-specific manner (Filice, et al., 2016; Xia, et al., 2021). PNN+ cell density is often investigated as a secondary marker for PV+FSIs with reports of no alteration in PNN density within the striatum of murine models of ASD, this is in agreement with our findings of no difference in PNN+ cell density in the DS of BTBR mice, irrespective of sex or developmental stage (Filice, et al., 2016; Lauber, et al., 2016; 2018; Briones, et al., 2022).

Though often unexplored, the density of cells with colocalised PV+PNN+ staining was also investigated in this study to gain a better understanding of potential colocalisation alterations in ASD. No significant difference was identified in the density of PV+PNN+ cells in the DS of BTBR mice relative to C57 mice, irrespective of sex and developmental stage. Colocalisation studies investigating alterations in the proportion of striatal PV+ cells with colocalised PNN expression in ASD present mixed results, with increases noted in SHANK3B-/-, CNTNAP2-/-, and BTBR mouse models in contrast to no significant difference found in both VPA and CNTNAP2-/- mice (Filice, et al., 2016; Briones, et al., 2022; Lauber, et al., 2016; 2018). The findings of this study support the latter, reporting no significant difference in the proportion of PV+ cells with colocalised PNN staining in the DS of BTBR mice irrespective of sex, developmental stage, or DS subregion. Further investigation of the percentage of PNN+ cells (and inversely) expressing colocalised PV staining, again, revealed no significant difference between BTBR and

C57 mice irrespective of sex and developmental strain. This is in contrast with prior reports of significant

reduction in the percentage of PNN+ cells with PV staining in murine models of ASD (Filice, et al., 2016;

Lauber, et al., 2016; 2018).

Investigation of gene expression alterations in ASD via qPCR analysis continued this trend of no

significance, with no significant reduction in the relative expression of pvalb, hapln1, tnr, and acan mRNA

in BTBR mice, irrespective of sex and developmental stage. This is in contrast with prior reports of

significant reductions in pvalb mRNA of up to 50% in both SHANK3B-/- and VPA mice, but consistent

with expression in CNTNAP2-/- mice, which report a non-significant 10% reduction in pvalb mRNA

expression (Filice, et al., 2016; Lauber, et al., 2016).

The discrepancies between the lack of significant differences in PV and PNN expression in a murine

model of ASD relative to C57 mice in this study, compared to the significant differences reported in the

studies described above may be due to the differences in ASD murine model utilised. Previous

investigations of PV and PNN expression in genetic, environmental, and idiopathic models of ASD report

both significant increased and decreases in expression in a strain dependent manner (Briones, et al.,

2022). This may reflect the heterogeneity in ASD behavioural phenotype expressed between these

different murine models (Ferhat, et al., 2017; Ey, et al., 2011). Attempts to cluster both behavioural and

biological phenotypes across different murine models of ASD have previously grouped BTBR mice in a

separate cluster than genetic models such as CNTNAP2-/- and SHANK3B-/- mice; this may support our

lack of similar alterations in PV and PNN expression in BTBR mice in this study (Ellegood, et al., 2015;

Zeribi, et al., 2021). However, significant differences in PV and PNN expression have been reported in

the striatum of male BTBR mice of one developmental stage (Briones, et al., 2022). Thus, the findings of

this study may instead suggest that previously observed differences in BTBR mice are not consistent

between DS subregion, sexes, and developmental stages. Indeed, significant alterations in PV and PNN

expression were only found within this study when variables of DS subregion, sex, and developmental

stage were considered.

(4.2) Altered PV and PNN expression in BTBR mice relative to DS subregion

A significantly greater density of PV+ cells was observed in the DLS relative to the DMS in this

study, irrespective of strain, sex, and developmental stage of the animal. This agrees with prior reports of

more abundant PV expression laterally than medially within the striatum (Bengtsson, et al., 2020; Kita, et

1109 al., 1990; Lee, et al., 2012; Monteiro, et al., 2018; O'Connor, et al., 2019; Todtenkopf, et al., 2004). A

1110 greater density within the DLS than DMS was maintained whilst examining both mouse strains separately,

1111 however the size of this subregional difference was not identical within C57 (691 cells/mm^3) and BTBR

1112 (1566 cells/mm^3) mice. Though not statistically explored in this study, this difference may suggest an

1113 exacerbation of the typically observed lateromedial gradient of PV+FSI expression in ASD. Future

1114 research may explore this possibility and examine if this steeper lateromedial gradient across the DS is

1115 also present within the previously reported electrophysiological differences of PV+FSIs between the DLS

1116 and DMS (Monteiro, et al., 2018; Fino, et al., 2018). Variance in network level connectivity may

1117 contribute to the observed lateral bias of PV+FSI density, with differential extrastriatal signalling input to

1118 FSIs within the DMS and DLS previously identified (Sreenivasan, et al., 2022; Bengtsson, et al., 2020;

1119 Wegman, et al., 2024). Alterations in the connectivity of corticostriatal signalling inputs (as previously

1120 identified in ASD (Abbott, et al., 2018)) are suggested to alter the density of striatal PV+FSIs throughout

1121 development (Fino, et al., 2018; Sreenivasan, et al., 2022). This may indicate an underlying mechanism

1122 for differences in PV+FSI density between DS subregions to manifest in TD and be attenuated in ASD.

1123 However, this regulatory role of corticostriatal signalling on neuronal development is bidirectional,-

1124 potentially functioning as a developmental feedback loop; future research may thus investigate if early

1125 PV+FSI alterations may initially impact these corticostriatal connections leading to differential

1126 compensatory mechanisms later in cortical development in ASD (Deemyad, et al., 2024 [preprint];

1127 Sreenivasan, et al., 2022).

1128 Despite differences in PV+FSI morphology and function between the DMS and DLS, few studies have

1129 investigated if striatal PV+FSI alteration in ASD occurs in a subregion specific manner. This study reports

1130 contrasting alterations in PV+FSI density in BTBR mice within the DMS (~29% reduction) and the DLS

1131 (~5% increase) relative to C57 mice. A reduced PV+FSI density in the DMS in BTBR mice observed in

1132 this study is consistent with prior reports of reduced PV+FSI density in the DMS of both BTBR and VPA

1133 male mice (PND 70-168; Briones, et al., 2022). However, an increased density of PV+FSIs in the DLS of

1134 BTBR mice has not been previously observed (Briones, et al., 2022). Investigation of the relative intensity

1135 of PV staining identified the expected lateromedial gradient across the DS. No significant difference in

1136 the relative intensity of PV expression between strains in either striatal subregion may suggest the

1137 observed differences in PV+FSI density between strains are not due to differences in PV expression

1138   influencing the number of identifiable PV+FSIs (as previously suggested in genetic models of ASD by

1139   Filice, et al., 2020; Lauber, et al., 2018).

1140   The potential functional consequences of these PV+FSI expression alterations in BTBR mice, and how

1141   they may relate to the ASD-like behavioural phenotype of this idiopathic model may be extrapolated from

1142   investigations of the functional and behavioural outcomes of PV+FSI ablation and modulation in typically

1143   developing (TD) mice (O'Hare, et al., 2017; Rapanelli, et al., 2017; Xu, et al., 2016). Reduced PV+FSI

1144   density within the DS has been previously achieved via combination transgenic-viral cell ablation

1145   approaches, wherein reductions of PV+FSIs (by ~40%) within the DS wholly resulted in increased

1146   stereotypic behaviour in response to stressors in addition to increased anxiety-like behaviour in

1147   otherwise TD adult male mice (Xu, et al., 2016; Rapanelli, et al., 2017). This may suggest reductions in

1148   the DS wholly to contribute to an RRBI-associated mechanism however not in the spontaneous manner

1149   often reported in BTBR mice and ASD (Xu, et al., 2016). Of note, when this ablation of GABAergic

1150   interneurons was performed more medially in the DS, mice presented with increased spontaneous

1151   stereotypy and deficits in social interaction (Rapanelli, et al., 2017). The observed incidence of ASD-like

1152   behaviours after partial PV+FSI ablation in otherwise TD adult male mice may further emphasise the

1153   potential role of PV+FSI reductions to contribute to an ASD-like behavioural phenotype, further

1154   supported by a similar reduction in PV+FSIs in the DMS of BTBR mice, known to express a similar

1155   behavioural profile, in this study. In contrast, chemogenic inhibition of PV+FSIs in the DLS of TD mice

1156   reportedly prevents the expression of habitual behaviours, suggesting that increased PV+FSI activity (a

1157   potential consequence of increased PV+FSI density) may drive habitual behaviour (O'Hare, et al., 2017).

1158   This in turn may suggest the subregional differences in PV+FSI density reported in this study to

1159   differentially contribute to RRBIs in BTBR mice. However, whilst alterations of PV+FSIs in TD adult male

1160   mice may support a potential role of striatal subregion-specific PV+FSI alterations to facilitate RRBIs

1161   these studies cannot be utilised as direct comparisons to potential mechanisms in ASD as a

1162   neurodevelopmental condition, as reductions in PV+FSIs were performed in brains which have developed

1163   with PV+FSIs present at typical levels. Therefore, this will likely not fully reflect the brain wide

1164   consequential and compensatory mechanisms that may be present in ASD due to altered PV+FSI density

1165   at earlier stages of neurodevelopment (Azim, et al., 2009; Carceller, et al., 2020; Topchiy, et al., 2024).

1166   Future research could further explore if similar mechanisms of habitual behaviour are present in BTBR

1167   mice by chemogenically inhibiting PV+FSIs in DLS and exploring the impact on expressed RRBI

1168   behaviours from baseline.

1169   Apparent alterations in PV+FSI density in ASD have been suggested to be the result of downregulated

1170   PV protein expression, resulting in a significant number of PV+FSIs to not be included in counts due to

1171   the intensity of fluorescent staining not reaching limits of detection (Filice, et al., 2020; Lauber, et al.,

1172   2018). To address this, recent investigations utilise secondary markers to double stain PV+FSIs –with

1173   labelling PNNs most often adopted (Filice, et al., 2016; Lauber, et al., 2016; 2018). In turn, reports have

1174   begun to understand the presence of PNNs in the striatum wholly as to represent PV+FSIs irrespective of

1175   PV staining intensity of presence, this reporting no significant differences PV+FSIs in various genetic and

1176   pharmacological murine models of ASD relative to TD controls (Filice, et al., 2016; Lauber, et al., 2016;

1177   2018; though see Briones, et al., 2022). Whilst a lateromedial gradient of PNN+ cell density within the

1178   DS was identified in this study, potentially expected based on prior reports (Lee, et al., 2008; Miyamoto,

1179   et al., 2018; O'Connor, et al., 2019; though see Lupori, et al., 2023). Alterations in PNN expression have

1180   previously been reported in ASD within the GPe and denate nucleus in postmortem ASD, and a recent

1181   report has noted an increase in PNN+ cells within the DLS of BTBR mice, a finding this study has been

1182   unable to replicate (Brandenburg & Blatt, 2022; Briones, et al., 2022). Indeed, no significant differences

1183   in PNN+ cell density were observed in BTBR mice relative to C57 mice within the DMS or DLS in this

1184   study, potentially suggesting PNN alterations to be region specific and not found within the DS. Utilising

1185   the reasoning of PNN+ cells to represent PV+FSIs in this study would suggest the previously noted

1186   differences in PV+ cells in this study to represent a reduction in PNN expression in BTBR mice. Though

1187   as we found no significant difference in PV fluorescent intensity in PV+FSIs between strain in either DS

1188   subregion. Furthermore, the proportion of PNN+ cells expressing colocalised PV in the DS of C57 mice in

1189   our study (~60%) was relatively low compared to past research, with the identity of PV-PNN+ cells yet to

1190   be determined (O'Connor, et al., 2019; Wingert & Sorg, 2021). Due to this, we are hesitant to assume

1191   PNN+ cell density to accurately reflect PV+FSI density in this study but continue to explore PV-PNN

1192   colocalisation without this assumption.

1193   The density of colocalised PV+PNN+ cells within the DS observed the same lateromedial gradient

1194   reported for PV+ and PNN+ cells, irrespective of strain, sex, or developmental stage in this study. This

1195   finding agrees with gradients observed in TD mice at PND 15 and 60 by O'Connor, et al. (2019).

1196   However, whilst this gradient holds true for both BTBR and C57 mice the difference in PV+PNN+ cell

1197 density between DS subregions again appears larger in BTBR (949 cells/mm^3) than C57 mice (744

1198 cells/mm^3). A significant reduction in PV+PNN+ cell density in BTBR mice relative to C57 mice (~16%)

1199 follows the same trend in reductions to PV+ cell density overall, whilst no significant difference in

1200 PV+PNN+ cell density was observed in the DLS in BTBR mice. Reductions in both PV+PNN+ and PV+

1201 cell density may suggest the reduced density of PV+ cells in ASD may equally impact PV+FSIs with and

1202 without PNNs. Investigation of the proportion of PV+ cells expressing colocalised PNNs within the DMS

1203 and DLS revealed a significantly greater percentage of PV+ cells with colocalised PNN staining within the

1204 DLS than the DMS, a finding not previously reported by investigations of colocalisation in the striatum

1205 (Briones, et al., 2022; Lee, at al., 2012). In agreement with previous reports (Lee, et al., 2012) a similar

1206 lateromedial gradient was also identified for the proportion of PNN+ cells with PV colocalised staining,

1207 irrespective of mouse strain, sex, and developmental stage. A significantly greater percentage of PV+

1208 cells expressed PNN staining within the DMS of BTBR mice in a recent report by Briones and colleagues

1209 (2022), a finding not replicated in this study as no significant differences in percentage colocalisation

1210 were identified between BTBR and C57 mice within the DMS or DLS. Whilst no significant difference in

1211 the percentage of PV+ cells with colocalised PNN staining may be expected, due to reductions in PV+

1212 cells in this study not observed to being exclusive to PV+ cells without PNNs, a lack of difference in the

1213 percentage of PNN+ cells with PV staining between strains in the DMS and DLS was unexpected due to

1214 the lack of overall PNN+ density in this study. Our findings may not have identified these alterations in

1215 colicalisation irrespective of sex and developmental stage, potentially suggesting sex- and age-

1216 dependent alterations in ASD as explored below.

1217 (4.3) Altered PV and PNN expression in BTBR mice relative to Sex and DS Subregion

1218   No significant difference in the density of PV+ cells in the DS wholly between sexes was

1219 observed in this study, in contrast to a recent report of greater density of PV+FSIs in the DS of male

1220 mice (Van Zandt, et al., 2024). However, when the difference in density of PV+ cells between sexes was

1221 explored relative to DS subregion, significant differences were observed within each subregion. A greater

1222 density of PV+ cells in the DMS was observed in male mice, in agreement with the increase noted in the

1223 DS wholly by Van Zandt, et al., 2024). Whilst within the DLS a greater density of PV+ cells was found in

1224 female mice. These subregion dependent sex differences in PV+ cell density may explain why no sex

1225 difference was found overall within this study. The density of PV+ cells remains greater in the DLS than

1226 the DMS for both sexes, maintaining the lateromedial gradient between these regions previously

1227 established (see section (4.2)). However, this difference in PV+ cell density between subregions was

1228 greater in female mice due to this increased density within the DLS and reduced density in the DMS,

1229 relative to male mice. The functional consequences of this observed sex difference in basal densities of

1230 PV+FSIs within the DMS and DLS is beyond the scope of this study, though previous reports identify sex

1231 differences in dopamine release and MSN excitability in the DS of female mice that may relate these

1232 observed basal differences between sexes (Cao, et al., 2018; Zachry, et al., 2021).

1233 Sexually dimorphic basal differences in PV+ cell density across the dorsal striatum may be important to

1234 consider as no significant difference in the pattern of reductions in PV+ cell density was observed in

1235 BTBR mice relative to C57 mice of both sexes. Different basal densities within the DMS and DLS between

1236 sexes may suggest male or female mice may more strongly rely of PV+FSIs within one striatal

1237 subdivision, or that PV+FSI populations within subregions to be differentially resilient to pathological

1238 disruption in ASD (Van Zandt, et al., 2024). This may partially explain the differential functional and

1239 behavioural consequences of similar PV+FSI alterations between sexes in BTBR mice (Van Zandt, et al.,

1240 2024). This in turn may underlie some of the previously reported sex differences of ASD-like behaviour in

1241 BTBR mice, with greater RRBIs (e.g. excessive grooming and marble burying) in male mice, but similar

1242 social/communication deficits observed between sexes (Amodeo, et al., 2019; Bove, et al., 2024). This

1243 concept may be further supported by previously discussed PV+FSI ablation studies, as PV+FSI ablation

1244 only produced ASD-like behavioural profiles in male mice (Rapanelli, et al., 2017). Initially this may seem

1245 surprising within the context of the findings from this study, as female mice presented with a reduced

1246 basal density relative to male mice however this may indicate a greater reliance of PV+FSIs in the DMS of

1247 male mice with reduced ability to accommodate this ablation (Rapanelli, et al., 2017; Van Zandt, et al.,

1248 2024). Further, reports of putamen volumetric alterations predicting RRBI severity in autistic males but

1249 not females may demonstrate similar sexually dimorphic regional dependence in ASD (van't Westeinde, et

1250 al., 2020; Supekar, et al., 2015). Future work may explore potential differences in reliance of PV+FSIs in

1251 the DMS and DLS in RRBI-associated behaviours through investigation of PV+FSI activity at baseline

1252 relative to when repetitive behaviours are performed between sexes in both control mice and models of

1253 ASD.

1254 A greater PV fluorescent intensity was identified in male relative to female mice, suggesting greater PV

1255 protein expression in PV+FSIs in male mice. Few studies have investigated sex differences in PV

1256 fluorescent intensity in the striatum, however this finding mirrors the greater PV protein expression

reported in male mice in the hippocampus (Wu, et al., 2014). Sex differences in the relative expression of PV in PV+FSIs may be in part due to the influence of gonadal hormones such as estrogen, with estrogen receptor beta present on PV+FSIs (Blurton-Jones, et al., 2002; Du, et al., 2018; Wu, et al., 2014). Estrogen receptors are suggested to support PV expression, with previous research noting PV levels in pvalb homo- and hetero-zygous mice to be increased after estrogen administration (Filice, et al., 2018). In contrast no significant differences in pvalb gene expression were found between sexes, which may suggest alterations in PV expression to be due to post-translational differences.

How PV intensity is regulated is poorly understood, though PNNs are noted to play a role (Xia, et al., 2021; Hanssen, et al., 2023). Sexually dimorphic PNN expression was reported in various cortical and subcortical regions, however the direction of these differences appears to vary in a region dependent manner (John, et al., 2022; Cicarelli, et al., 2021). This study identified a greater density of PNN+ cells in female mice. Prior investigations of sex differences in PNN expression within the striatum are limited, though sex differences in PNN expression within the BG has been reported in songbirds with reduced expression noted in female birds (Meyer, et al., 2014). Albeit comparisons with PNN expression in songbirds may be limited due to the greater sexual dimorphism in function of these regions, with respect to song production and perception. The presence of sex differences in PNN expression in mice within this study may highlight a need for recently developed PNN expression brain atlases to explore sex differences in PNN expression to be of greatest use in guiding future research (Lupori, et al., 2023).

Investigation of PV+PNN+ colocalised cell density within the DS indicated a similar sexual dimorphism to that observed for PNN+ cells. Though consideration of DS subregions suggests this increased density of PV+PNN+ cells in female mice to be due to increased density within the DLS, with comparable densities observed between sexes in the DMS. Whilst a lateromedial gradient of PV+PNN+ cell density was present within both sexes, the greater density of PV+PNN+ cells within the DLS of female mice indicates a greater difference between DS subregions in female mice. Due to the noted role of PNNs in the facilitation of PV+FSI function (as described in section (1.5)), an increased density of PV+PNN+ cells in the DLS of female mice may underlie prior reports of increased habit formation in typically developing females (Schoenberg, et al., 2019; LaClair, et al., 2019). No significant differences in PV+PNN+ cell density were identified between strains relative to sex, potentially further emphasising similar reductions in both sexes in ASD.

1286 Further exploration of PV-PNN colocalisation differences between sexes demonstrated a significantly

1287 higher proportions of PV+ cells to have colocalised PNN expression female mice within the DS. This

1288 increase, which may suggest a greater proportion of mature PV+FSIs in female mice, may be expected

1289 based on the observed increase in PNN+ cells and PV+PNN+ cell density, but no significant increase in

1290 PV+ cell density in female mice. No sex dependent differences between strains in the proportion of PV+

1291 cells with colocalised PNN staining were identified in this study, in agreement with prior reports of no

1292 difference in the percentage of PV+ cells expressing colocalised PNN staining in the DS wholly in male

1293 CNTNAP2-/- and VPA mice (Lauber, et al., 2016; 2018; though see Filice, et al., 2016). Of note, a

1294 greater percentage of PV+ cells with colocalised PNN staining was observed in the DMS of male BTBR

1295 mice relative to sex matched controls, as previously identified by Briones, et al., (2022), however a

1296 similar difference was not observed in female BTBR mice. Inversely, male mice presented with a greater

1297 percentage of PNN+ cells with colocalised PV staining than female mice in the DS wholly. Notably, in

1298 contrast with prior reports noting a reduced percentage of PNN+ cells with colocalised PV staining in the

1299 striatum wholly, this study found no difference in this proportion of PNN+ cells between strain in either

1300 sex, irrespective of age (Filice, et al., 206; Lauber, et al., 2016; 2018). Thes conflicting findings

1301 presented here relative to prior work may be due to exclusive investigation of the DS in this study,

1302 therefore eliminating potential differences that may arise due to altered colocalisation within the central

1303 striatum (Lee, et al., 2012).

1304 No significant differences in the relative expression of pvalb, hapln1, tnr, or acan mRNA were identified

1305 between sex, with and without respect to strain.

1306 (4.4) Altered PV and PNN expression in BTBR mice relative to Developmental Stage, Sex and

1307 DS Subregion

1308 The protracted maturation of PV+FSIs has been suggested to increase their efficacy as powerful

1309 inhibitors across development, however this may also underlie a particular vulnerability of these neurons

1310 to pathological disruption in conditions such as ASD (Plotkin, et al., 2005; Topchiy, et al., 2024). The

1311 postnatal morphological development of the striatum reportedly follows an inverted "U" shape, with peak

1312 volume in late childhood, reflected by reports of increased PV+FSI density in the striatum through

1313 development (Langen, et al., 2009; Hazlett, et al., 2024; Eto, et al., 2010; O'Connor, et al., 2019). In

1314 contrast, a significant reduction in the density of striatal PV+ cells was observed between PNW 3-4 and

1315 6-8 mice irrespective of sex, strain, or DS subregion. This discrepancy could be attributed to differences

1316   in the age ranges explored between studies. Striatal PV expression reportedly emerges from PND 0 from

1317   which PV+FSIs reportedly undergo significant developmentally programmed cell death, beginning with a

1318   steep drop until PND 15 when reductions slow until PND 21 in the striatum (Sreenivasan, et al., 2022).

1319   Beyond this developmental period, however, increases in PV+FSI density are reported in the striatum

1320   wholly up to PND 90, again noting a gradual slowing of PV+FSI density alteration after PND 30 (Hazlett,

1321   et al., 2024; Eto, et al., 2010; Plotkin, et al., 2005). The apparent reduction in PV+FSI density within the

1322   DS between PNW 3-4 and 6-8 mice may be attributed to synaptic pruning within this region, with PNW

1323   6-8 mice potentially past the developmental "peak" of striatal development in adolescence earlier

1324   described (Fish, et al., 2013; Gildawie et al., 2020).

1325   Despite the temporal differences in PV+FSI density previously reported between brain regions, no

1326   significant difference in the density of PV+FSIs between the DMS and DLS of PNW 3-4 and 6-8 mice in

1327   this study, suggesting no significant temporal differences in PV+FSI density between DS subregions (Eto,

1328   et al., 2010; Gildawie, et al., 2020). Whilst PV+FSIs are reported to initially emerge following a

1329   lateromedial progression through the DS, this is suggested to occur at PNW 1-3, before the age range

1330   utilised in this study (Schlösser, et al., 1999). This may be further highlighted within this study due to the

1331   presence of defined lateromedial gradients in PV+ cell density in the DS of both PNW 3-4 and 6-8 mice.

1332   Notably, a greater density of PV+ cells was identified in male relative to female mice at PNW 3-4,

1333   however this sex difference was not observed at PNW 6-8. Further investigation of temporal differences

1334   in PV+ cell density between sexes highlights the above reduction through development to only be

1335   significant in male mice. This may imply the continued reduction of PV+FSIs to only occur in male mice

1336   through development. The potential mechanism underlying this sex difference in dynamic PV+FSI

1337   expression is hard to parse however dynamic levels of circulating gonadal hormones may play a role due

1338   to the suggested neuroprotective function of estrogen on PV+FSIs (Filice, et al., 2018; Wu, et al., 2014).

1339   Investigation of PV+FSI density in animal models of ASD is often performed utilising mice of only one

1340   developmental stage despite the inherent nature of ASD as a neurodevelopmental disorder implying

1341   alterations to occur across developmental stages. Reports of altered striatal PV+FSI density in "adult"

1342   developmental stages in animal models of ASD are mixed, with a reduction identified in the DMs of BTBR

1343   mice whereas no significant differences were observed in SHANK3B-/-. CNTNAP2-/-, and VPA mice

1344   (Briones, et al., 2022; Ghandi, et al., 2023). In contrast this study observed an increased dorsostriatal

1345   PV+FSI density in BTBR mice at PNW 6-8. This conflicting finding may be due to the striatal region

1346   investigated, as greater densities of PV+FSIs in the DLS of BTBR have been previously identified (see

1347   section (4.2)). Within the dorsal striatum of PNW 3-4 mice, a reduced density of PV+FSIs was noted in

1348   BTBR mice relative to C57 mice, in agreement with previous reports in the striatum wholly in VPA,

1349   CNTNAP2-/-, and SHANK3B-/- mice (Lauber, et al., 2016; 2018; Filice, et al., 2020).

1350   Though more pertinently, investigation of multiple developmental stages in this study permits the

1351   assessment of PV+FSI density on a temporal axis. A reduction in the density of PV+FSIs was maintained

1352   in C57 mice through development, but strikingly no significant difference in PV+ cell density was

1353   identified in BTBR mice. This may suggest typical pruning of PV+FSIs to not occur in BTBR mice.

1354   Alterations in synaptic pruning have been previously identified in ASD, with dysregulation suggested to

1355   contribute to attenuated signal to noise ratio and hyperconnectivity in ASD (Beopoulous, et al., 2022;

1356   Xiong, et al., 2023; Abbott, et al., 2018). This potential altered temporal development of PV+FSI

1357   expression in ASD may speak to the observed RRBI phenotype as the persistence of stereotyped

1358   behaviours, through present within all children in early life, prolonged past expected developmental

1359   reductions classifies motor stereotypies as pathological in conditions such as ASD (Kohls, et al., 2014;

1360   Kumar, et al., 2022). When further considered with respect to sex, a greater density of PV+ cells is

1361   specifically apparent in female BTBR mice at PNW 6-8, relative to age- and sex- matched C57 mice.

1362   Whereas general trends of reduced PV+FSI density are apparent within all other BTBR subgroups, The

1363   potential impact of this morphological difference in the DS of female BTBR mice is hard to parse without

1364   further investigation, though it is notable that the greatest difference in PV+FSI densities between DS

1365   subregions was observed in this subgroup.

1366   Despite previous reports of increased PV protein expression and related relative intensity of PV staining

1367   through development, no significant difference in the relative fluorescent intensity of PV staining was

1368   identified between developmental stages in this study (Ueno, et al., 2017; Woodard & Coutellier, 2021).

1369   Reflecting the developmental differences observed in PV+ cell density at PNW 3-4 and 6-8, a significant

1370   reduction in PNN+ cell density was observed throughout the DS in this study. Few similar investigations

1371   of PNN density through development have been conducted within this age range, however an

1372   investigation of PNN density between PND 10 and 40 did identify a trend towards PNN density

1373   reduction between PND 21 and 40 (Lee & Lee, 2021).

1374   No significant difference in the density of PV+PNN+ colocalised cells was observed between PNW 3-4

1375   and 6-8 within the DS wholly, but temporal alterations similar to those observed for PV+ cell density

1376   between mouse strains were noted for PV+PNN+ cell density. Whilst further investigation of temporal

1377   differences in PV-PNN colocalisation found no significant difference in the percentage of PV+ cells with

1378   colocalised PNN staining in the DS of PNW 3-4 and 6-8 mice, a significantly greater proportion of PNN+

1379   cell with colocalised PV staining was observed in PNW 6-8 mice relative to PNW 3-4 mice. This may

1380   indicate colocalisation of PV and PNNs to still be increasing within this stage of development. With

1381   consideration of sex and DS subregion, the difference in the percentage of PNN+ cells with colocalised

1382   PV staining appears more clearly, with greater subregional differences in colocalisation observed in PNW

1383   3-4 female mice, due to a lower % of PNN+ cells with colocalised PV staining within the DMS noted to

1384   be increased at PNW 6-8.

1385   Whilst the relative expression of pvalb, hapln1, tnr, and acan mRNA were not significantly different

1386   between developmental stages in this study, consideration of mouse strain and sex emphasised

1387   emerging differences between sexes present in BTBR mice that were not seen in C57 mice for any gene

1388   of interest. A significantly greater relative expression of plvalb, hapln1, and tnr mRNA was identified in in

1389   in female PNW 3-4 BTBR mice relative to age- and strain- matched males, though no significant sex

1390   difference in acan mRNA expression in juvenile BTBR mice. Further, a greater expression of hapln1 mRNA

1391   was identified in male PNW 6-8 BTBR mice relative to age- and strain- matched females. To our

1392   knowledge these alterations the relative expression in PNN associated genes has not previously been

1393   reported in the BTBR model and the potential functional implications of these complex multi-way

1394   interactions of gene expression in the dorsal striatum in BTBR mice on PV+FSI morphology and function

1395   are yet to be elucidated but may present a prime starting point for future research.

1396   However, it is important to acknowledge the difference between the calculated total sample size of 54

1397   (from G*Power, see appendix A) and the actual sample size of 40 for IHC, and 34 for qPCR analysis. This

1398   discord between the calculated and actual sample size was due combines resource constraints on

1399   available animal tissue in conjunction with the low yield of RNA available from FFPE tissue. FFPE brain

1400   tissue is often considered suboptimal for gene expression analysis due to the low yield of quality RNA

1401   which is typically extracted (Mathieson & Thomas, 2019). RNA fragmentation in these samples can occur

1402   due to formalin exposure wherein RNA becomes crosslinked with DNA and proteins which, when

1403   dissociated during RNA purification, can lead to severe RNA fragmentation (Zeka, et al., 2016; Mathieson

1404   & Thomas, 2019). This RNA fragmentation can lead to reduced qPCR sensitivity and reproducibility,

1405   reflected by the higher Cq values obtained in this study. Typically, higher Cq values (reflecting a lower

1406 RNA yield) would suggest for increasing the input of RNA, however due to the initial limited tissue

1407 available this was not possible. In turn, the qPCR data collected in this study did not near the calculated

1408 total sample size by the initial power analysis. Therefore, caution must be taken in interpreting these

1409 results due to the increased risk of type 1 and type 2 errors. Future studies may wish to replicate this

1410 study of BTBR mice with fresh-frozen tissue which typically results in a higher quality and yield of RNA

1411 for a more reliable comparison with prior gene expression studies by Filice, et al., (2016) and Lauber, et

1412 al., (2016), with an n of 5/6 for each group investigated.

1413

1414 (5.0) Conclusion

1415 The aim of this study was to explore potential differences in PV and PNN expression in PV+FSIs

1416 of the dorsal striatum relative to DS subregion (DMS and DLS), sex, and developmental stage (PNW 3-4

1417 and PNW 6-8) between C57 and BTBR mice, an idiopathic model of ASD. To our knowledge this was the

1418 first study to identify sex differences in PV+ and PV+PNN+ cell density between the DMS and DLS in

1419 typical development, with this sex difference maintained in BTBR mice. The similar differences observed

1420 in BTBR mice from these differential baselines may contribute to the observed sexually dimorphic profile

1421 in ASD with regards to RRBI expression. This study also noted no reduction in PV+FSI density within

1422 BTBR mice through development, potentially explaining previous contradictory findings of PV+FSI

1423 expression in ASD models investigated in juvenile and adult stages separately. Further research may

1424 consider if PV+FSI alterations in these DS subregions in male or female mice may have differential

1425 impacts on the generation ASD-like behaviour.

1426

1427

1428

1429

1430

1431

References

Abbott, A. E., Linke, A. C., Nair, A., Jahedi, A., Alba, L. A., Keown, C. L., Fishman, I., & Müller, R. A. (2018). Repetitive behaviors in autism are linked to imbalance of corticostriatal connectivity: a functional connectivity MRI study. *Social cognitive and affective neuroscience*, *13*(1), 32-42.

Adak, P., Banerjee, N., Sinha, S., & Bandyopadhyay, A. K. (2023). Gamma-aminobutyric acid type A receptor variants are associated with autism spectrum disorders. *Journal of Molecular Neuroscience*, *73*(4), 237-249.

American Psychiatric Association (2013). Diagnostic and statistical manual of mental disorders.

Ariza, J., Rogers, H., Hashemi, E., Noctor, S. C., & Martínez-Cerdeño, V. (2018). The number of chandelier and basket cells are differentially decreased in prefrontal cortex in autism. *Cerebral Cortex*, *28*(2), 411-420.

Azim, E., Jabaudon, D., Fame, R. M., & Macklis, J. D. (2009). SOX6 controls dorsal progenitor identity and interneuron diversity during neocortical development. *Nature neuroscience*, *12*(10), 1238-1247.

Balmer, T. S. (2016). Perineuronal nets enhance the excitability of fast-spiking neurons. *ENeuro*, *3*(4).

Balmer, T. S., Carels, V. M., Frisch, J. L., & Nick, T. A. (2009). Modulation of perineuronal nets and parvalbumin with developmental song learning. *Journal of Neuroscience*, *29*(41), 12878-12885.

Bengtsson Gonzales, C., Hunt, S., Munoz-Manchado, A. B., McBain, C. J., & Hjerling-Leffler, J. (2020). Intrinsic electrophysiological properties predict variability in morphology and connectivity among striatal Parvalbumin-expressing Pthlh-cells. *Scientific Reports*, *10*(1), 15680.

Beopoulos, A., Géa, M., Fasano, A., & Iris, F. (2022). Autism spectrum disorders pathogenesis: Toward a comprehensive model based on neuroanatomic and neurodevelopment considerations. *Frontiers in Neuroscience*, *16*, 988735.

Bolam, J. P., Clarke, D. J., Smith, A. D., & Somogyi, P. (1983). A type of aspiny neuron in the rat neostriatum accumulates [3H] γ-aminobutyric acid: combination of Golgi-staining, autoradiography, and electron microscopy. *Journal of Comparative Neurology*, *213*(2), 121-134.

1457 Boyd, B. A., McDonough, S. G., Rupp, B., Khan, F., & Bodfish, J. W. (2011). Effects of a family-

1458 implemented treatment on the repetitive behaviors of children with autism. Journal of autism and

1459 developmental disorders, 41, 1330-1341.

1460 Brandenburg, C., & Blatt, G. J. (2022). Region-specific alterations of perineuronal net expression in

1461 postmortem autism brain tissue. *Frontiers in Molecular Neuroscience*, *15*, 838918.

1462 Briones, B. A., Pitcher, M. N., Fleming, W. T., Libby, A., Diethorn, E. J., Haye, A. E., MacDowell, C.J., Zynch,

1463 A.D., Waters, R.C., Buschman, T.J., Witten, I.B., & Gould, E. (2022). Perineuronal nets in the dorsomedial

1464 striatum contribute to behavioral dysfunction in mouse models of excessive repetitive

1465 behavior. *Biological Psychiatry Global Open Science*, *2*(4), 460-469.

1466 Bruining, H., Hardstone, R., Juarez-Martinez, E. L., Sprengers, J., Avramiea, A. E., Simpraga, S., Houtman,

1467 S.J., Poil, S., Dallares, E., Palva, S., Oranje, B., Palva, J.M., Mansvelder, H.D., & Linkenkaer-Hansen, K.

1468 (2020). Measurement of excitation-inhibition ratio in autism spectrum disorder using critical brain

1469 dynamics. *Scientific reports*, *10*(1), 9195.

1470 Burket, J. A., Webb, J. D., & Deutsch, S. I. (2021). Perineuronal nets and metal cation concentrations in

1471 the microenvironments of fast-spiking, parvalbumin-expressing GABAergic interneurons: relevance to

1472 neurodevelopment and neurodevelopmental disorders. Biomolecules, 11(8), 1235.

1473 Carayol, J., Schellenberg, G. D., Dombroski, B., Genin, E., Rousseau, F., & Dawson, G. (2011). Autism risk

1474 assessment in siblings of affected children using sex-specific genetic scores. *Molecular autism*, *2*, 1-8.

1475 Carceller, H., Gramuntell, Y., Klimczak, P., & Nacher, J. (2023). Perineuronal nets: subtle structures with

1476 large implications. *The Neuroscientist*, *29*(5), 569-590.

1477 Carceller, H., Guirado, R., Ripolles-Campos, E., Teruel-Marti, V., & Nacher, J. (2020). Perineuronal nets

1478 regulate the inhibitory perisomatic input onto parvalbumin interneurons and γ activity in the prefrontal

1479 cortex. *Journal of Neuroscience*, *40*(26), 5008-5018.

1480 Carvalho Pereira, A., Violante, I. R., Mouga, S., Oliveira, G., & Castelo-Branco, M. (2018). Medial frontal

1481 lobe neurochemistry in autism spectrum disorder is marked by reduced N-acetylaspartate and unchanged

1482 gamma-aminobutyric acid and glutamate+ glutamine levels. *Journal of Autism and Developmental*

1483 *Disorders*, *48*, 1467-1482.

1484   Casanova, M. F., Casanova, E. L., Frye, R. E., Baeza-Velasco, C., LaSalle, J. M., Hagerman, R. J., Scherer,

1485   S.W., & Natowicz, M. R. (2020). Secondary vs. idiopathic autism. Frontiers in psychiatry, 11, 297.

1486   Cellot, G., & Cherubini, E. (2013). Functional role of ambient GABA in refining neuronal circuits early in

1487   postnatal development. Frontiers in neural circuits, 7, 136.

1488   Chapman, J. R., & Waldenström, J. (2015). With reference to reference genes: a systematic review of

1489   endogenous controls in gene expression studies. *PloS one*, *10*(11), e0141853.

1490   Ciccarelli, A., Weijers, D., Kwan, W., Warner, C., Bourne, J., & Gross, C. T. (2021). Sexually dimorphic

1491   perineuronal nets in the rodent and primate reproductive circuit. *Journal of Comparative*

1492   *Neurology*, *529*(13), 3274-3291.

1493   Cox, N. J. (2011). Stata tip 96: Cube roots. The stata journal, 11(1), 149-154.

1494   D'Cruz, A. M., Ragozzino, M. E., Mosconi, M. W., Shrestha, S., Cook, E. H., & Sweeney, J. A. (2013).

1495   Reduced behavioral flexibility in autism spectrum disorders. *Neuropsychology*, *27*(2), 152.

1496   Deemyad, T., M. Janeček, Y. Shih, V. Valle, A. D'Agostino, M. S. Perez, K. D. Ketchesin, S. da Silva, and R.

1497   T. Peixoto. "Striatal output regulates the postnatal maturation of cortical circuits." (2024).

1498   Delmonte, S., Gallagher, L., O'hanlon, E., McGrath, J., & Balsters, J. H. (2013). Functional and structural

1499   connectivity of frontostriatal circuitry in Autism Spectrum Disorder. *Frontiers in human neuroscience*, *7*,

1500   430.

1501   Di, J., Li, J., O'Hara, B., Alberts, I., Xiong, L., Li, J., & Li, X. (2020). The role of GABAergic neural circuits in

1502   the pathogenesis of autism spectrum disorder. *International Journal of Developmental*

1503   *Neuroscience*, *80*(2), 73-85.

1504   Dorsey, S. G., Mocci, E., Lane, M. V., & Krueger, B. K. (2023). Rapid effects of valproic acid on the fetal

1505   brain transcriptome: Implications for brain development and autism. *Research Square*. [PREPRINT]

1506   Drago, A., Calabro, M., Crisafulli, C., & Rasmussen, S. K. (2018). Genetic Insights from a Molecular

1507   Pathway Analysis on Two Independent Samples of Autistic Patients. *J Mol Genet Med*, *12*(326), 1747-

1508   0862.

1509 Dufour, B. D., McBride, E., Bartley, T., Juarez, P., & Martínez-Cerdeño, V. (2023). Distinct patterns of
1510 GABAergic interneuron pathology in autism are associated with intellectual impairment and stereotypic
1511 behaviors. *Autism*, *27*(6), 1730-1745.

1512 Dutta, S., & Sengupta, P. (2016). Men and mice: relating their ages. *Life sciences*, *152*, 244-248.

1513 Edmondson, D. A., Xia, P., McNally Keehn, R., Dydak, U., & Keehn, B. (2020). A magnetic resonance
1514 spectroscopy study of superior visual search abilities in children with autism spectrum disorder. *Autism*
1515 *Research*, *13*(4), 550-562.

1516 Elkin, L. A., Kay, M., Higgins, J. J., & Wobbrock, J. O. (2021, October). An aligned rank transform
1517 procedure for multifactor contrast tests. In *The 34th annual ACM symposium on user interface software*
1518 *and technology* (pp. 754-768).

1519 Ellegood, J., Babineau, B. A., Henkelman, R. M., Lerch, J. P., & Crawley, J. N. (2013). Neuroanatomical
1520 analysis of the BTBR mouse model of autism using magnetic resonance imaging and diffusion tensor
1521 imaging. *Neuroimage*, *70*, 288-300.

1522 Eskici, N. F., Erdem-Ozdamar, S., & Dayangac-Erden, D. (2018). The altered expression of perineuronal
1523 net elements during neural differentiation. *Cellular & molecular biology letters*, *23*, 1-12.

1524 Eto, R., Abe, M., Kimoto, H., Imaoka, E., Kato, H., Kasahara, J., & Araki, T. (2010). Alterations of
1525 interneurons in the striatum and frontal cortex of mice during postnatal development. *International*
1526 *Journal of Developmental Neuroscience*, *28*(5), 359-370.

1527 Evans, M. M., Kim, J., Abel, T., Nickl-Jockschat, T., & Stevens, H. E. (2024). Developmental disruptions of
1528 the dorsal striatum in autism spectrum disorder. *Biological Psychiatry*, *95*(2), 102-111.

1529 Ey, E., Leblond, C. S., & Bourgeron, T. (2011). Behavioral profiles of mouse models for autism spectrum
1530 disorders. Autism research, 4(1), 5-16.

1531 Fatemi, S. H., Reutiman, T. J., Folsom, T. D., Rooney, R. J., Patel, D. H., & Thuras, P. D. (2010). mRNA and
1532 protein levels for GABA A α4, α5, β1 and GABA B R1 receptors are altered in brains from subjects with
1533 autism. *Journal of autism and developmental disorders*, *40*, 743-750.

1534 Fatemi, S. H., Reutiman, T. J., Folsom, T. D., Rustan, O. G., Rooney, R. J., & Thuras, P. D. (2014).

1535 Downregulation of GABA A receptor protein subunits α6, β2, δ, ε, γ2, θ, and ρ2 in superior frontal cortex

1536 of subjects with autism. *Journal of autism and developmental disorders*, *44*, 1833-1845.

1537 Faul, F., Erdfelder, E., Lang, A.-G., & Buchner, A. (2007). G*Power 3: A flexible statistical power analysis

1538 program for the social, behavioral, and biomedical sciences. *Behavior Research Methods*, *39*, 175-191.

1539 Fawcett, J. W., Oohashi, T., & Pizzorusso, T. (2019). The roles of perineuronal nets and the perinodal

1540 extracellular matrix in neuronal function. *Nature Reviews Neuroscience*, *20*(8), 451-465.

1541 Ferguson, B. R., & Gao, W. J. (2018). PV interneurons: critical regulators of E/I balance for prefrontal

1542 cortex-dependent behavior and psychiatric disorders. *Frontiers in neural circuits*, *12*, 37.

1543 Ferhat, A. T., Halbedl, S., Schmeisser, M. J., Kas, M. J., Bourgeron, T., & Ey, E. (2017). Behavioural

1544 phenotypes and neural circuit dysfunctions in mouse models of autism spectrum disorder. Translational

1545 anatomy and cell biology of autism spectrum disorder, 85-101.

1546 Filice, F., Janickova, L., Henzi, T., Bilella, A., & Schwaller, B. (2020). The parvalbumin hypothesis of autism

1547 spectrum disorder. *Frontiers in Cellular Neuroscience*, *14*, 577525.

1548 Filice, F., Vörckel, K. J., Sungur, A. Ö., Wöhr, M., & Schwaller, B. (2016). Reduction in parvalbumin

1549 expression not loss of the parvalbumin-expressing GABA interneuron subpopulation in genetic

1550 parvalbumin and shank mouse models of autism. *Molecular brain*, *9*, 1-17.

1551 Fino, E., Vandecasteele, M., Perez, S., Saudou, F., & Venance, L. (2018). Region-specific and state-

1552 dependent action of striatal GABAergic interneurons. *Nature communications*, *9*(1), 3339.

1553 Fiorentino, H., Kuczewski, N., Diabira, D., Ferrand, N., Pangalos, M. N., Porcher, C., & Gaiarsa, J. L. (2009).

1554 GABAB receptor activation triggers BDNF release and promotes the maturation of GABAergic synapses.

1555 Journal of Neuroscience, 29(37), 11650-11661.

1556 Fish, K. N., Hoftman, G. D., Sheikh, W., Kitchens, M., & Lewis, D. A. (2013). Parvalbumin-containing

1557 chandelier and basket cell boutons have distinctive modes of maturation in monkey prefrontal

1558 cortex. *Journal of Neuroscience*, *33*(19), 8352-8358.

1559 Fuccillo, M. V. (2016). Striatal circuits as a common node for autism pathophysiology. *Frontiers in*

1560 *neuroscience*, *10*, 27.

1561 Gandhi, T., Liu, C. C., Adeyelu, T. T., Canepa, C. R., & Lee, C. C. (2023). Behavioral regulation by

1562 perineuronal nets in the prefrontal cortex of the CNTNAP2 mouse model of autism spectrum

1563 disorder. *Frontiers in Behavioral Neuroscience*, *17*, 1114789.

1564 Gandhi, T., Liu, C. C., Adeyelu, T. T., Canepa, C. R., & Lee, C. C. (2023). Behavioral regulation by

1565 perineuronal nets in the prefrontal cortex of the CNTNAP2 mouse model of autism spectrum

1566 disorder. *Frontiers in Behavioral Neuroscience*, *17*, 1114789.

1567 Giamanco, K. A., & Matthews, R. T. (2012). Deconstructing the perineuronal net: cellular contributions

1568 and molecular composition of the neuronal extracellular matrix. *Neuroscience*, *218*, 367-384.

1569 Gildawie, K. R., Honeycutt, J. A., & Brenhouse, H. C. (2020). Region-specific effects of maternal separation

1570 on perineuronal net and parvalbumin-expressing interneuron formation in male and female

1571 rats. *Neuroscience*, *428*, 23-37.

1572 Gonçalves, J., Violante, I. R., Sereno, J., Leitão, R. A., Cai, Y., Abrunhosa, A., Silva, A.P., Silva, A.J., &

1573 Castelo-Branco, M. (2017). Testing the excitation/inhibition imbalance hypothesis in a mouse model of

1574 the autism spectrum disorder: in vivo neurospectroscopy and molecular evidence for regional

1575 phenotypes. *Molecular Autism*, *8*, 1-8.

1576 Gritton, H. J., Howe, W. M., Romano, M. F., DiFeliceantonio, A. G., Kramer, M. A., Saligrama, V., Bucklin,

1577 M.E., Zemel, D., & Han, X. (2019). Unique contributions of parvalbumin and cholinergic interneurons in

1578 organizing striatal networks during movement. *Nature neuroscience*, *22*(4), 586-597.

1579 Han, S., Tai, C., Jones, C. J., Scheuer, T., & Catterall, W. A. (2014). Enhancement of inhibitory

1580 neurotransmission by GABAA receptors having α2, 3-subunits ameliorates behavioral deficits in a mouse

1581 model of autism. *Neuron*, *81*(6), 1282-1289.

1582 Hanssen, K. Ø., Grødem, S., Fyhn, M., Hafting, T., Einevoll, G. T., Ness, T. V., & Halnes, G. (2023).

1583 Responses in fast-spiking interneuron firing rates to parameter variations associated with degradation of

1584 perineuronal nets. *Journal of Computational Neuroscience*, *51*(2), 283-298.

1585 Hashemi, E., Ariza, J., Rogers, H., Noctor, S. C., & Martínez-Cerdeño, V. (2017). The number of

1586 parvalbumin-expressing interneurons is decreased in the prefrontal cortex in autism. *Cerebral*

1587 *cortex*, *27*(3), 1931-1943.

1588 Hazlett, M. F., Hall, V. L., Patel, E., Halvorsen, A., Calakos, N., & West, A. E. (2024). The Perineuronal Net

1589 Protein Brevican Acts in Nucleus Accumbens Parvalbumin-Expressing Interneurons of Adult Mice to

1590 Regulate Excitatory Synaptic Inputs and Motivated Behaviors. *Biological Psychiatry*.

1591 Hong, T., Falcone, C., Dufour, B., Amina, S., Castro, R. P., Regalado, J., Pearson, W., Noctor, S.C., &

1592 Martínez-Cerdeño, V. (2020). GABAARα2 is decreased in the axon initial segment of pyramidal cells in

1593 specific areas of the prefrontal cortex in autism. *Neuroscience*, *437*, 76-86.

1594 Horder, J., Petrinovic, M. M., Mendez, M. A., Bruns, A., Takumi, T., Spooren, W., Barker, G.J., Künnecke, B.,

1595 & Murphy, D. G. (2018). Glutamate and GABA in autism spectrum disorder—a translational magnetic

1596 resonance spectroscopy study in man and rodent models. *Translational psychiatry*, *8*(1), 106.

1597 Hussman, J. P., Chung, R. H., Griswold, A. J., Jaworski, J. M., Salyakina, D., Ma, D., Konidari, I, Whitehead,

1598 P.L., Vance, J., Martin, E.R., Cuccaro, M.L., Gilbert, J.R., Haines, J.L., & Pericak-Vance, M. A. (2011). A

1599 noise-reduction GWAS analysis implicates altered regulation of neurite outgrowth and guidance in

1600 autism. *Molecular autism*, *2*, 1-16.

1601 Ikeda, Y., Nishiyama, N., Saito, H., & Katsuki, H. (1997). GABAA receptor stimulation promotes survival of

1602 embryonic rat striatal neurons in culture. Developmental Brain Research, 98(2), 253-258.

1603 Inan, M., Zhao, M., Manuszak, M., Karakaya, C., Rajadhyaksha, A. M., Pickel, V. M., ... & Manfredi, G.

1604 (2016). Energy deficit in parvalbumin neurons leads to circuit dysfunction, impaired sensory gating and

1605 social disability. *Neurobiology of disease*, *93*, 35-46.

1606 Jakovljević, A., Tucić, M., Blažiková, M., Korenić, A., Missirlis, Y., Stamenković, V., & Andjus, P. (2021).

1607 Structural and functional modulation of perineuronal nets: in search of important players with highlight

1608 on tenascins. *Cells*, *10*(6), 1345.

1609 John, U., Patro, N., & Patro, I. (2022). Perineuronal nets: Cruise from a honeycomb to the safety

1610 nets. *Brain Research Bulletin*, *190*, 179-194.

1611 Kita, H., & Kitai, S. T. (1990). Amygdaloid projections to the frontal cortex and the striatum in the

1612 rat. *Journal of Comparative Neurology*, *298*(1), 40-49.

1613 Kohls, G., Yerys, B. E., & Schultz, R. T. (2014). Striatal development in autism: repetitive behaviors and

1614 the reward circuitry. *Biological Psychiatry*, *76*(5), 358-359.

1615 Kolodny, T., Schallmo, M. P., Gerdts, J., Edden, R. A., Bernier, R. A., & Murray, S. O. (2020). Concentrations

1616 of cortical GABA and glutamate in young adults with autism spectrum disorder. *Autism Research*, *13*(7),

1617 1111-1129.

1618 Kumar, N. S., Malhi, P., Bharti, B., & Saini, L. (2022). Restricted and Repetitive Behaviors and Interests in

1619 Young Children with Autism: A Comparative Study. *Indian Journal of Pediatrics*, *89*(12), 1216-1221.

1620 Langen, M., Schnack, H. G., Nederveen, H., Bos, D., Lahuis, B. E., de Jonge, M. V., Engeland, H., & Durston,

1621 S. (2009). Changes in the developmental trajectories of striatum in autism. *Biological psychiatry*, *66*(4),

1622 327-333.

1623 Lauber, E., Filice, F., & Schwaller, B. (2016). Prenatal valproate exposure differentially affects

1624 parvalbumin-expressing neurons and related circuits in the cortex and striatum of mice. *Frontiers in*

1625 *molecular neuroscience*, *9*, 150.

1626 Lauber, E., Filice, F., & Schwaller, B. (2018). Dysregulation of parvalbumin expression in the Cntnap2−/−

1627 mouse model of autism spectrum disorder. *Frontiers in molecular neuroscience*, *11*, 262.

1628 Lee, D. K. (2020). Data transformation: a focus on the interpretation. *Korean journal of*

1629 *anesthesiology*, *73*(6), 503-508.

1630 Lee, H., Leamey, C. A., & Sawatari, A. (2008). Rapid reversal of chondroitin sulfate proteoglycan

1631 associated staining in subcompartments of mouse neostriatum during the emergence of behaviour. *PLoS*

1632 *One*, *3*(8), e3020.

1633 Lee, H., Leamey, C. A., & Sawatari, A. (2012). Perineuronal nets play a role in regulating striatal function

1634 in the mouse. *PloS one*, *7*(3), e32747.

1635 Lee, J., & Lee, K. (2021). Parvalbumin-expressing GABAergic interneurons and perineuronal nets in the

1636 prelimbic and orbitofrontal cortices in association with basal anxiety-like behaviors in adult

1637 mice. *Behavioural Brain Research*, *398*, 112915.

1638 Lee, Y., Kim, H., Kim, J. E., Park, J. Y., Choi, J., Lee, J. E., Lee, E.H., & Han, P. L. (2018). Excessive D1

1639 dopamine receptor activation in the dorsal striatum promotes autistic-like behaviors. *Molecular*

1640 *neurobiology*, *55*, 5658-5671.

1641   Lefebvre, A., Traut, N., Pedoux, A., Maruani, A., Beggiato, A., Elmaleh, M., Germanaud, D., Amestoy, A., Ly-

1642   Le Moal, M., Chatham, C., Murtagh, L., Bouvard, M., Alisson, M., Lenoyer, M., Bourgeron, T., Toro, R.,

1643   Dumax, G., Moreau, C., & Delorme, R. (2023). Exploring the multidimensional nature of repetitive and

1644   restricted behaviors and interests (RRBI) in autism: neuroanatomical correlates and clinical

1645   implications. *Molecular Autism*, *14*(1), 45.

1646   Lupori, L., Totaro, V., Cornuti, S., Ciampi, L., Carrara, F., Grilli, E., Vigilone, A., Tozzi, F., Putignano, E.,

1647   Mazzoitti, R., Amato, G., Gennaro, C., Tognino, P., & Pizzorusso, T. (2023). A comprehensive atlas of

1648   perineuronal net distribution and colocalization with parvalbumin in the adult mouse brain. *Cell*

1649   *Reports*, *42*(7).

1650   Mangiafico, S. S. (2016). Summary and analysis of extension program evaluation in R. *Rutgers*

1651   *Cooperative Extension: New Brunswick, NJ, USA*, *125*, 16-22.

1652   Mathieson, W., & Thomas, G. (2019). Using FFPE tissue in genomic analyses: advantages, disadvantages

1653   and the role of biospecimen science. Current Pathobiology Reports, 7, 35-40.

1654   McConkey, R. (2020). The rise in the numbers of pupils identified by schools with autism spectrum

1655   disorder (ASD): A comparison of the four countries in the United Kingdom. *Support for learning*, *35*(2),

1656   132-143.

1657   McDonald, J. H. (2009). *Handbook of biological statistics* (Vol. 2, pp. 6-59). Baltimore, MD: sparky house

1658   publishing.

1659   Melo, C., Ruano, L., Jorge, J., Pinto Ribeiro, T., Oliveira, G., Azevedo, L., & Temudo, T. (2020). Prevalence

1660   and determinants of motor stereotypies in autism spectrum disorder: A systematic review and meta-

1661   analysis. *Autism*, *24*(3), 569-590.

1662   Miyata, S., & Kitagawa, H. (2017). Formation and remodeling of the brain extracellular matrix in neural

1663   plasticity: Roles of chondroitin sulfate and hyaluronan. *Biochimica et Biophysica Acta (BBA)-General*

1664   *Subjects*, *1861*(10), 2420-2434.

1665   Molenhuis, R. T., de Visser, L., Bruining, H., & Kas, M. J. (2014). Enhancing the value of psychiatric mouse

1666   models; differential expression of developmental behavioral and cognitive profiles in four inbred strains

1667   of mice. *European Neuropsychopharmacology*, *24*(6), 945-954.

1668   Monteiro, P., Barak, B., Zhou, Y., McRae, R., Rodrigues, D., Wickersham, I. R., & Feng, G. (2018).

1669   Dichotomous parvalbumin interneuron populations in dorsolateral and dorsomedial striatum. *The Journal*

1670   *of physiology*, *596*(16), 3695-3707.

1671   Mostert-Kerckhoffs, M. A., Staal, W. G., Houben, R. H., & de Jonge, M. V. (2015). Stop and change:

1672   Inhibition and flexibility skills are related to repetitive behavior in children and young adults with autism

1673   spectrum disorders. *Journal of autism and developmental disorders*, *45*, 3148-3158.

1674   Mueller-Buehl, C., Reinhard, J., Roll, L., Bader, V., Winklhofer, K. F., & Faissner, A. (2022). Brevican,

1675   neurocan, tenascin-C, and tenascin-R act as important regulators of the interplay between perineuronal

1676   nets, synaptic integrity, inhibitory interneurons, and Otx2. *Frontiers in Cell and Developmental*

1677   *Biology*, *10*, 886527.

1678   Mueller-Buehl, C., Wegrzyn, D., Bauch, J., & Faissner, A. (2023). Regulation of the E/I-balance by the

1679   neural matrisome. *Frontiers in Molecular Neuroscience*, *16*, 1102334.

1680   Nardi, L., Chhabra, S., Leukel, P., Krueger-Burg, D., Sommer, C. J., & Schmeisser, M. J. (2023).

1681   Neuroanatomical changes of ionotropic glutamatergic and GABAergic receptor densities in male mice

1682   modeling idiopathic and syndromic autism spectrum disorder. *Frontiers in Psychiatry*, *14*, 1199097.

1683   O'Connor, A. M., Burton, T. J., Mansuri, H., Hand, G. R., Leamey, C. A., & Sawatari, A. (2019).

1684   Environmental enrichment from birth impacts parvalbumin expressing cells and wisteria floribunda

1685   agglutinin labelled peri-neuronal nets within the developing murine striatum. *Frontiers in*

1686   *neuroanatomy*, *13*, 90.

1687   O'Hare, J. K., Li, H., Kim, N., Gaidis, E., Ade, K., Beck, J., ... & Calakos, N. (2017). Striatal fast-spiking

1688   interneurons selectively modulate circuit output and are required for habitual behavior. *Elife*, *6*, e26231.

1689   Oohashi, T., Edamatsu, M., Bekku, Y., & Carulli, D. (2015). The hyaluronan and proteoglycan link proteins:

1690   Organizers of the brain extracellular matrix and key molecules for neuronal function and

1691   plasticity. *Experimental neurology*, *274*, 134-144.

1692   Owens, D. F., & Kriegstein, A. R. (2002). Is there more to GABA than synaptic inhibition?. Nature Reviews

1693   Neuroscience, 3(9), 715-727.

1694   Parikshak, N. N., Swarup, V., Belgard, T. G., Irimia, M., Ramaswami, G., Gandal, M. J., Harlt, C., Leppa, V.,

1695   Ubieta, L., Huang, J., Lowe, J.K., Blencowe, B. J, Horvath, S., & Geschwind, D. H. (2016). Genome-wide

1696   changes in lncRNA, splicing, and regional gene expression patterns in autism. *Nature*, *540*(7633), 423-

1697   427.

1698   Paxinos, G. & Franklin, K. (2007). The Mouse Brain in Stereotaxic Coordinates. 3rd ed. New York:

1699   Elsevier/Academic Press.

1700   Pellicano, E., Dinsmore, A., & Charman, T. (2014). What should autism research focus upon? Community

1701   views and priorities from the United Kingdom. *Autism*, *18*(7), 756-770.

1702   Plotkin, J. L., Wu, N., Chesselet, M. F., & Levine, M. S. (2005). Functional and molecular development of

1703   striatal fast-spiking GABAergic interneurons and their cortical inputs. *European Journal of*

1704   *Neuroscience*, *22*(5), 1097-1108.

1705   Plueckebaum, H., Meyer, L., Beck, A. K., & Menn, K. H. (2023). The developmental trajectory of functional

1706   excitation-inhibition balance relates to language abilities in autistic and allistic children. *Autism*

1707   *Research*, *16*(9), 1681-1692.

1708   R Core Team (2024). R: A language and environment for statistical computing. R Foundation for

1709   Statistical Computing, Vienna, Austria. URL https://www.R-project.org/.

1710   Rapanelli, M., Frick, L. R., Xu, M., Groman, S. M., Jindachomthong, K., Tamamaki, N., Tanahira, C., Taylor,

1711   J.R., & Pittenger, C. (2017). Targeted interneuron depletion in the dorsal striatum produces autism-like

1712   behavioral abnormalities in male but not female mice. *Biological psychiatry*, *82*(3), 194-203.

1713   Richler, J., Huerta, M., Bishop, S. L., & Lord, C. (2010). Developmental trajectories of restricted and

1714   repetitive behaviors and interests in children with autism spectrum disorders. *Development and*

1715   *psychopathology*, *22*(1), 55-69.

1716   Rowlands, D., Lensjø, K. K., Dinh, T., Yang, S., Andrews, M. R., Hafting, T., Fyhn, M., Fawcettm J.W., & Dick,

1717   G. (2018). Aggrecan directs extracellular matrix-mediated neuronal plasticity. *Journal of*

1718   *Neuroscience*, *38*(47), 10102-10113.

1719   Rubenstein, J. L. R., & Merzenich, M. M. (2003). Model of autism: increased ratio of excitation/inhibition in

1720   key neural systems. *Genes, Brain and Behavior*, *2*(5), 255-267.

Salari, N., Rasoulpoor, S., Rasoulpoor, S., Shohaimi, S., Jafarpour, S., Abdoli, N., Khaledi-Paveh, B., & Mohammadi, M. (2022). The global prevalence of autism spectrum disorder: a comprehensive systematic review and meta-analysis. *Italian Journal of Pediatrics*, *48*(1), 112.

Sapey-Triomphe, L. A., Lamberton, F., Sonié, S., Mattout, J., & Schmitz, C. (2019). Tactile hypersensitivity and GABA concentration in the sensorimotor cortex of adults with autism. *Autism Research*, *12*(4), 562-575.

Schlösser, B., Klausa, G., Prime, G., & Ten Bruggencate, G. (1999). Postnatal development of calretinin- and parvalbumin-positive interneurons in the rat neostriatum: An immunohistochemical study. *Journal of Comparative Neurology*, *405*(2), 185-198.

Schmidt, S., Arendt, T., Morawski, M., & Sonntag, M. (2020). Neurocan contributes to perineuronal net development. *Neuroscience*, *442*, 69-86.

Schmittgen, T. D., & Livak, K. J. (2008). Analyzing real-time PCR data by the comparative CT method. *Nature protocols*, *3*(6), 1101-1108.

Schwede, M., Nagpal, S., Gandal, M. J., Parikshak, N. N., Mirnics, K., Geschwind, D. H., & Morrow, E. M. (2018). Strong correlation of downregulated genes related to synaptic transmission and mitochondria in post-mortem autism cerebral cortex. *Journal of neurodevelopmental disorders*, *10*, 1-9.

Semple, B. D., Blomgren, K., Gimlin, K., Ferriero, D. M., & Noble-Haeusslein, L. J. (2013). Brain development in rodents and humans: Identifying benchmarks of maturation and vulnerability to injury across species. *Progress in neurobiology*, *106*, 1-16.

Shan, X., Uddin, L. Q., Xiao, J., He, C., Ling, Z., Li, L., Huang, X., Chen, H., & Duan, X. (2022). Mapping the heterogeneous brain structural phenotype of autism spectrum disorder using the normative model. *Biological Psychiatry*, *91*(11), 967-976.

Slaker, M. L., Harkness, J. H., & Sorg, B. A. (2016). A standardized and automated method of perineuronal net analysis using Wisteria floribunda agglutinin staining intensity. *IBRO reports*, *1*, 54-60.

Slaker, M., Blacktop, J. M., & Sorg, B. A. (2016). Caught in the net: perineuronal nets and addiction. *Neural plasticity*, *2016*(1), 7538208.

1747   Sohal, V. S., & Rubenstein, J. L. (2019). Excitation-inhibition balance as a framework for investigating

1748   mechanisms in neuropsychiatric disorders. *Molecular psychiatry*, *24*(9), 1248-1257.

1749   Sreenivasan, V., Serafeimidou-Pouliou, E., Exposito-Alonso, D., Bercsenyi, K., Bernard, C., Bae, S. E.,

1750   Oozeer, F., Hanusz-Godoy, A., Edwards, R. H., & Marín, O. (2022). Input-specific control of interneuron

1751   numbers in nascent striatal networks. *Proceedings of the National Academy of Sciences*, *119*(20),

1752   e2118430119.

1753   Sreenivasan, V., Serafeimidou-Pouliou, E., Exposito-Alonso, D., Bercsenyi, K., Bernard, C., Bae, S. E.,

1754   Oozenr, F., Hanusz-Godoy, A., Edwards, R.H., & Marín, O. (2022). Input-specific control of interneuron

1755   numbers in nascent striatal networks. *Proceedings of the National Academy of Sciences*, *119*(20),

1756   e2118430119.

1757   St-Pierre, Anne P., Violaine Shikon, and David C. Schneider. "Count data in biology—Data transformation

1758   or model reformation?." *Ecology and evolution* 8, no. 6 (2018): 3077-3085.

1759   Sussman, D., Leung, R. C., Vogan, V. M., Lee, W., Trelle, S., Lin, S., Cassel, D.B., Chakravarty, M.M., Lerch,

1760   J.P., Anagnoustou, E., & Taylor, M. J. (2015). The autism puzzle: Diffuse but not pervasive

1761   neuroanatomical abnormalities in children with ASD. *NeuroImage: Clinical*, *8*, 170-179.

1762   Tepper, J. M., Koós, T., Ibanez-Sandoval, O., Tecuapetla, F., Faust, T. W., & Assous, M. (2018).

1763   Heterogeneity and diversity of striatal GABAergic interneurons: update 2018. *Frontiers in*

1764   *neuroanatomy*, *12*, 91.

1765   Tepper, J. M., Tecuapetla, F., Koós, T., & Ibáñez-Sandoval, O. (2010). Heterogeneity and diversity of

1766   striatal GABAergic interneurons. *Frontiers in neuroanatomy*, *4*, 150.

1767   Thabault, M., Turpin, V., Balado, E., Fernandes-Gomes, C., Huot, A. L., Cantereau, A., Fernagut, P., Jaber,

1768   M., & Galvan, L. (2023). Age-related behavioural and striatal dysfunctions in Shank3ΔC/ΔC mouse model

1769   of autism spectrum disorder. *European Journal of Neuroscience*, *57*(4), 607-618.

1770   Todtenkopf, M. S., Stellar, J. R., Williams, E. A., & Zahm, D. S. (2004). Differential distribution of

1771   parvalbumin immunoreactive neurons in the striatum of cocaine sensitized rats. *Neuroscience*, *127*(1),

1772   35-42.

1773 Trakoshis, S., Martínez-Cañada, P., Rocchi, F., Canella, C., You, W., Chakrabarti, B., Ruigrok, A.N.V.,

1774 Bullmore, E.T., Suckling, J., Markicevic, M., Zerbi, V., Baron-Cohen, S., Gozzi, A., Lai, M., Panzeri, S., &

1775 Lombardo, M. V. (2020). Intrinsic excitation-inhibition imbalance affects medial prefrontal cortex

1776 differently in autistic men versus women. *elife*, *9*, e55684.

1777 Trent, S., Fry, J. P., Ojarikre, O. A., & Davies, W. (2014). Altered brain gene expression but not steroid

1778 biochemistry in a genetic mouse model of neurodevelopmental disorder. *Molecular Autism*, *5*, 1-11.

1779 Turner, A. H., Greenspan, K. S., & van Erp, T. G. (2016). Pallidum and lateral ventricle volume enlargement

1780 in autism spectrum disorder. *Psychiatry Research: Neuroimaging*, *252*, 40-45.

1781 Ueno, H., Suemitsu, S., Okamoto, M., Matsumoto, Y., & Ishihara, T. (2017). Parvalbumin neurons and

1782 perineuronal nets in the mouse prefrontal cortex. *Neuroscience*, *343*, 115-127.

1783 Ueno, H., Takao, K., Suemitsu, S., Murakami, S., Kitamura, N., Wani, K., Okamoto, M., Aoki, S., & Ishihara, T.

1784 (2018). Age-dependent and region-specific alteration of parvalbumin neurons and perineuronal nets in

1785 the mouse cerebral cortex. *Neurochemistry international*, *112*, 59-70.

1786 van Rooij, D., Anagnostou, E., Arango, C., Auzias, G., Behrmann, M., Busatto, G. F., Calderoni, S., Daly, E.,

1787 Deruelle, C., Di Martino, A., Dinstein, I., Duran, F. L. S., Durston, S., Ecker, C., Fair, D., Fedor, J., Fitzgerald,

1788 J., Freitag, C. M., Gallagher, L., & Gori, I. (2018). Cortical and Subcortical Brain Morphometry Differences

1789 Between Patients With Autism Spectrum Disorder and Healthy Individuals Across the Lifespan: Results

1790 From the ENIGMA ASD Working Group. American Journal of Psychiatry, 175(4), 359–369.

1791 https://doi.org/10.1176/appi.ajp.2017.17010100Topchiy, I., Mohbat, J., Folorunso, O. O., Lazcano-

1792 Etchebarne, C., & Engin, E. (2024). GABA System as the Cause and Effect in Early

1793 Development. *Neuroscience & Biobehavioral Reviews*, 105651.

1794 van't Westeinde, A., Cauvet, É., Toro, R., Kuja-Halkola, R., Neufeld, J., Mevel, K., & Bölte, S. (2020). Sex

1795 differences in brain structure: a twin study on restricted and repetitive behaviors in twin pairs with and

1796 without autism. Molecular autism, 11, 1-20.

1797 Van Zandt, M., Flanagan, D., & Pittenger, C. (2024). Sex differences in the distribution and density of

1798 regulatory interneurons in the striatum. *Frontiers in cellular neuroscience*, *18*, 1415015.

1799 https://doi.org/10.3389/fncel.2024.1415015

1800 Van't Spijker, H. M., & Richter, J. D. (2024). FMRP regulation of aggrecan mRNA translation controls

1801 perineuronal net development. *Journal of Neurochemistry*.

1802 Voorn, P., Vanderschuren, L. J., Groenewegen, H. J., Robbins, T. W., & Pennartz, C. M. (2004). Putting a

1803 spin on the dorsal–ventral divide of the striatum. *Trends in neurosciences*, *27*(8), 468-474.

1804 Wegiel, J., Flory, M., Kuchna, I., Nowicki, K., Ma, S. Y., Imaki, H., Wegiel, J., Coen, I.L., London, E.,

1805 Wisniewski, W., & Brown, W. T. (2014). Stereological study of the neuronal number and volume of 38

1806 brain subdivisions of subjects diagnosed with autism reveals significant alterations restricted to the

1807 striatum, amygdala and cerebellum. *Acta neuropathologica communications*, *2*, 1-18.

1808 Wegman, E., Wosiski-Kuhn, M., & Luo, Y. (2024). The dual role of striatal interneurons: circuit modulation

1809 and trophic support for the basal ganglia. *Neural Regeneration Research*, *19*(6), 1277-1283.

1810 Weiss, L., Arking, D., Daly, M., & Chakravarti, A. (2009). A genome-wide linkage and association scan

1811 reveals novel loci for autism. *Nature*, *461*(7265).

1812 Wingert, J. C., & Sorg, B. A. (2021). Impact of perineuronal nets on electrophysiology of parvalbumin

1813 interneurons, principal neurons, and brain oscillations: a review. *Frontiers in synaptic neuroscience*, *13*,

1814 673210.

1815 Wobbrock, J. O., Findlater, L., Gergle, D., & Higgins, J. J. (2011, May). The aligned rank transform for

1816 nonparametric factorial analyses using only anova procedures. In *Proceedings of the SIGCHI conference*

1817 *on human factors in computing systems* (pp. 143-146).

1818 Wöhr, M., Orduz, D., Gregory, P., Moreno, H., Khan, U., Vörckel, K. J., Wolger, D.P., Welzl, H., Gall, D.,

1819 Schiffmann, S.N., & Schwaller, B. (2015). Lack of parvalbumin in mice leads to behavioral deficits relevant

1820 to all human autism core symptoms and related neural morphofunctional abnormalities. *Translational*

1821 *psychiatry*, *5*(3), e525-e525.

1822 Woodward, E. M., & Coutellier, L. (2021). Age-and sex-specific effects of stress on parvalbumin

1823 interneurons in preclinical models: Relevance to sex differences in clinical neuropsychiatric and

1824 neurodevelopmental disorders. *Neuroscience & Biobehavioral Reviews*, *131*, 1228-1242.

1825 World Health Organization. (2022). ICD-11: International classification of diseases (11th revision).

1826   Wu, Y. C., Du, X., Van den Buuse, M., & Hill, R. A. (2014). Sex differences in the adolescent developmental

1827   trajectory of parvalbumin interneurons in the hippocampus: a role for

1828   estradiol. *Psychoneuroendocrinology*, *45*, 167-178.

1829   Wu, X., Fu, Y., Knott, G., Lu, J., Di Cristo, G., & Huang, Z. J. (2012). GABA signaling promotes synapse

1830   elimination and axon pruning in developing cortical inhibitory interneurons. Journal of Neuroscience,

1831   32(1), 331-343.

1832   Xia, D., Li, L., Yang, B., & Zhou, Q. (2021). Altered relationship between parvalbumin and perineuronal

1833   nets in an autism model. *Frontiers in Molecular Neuroscience*, *14*, 597812.

1834   Xiong, Y., Chen, J., & Li, Y. (2023). Microglia and astrocytes underlie neuroinflammation and synaptic

1835   susceptibility in autism spectrum disorder. *Frontiers in Neuroscience*, *17*, 1125428.

1836   Xu, M., Li, L., & Pittenger, C. (2016). Ablation of fast-spiking interneurons in the dorsal striatum,

1837   recapitulating abnormalities seen post-mortem in Tourette syndrome, produces anxiety and elevated

1838   grooming. *Neuroscience*, *324*, 321-329.

1839   Zeka, F., Vanderheyden, K., De Smet, E., Cuvelier, C. A., Mestdagh, P., & Vandesompele, J. (2016).

1840   Straightforward and sensitive RT-qPCR based gene expression analysis of FFPE samples. Scientific

1841   reports, 6(1), 21418.

1842   Zhao, H., Mao, X., Zhu, C., Zou, X., Peng, F., Yang, W., Li, B., Li, G., Ge, T., & Cui, R. (2022). GABAergic

1843   system dysfunction in autism spectrum disorders. *Frontiers in cell and developmental biology*, *9*,

1844   781327.

1845

1846

1847

1848

1849

1850

1851

1852

1853

1854

1855 APPENDICIES

1856 **Appendix A:** G*Power (ver. 3.1.9.7) output from the conducted power analysis performed in the

1857 planning of this study.

1858
1859
1860
1861
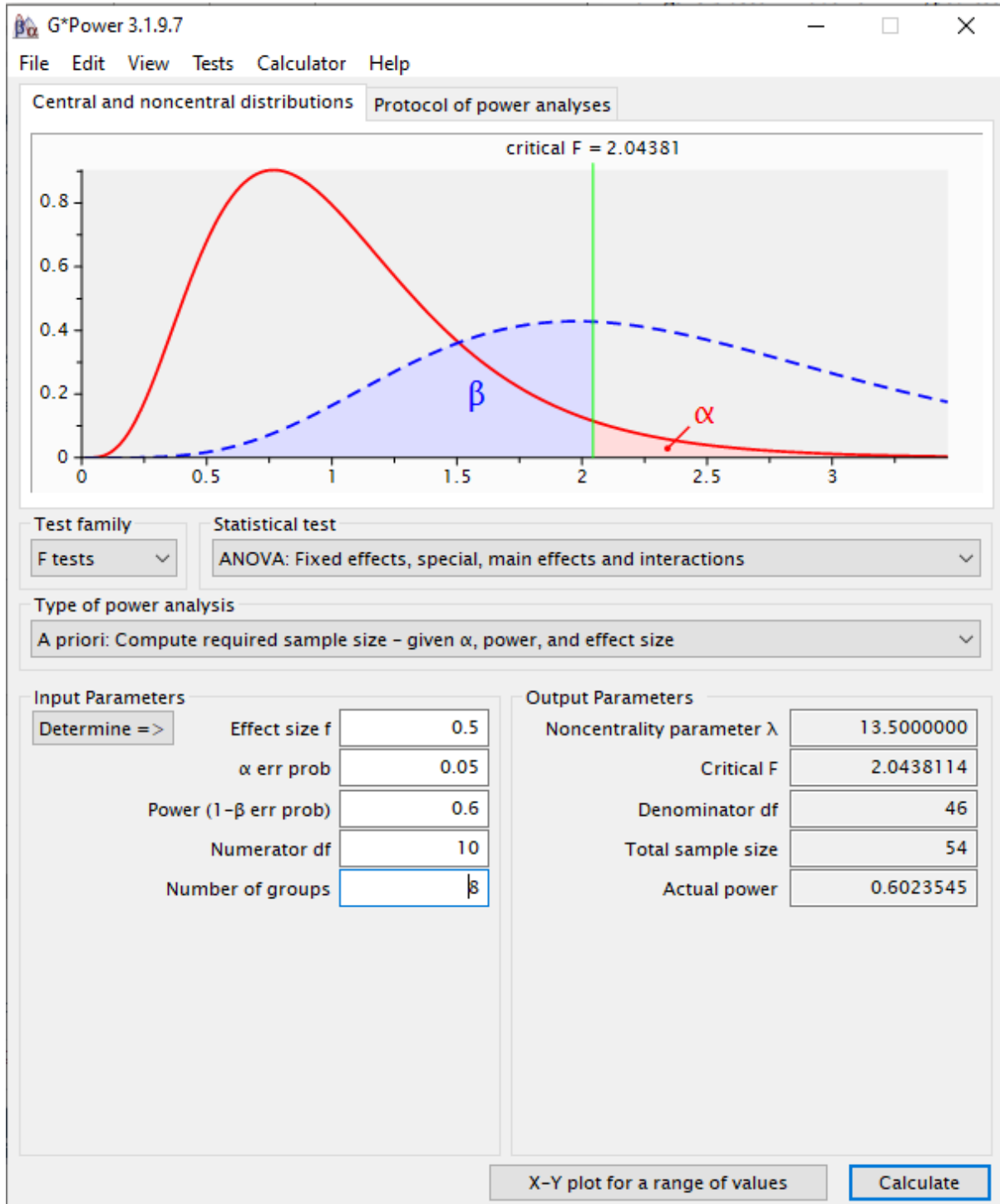
Appendix B: NanoDrop 2000 spectrophotometer logbook to assess the purity of RNA from all fixative-

1863   stripped tissue samples.

Sample ID	Nature of sample	Conc. Nucleic Acid (ng/uL)	A260	A280	260/280	260/230
J		11	0.275	0.14	1.96	0.43
K		7.3	0.181	0.088	2.07	1.21
L		8.3	0.207	0.104	1.98	0.15
M		4.8	0.12	0.065	1.85	0.47
N		9	0.224	0.106	2.11	0.08
O		16.5	0.412	0.234	1.77	0.83
P		7	0.174	0.088	1.99	0.89
Q		9	0.224	0.116	1.94	0.82
R		7.7	0.191	0.095	2.01	0.62
S		21.2	0.531	0.274	1.94	0.75
A		7.3	0.183	0.098	1.88	0.66
B		5.9	0.148	0.081	1.82	0.5
C		4.2	0.105	0.055	1.91	0.53
D		3.7	0.093	0.036	2.63	1.07
E		2.2	0.054	0.013	4.14	0.54
F		22.2	0.554	0.33	1.68	0.38
G		13.1	0.328	0.182	1.8	0.62
H		3.5	0.086	0.04	2.15	0.11
I		3.8	0.095	0.04	2.39	0.84
1		3.4	0.085	0.041	2.08	0.5
2		6.1	0.152	0.086	1.77	0.49
3		18.8	0.47	0.282	1.67	0.62
4		3	0.076	0.035	2.15	0.35
5		9.4	0.236	0.133	1.78	0.26
6		7.1	0.177	0.094	1.89	0.6
7		3.4	0.085	0.034	2.48	0.22
BEE		22.1	0.552	0.274	2.02	1.14
RET		17.9	0.449	0.21	2.14	0.94
COL		16.9	0.423	0.201	2.1	1.16
MON		10.7	0.267	0.131	2.04	0.13
GIG		17.7	0.443	0.221	2	1.16
JUG		12.4	0.331	0.145	2.14	0.41
PUY		16.7	0.418	0.186	2.24	0.95
TYE		16.6	0.415	0.196	2.16	0.89
MEL		9.6	0.241	0.104	2.32	0.92
PAM		13.6	0.341	0.157	2.17	1.15

1864

1865

1866

1867

1868

1869

1870

1871

1872

Appendix C: Assessment of suitability of primers for duplexing was assessed through primer efficiency

1874   curves, as displayed below for each duplexed pair in this study.
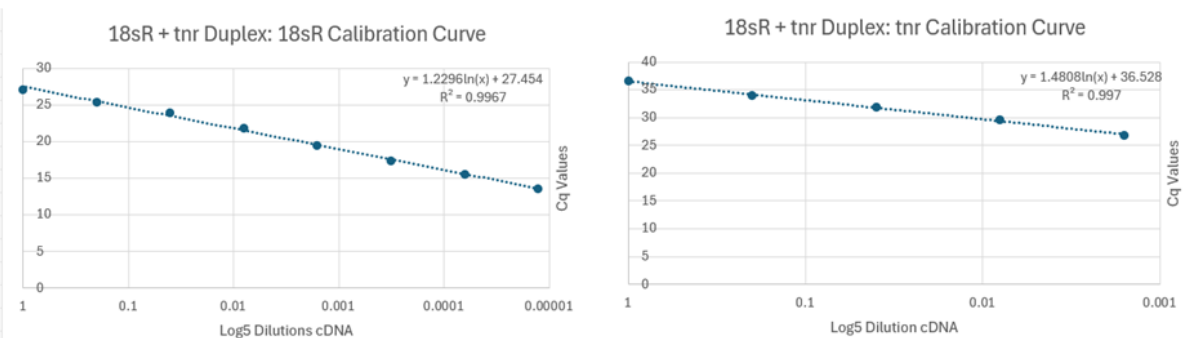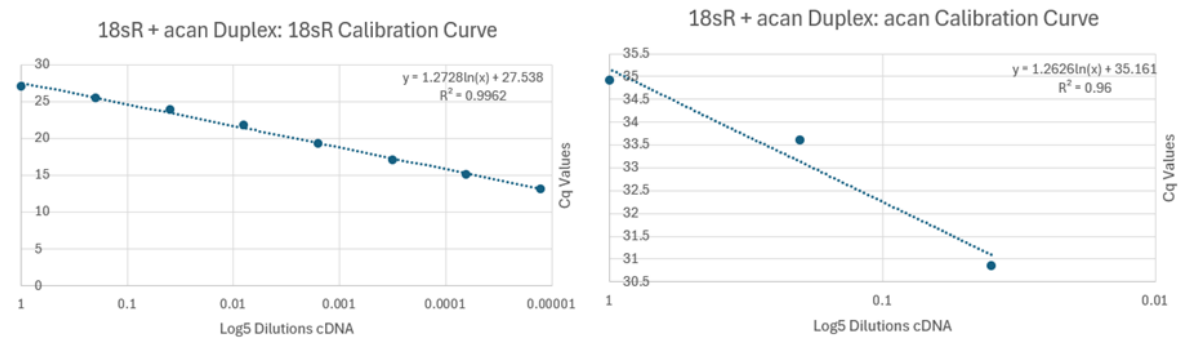
18sR pvalb Duplex Calibration Curves
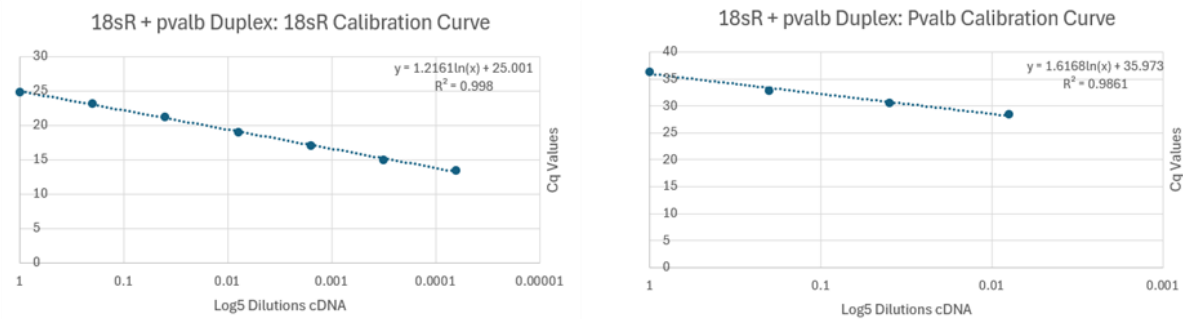
18sR hapln1 Duplex Calibration Curves
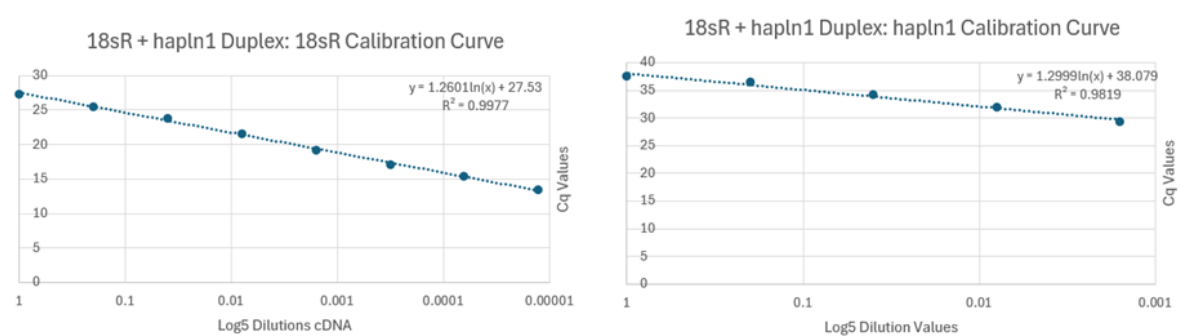
18sR tnr Duplex Calibration Curves

18sR acan Duplex Calibration Curves

1875